SPATIAL MODULATION MIMO SYSTEMS WITH DUAL-POLARIZED ANTENNAS

by

Golara Zafari

B.S., Electrical and Electronic Engineering, Khaje Nasir Toosi University of Technology, 2011

Submitted to the Institute for Graduate Studies in
Science and Engineering in partial fulfillment of
the requirements for the degree of
Master of Science

Graduate Program in Electrical and Electronics Engineering
Boğaziçi University

2014

SPATIAL MODULATION MIMO SYSTEMS WITH DUAL-POLARIZED ANTENNAS

APPROVED BY:

Assoc. Prof. Mutlu Koca (Thesis Supervisor)	.....
Assist. Prof. Ali Emre Pusane	.....
Assoc. Prof. Tuna Tuğcu	.....

DATE OF APPROVAL: 18.08.2014

ACKNOWLEDGEMENTS

I would like to express my special appreciation and thanks to my advisor Assoc. Prof. Mutlu Koca, you have been a tremendous mentor for me. I would like to thank you for encouraging my research. Your advices on my research have been priceless. I would also like to thank my committee members, Assist. Prof. Ali Emre Pusane and Assoc. Prof. Tuna Tuğcu, for serving as my committee members even at hardship. I also want to thank you for letting my defense be an enjoyable moment, and for your brilliant comments and suggestions, thanks to you.

My special thanks goes to my family. I know I always have my family to count on when times are rough. Words cannot express how grateful I am to my mother and father for all of the sacrifices that you've made on my behalf. Your prayer for me was what sustained me thus far. I would also express my deep thank to dear Zafar and Elahe for your unconditional support. I can sincerely assure you that I am with you in my spirit and thought.

Last but not least, I would like to thank all of my friends, especially WCL's people who supported me and incented me to strive towards my goal. Also my appreciation to all those who made my time in Turkey an experience that far surpassed my every expectation.

This thesis has been supported by the Scientific and Technological Research Council of Turkey (TÜBİTAK) under project number 111E274.

ABSTRACT

SPATIAL MODULATION MIMO SYSTEMS WITH DUAL-POLARIZED ANTENNAS

In wireless communication systems, multiple-input multiple-output (MIMO) systems have been widely used during the past decades to achieve better performance. However, there is an inevitable issue due to the usage of multi-antennas, which is known as inter-channel interference. Not only inter-channel interference, but also correlation, which is the result of inter-antenna spacing, deteriorate the performance. A promising solution to combat with these issues is to increase inter-antenna spacing or alternatively using orthogonal polarization and decrease the number of channels to eliminate inter-channel interference using spatial modulation (SM). In this work, we address the effect of dual-polarized antennas over MIMO system employing SM. The performance is evaluated for the general Rician channel with transmit and receive correlation. The equilibrium points, where dual-polarized and uni-polarized channels achieve the same performance, is derived in terms of exact performance as well as Chernoff bound and the equilibrium points are compared with the equilibrium points, where dual-polarized and uni-polarized systems have the same ergodic mutual information. It is theoretically shown that two cross points are the same in the Rayleigh scenario, where the number of transmit and receive antennas is equal. Later on, the results are extended to the case where there is channel estimation error and also generalized-SM (G-SM) where more than one antenna is used to transmit the same symbol and achieve diversity gain.

ÖZET

ÇİFT-KUTUPSAL ANTENLİ ÇOK-GİRDİLİ ÇOK-ÇIKTILI UZAMSAL KİPLENİM SİSTEMLERİ

Kablosuz iletişim sistemlerinden çok girdili çok çıktılı (MIMO) sistemleri, daha iyi performans elde edebilmek için son on yılda çok yaygın olarak kullanılmıştır. Öte yandan, çok anten kullanımının neden olduğu, kanallar-arası girişim olarak bilinen kaçınılmaz bir sorun vardır. Yalnızca kanallar-arası girişim değil, aynı zamanda antenler-arası aralığın sonucu olan ilinti de performansı kötüleştirmektedir. Bu sorunlarla mücadele etmek için ümit veren çözüm anten aralığını arttırmak ya da alternatif olarak dikgen kutuplama kullanarak ve kanal sayısını arttırarak kanallar-arası girişimi ortadan kaldıran uzamsal kiplenim (UK) kullanmaktır. Bu çalışmada çift kutuplanmış antenlerin etkileri, UK'nın uygulandığı MIMO sistemlerinde incelenmiştir. Performans alıcı ve verici ilintili genel Rice tipi kanallar için değerlendirilmiştir. Çift kutuplanmış ve tek kutuplanmış kanalların aynı performansı elde ettiği denge noktaları hem kesin performans hem de Chernoff sınırı açısından türetilmiş ve çift kutuplanmış be tek kutuplanmış sistemlerin aynı ergodik karşılıklı bilgiye sahip oldukları denge noktalarıyla karşılaştırılmıştır. Alıcı ve verici anten sayılarının eşit olduğu Rayleigh senaryolarında iki çapraz noktanın aynı olduğu teorik olarak gösterilmiştir. Daha sonra, sonuçlar kanal kestirim hatasının olduğu ve aynı zamanda birden çok antenin aynı sembolü iletmek ve çeşitleme kazancının elde etmek için kullandığı genelleşmiş-UK (G-UK) durumları için genişletilmiştir.

TABLE OF CONTENTS

LIST OF FIGURES

LIST OF TABLES

LIST OF SYMBOLS

a_{ij}	Description of a_{ij}
$\mathcal{CN}(m_x, \sigma_x^2)$	Complex Gaussian random variable with mean m_x and variance σ_x^2
$D(\cdot)$	Distance metric
$E\{\cdot\}$	Expectation operator
$\mathbf{G}$	Channel matrix with erroneous estimation
$\mathbf{g}_u$	uth column of $\mathbf{G}$
$\mathbf{H}$	Channel matrix
$\bar{\mathbf{H}}_w$	Fixed part of the channel $\mathbf{H}$
$\tilde{\mathbf{H}}_w$	Variable part of the channel $\mathbf{H}$
$\mathbf{h}_u$	uth column of $\mathbf{H}$
$h_{i,j}$	Channel coefficient between ith receive antenna and jth transmit antenna
$I_0(\cdot)$	Modified Bessel function of the first kind
K	Rician factor
L	L-ary digital modulation
ℓ	Number of bits assigned for constellation symbols
M	Number of transmit antennas
m	Number of bits assigned to antenna selection
N	Number of receive antennas
N_0	Noise variance
$\mathcal{N}(m_x, \sigma_x^2)$	Gaussian random variable with mean m_x and variance σ_x^2
P_r	Average received power
$\mathbf{Q}_t$	Coupling matrix for dual-polarized transmit antenna
$\mathbf{Q}_r$	Coupling matrix for dual-polarized receive antenna
$\mathbf{q}_u$	uth aggregate channel vector
q_r^{-1}	XPI for dual-polarized receive antenna
q_t^{-1}	XPI for dual-polarized transmit antenna
R	Spectral efficiency

$Re\{x\}$, x^R	Real part of a complex variable
$vec(\cdot)$	Vectorization of a matrix
X	Transmitted symbol
$\mathbf{x}$	Transmitted signal
$\mathbf{y}$	Received signal
α_r	Spatial correlation coefficient at the receiver
α_t	Spatial correlation coefficient at the transmitter
η	Signal-to-noise ratio (SNR)
γ_r	Receive polarization correlation coefficient
γ_t	Transmit polarization correlation coefficient
$\boldsymbol{\nu}$	Noise vector
$\Omega_{i,j}$	Transmit correlations between the ith and jth aggregate channels in presence of error estimation
$\Phi_{i,j}$	Transmit correlations between the ith and jth aggregate perfect channels
$\mathbf{\Pi}_r$	Polarization correlation matrix at the receiver
$\mathbf{\Pi}_t$	Polarization correlation matrix at the transmitter
$\mathbf{\Psi}_r$	Receive correlation matrix
$\mathbf{\Psi}_t$	Transmit correlation matrix
$\mathbf{\Sigma}_r$	Spatial correlation matrix at the receiver
$\mathbf{\Sigma}_t$	Spatial correlation matrix at the transmitter
σ_e^2	Variance of the channel estimation error
$\sigma_{i,j}^r$	i,jth element of receive spatial correlation matrix
$\sigma_{i,j}^t$	i,jth element of transmit spatial correlation matrix
$\mathbf{\Xi}_r$	Correlation matrix of the channel estimation error at the receiver
$\mathbf{\Xi}_t$	Correlation matrix of the channel estimation error at the transmitter
$\{\cdot\}^*$	Complex conjugation
$\lvert\cdot\rvert$	Determinant of a matrix

$\|\cdot\|_F$	Frobenius norm
$\{\cdot\}^H$	Hermitian
$\{\cdot\}^T$	Transposition
$\otimes$	Kronecker product

LIST OF ACRONYMS/ABBREVIATIONS

ABEP	Average Bit Error Probability
AM	Amplitude Modulation
AoA	Angle of Arrival
APEP	Average Pairwise Error Probability
AS	Angular Spread
BER	Bit Error Rate
C-SM	Conventional Spatial Modulation
DoT	Direction of Travel
exp	Exponential Function
FM	Frequency Modulation
G-SM	Generalized Spatial Modulation
i.i.d	Independent and Identically Distributed
LOS	Line Of Sight
MIMO	Multiple Input Multiple Output
ML	Maximum Likelihood
PDF	Probability Density Function
PEP	Pairwise Error Probability
SISO	Single Input Single Output
SM	Spatial Modulation
SNR	Signal to Noise Ratio
STBC	Space Time Block Coding
XPD	Cross-Polar Discrimination
XPR	Cross-Polar Ratio
XPI	Cross-Polar Isolation

1. INTRODUCTION

1.1. MIMO Communication

MIMO communication is an emerging technology to solve the traffic capacity. The technology, which also known as space-time wireless or smart antennas, has been widely used in various areas including broad band wireless systems, wireless local area networks (WLAN), third-generation (3D) networks [1] and it has been penetrated to several wireless communication standards such as IEEE 802.11, 802.16 (WiMAX), HSPDA, and LTE [2]. Given multiple antennas at transmitter and receiver, provide spatial dimension. High reliability and data rate arise from the use of the new dimension. Indeed, advantageous of MIMO systems stems from usage of multi-path created by multi-antennas at both ends, piping either the same or different informations, in such a manner that two main gains can be introduced as below.

(i) Diversity gain: Diversity gain is achieved when the same data stream undergoes from parallel channels. This increases the number of independent branches. Therefore; facing deep fading in all of the channels would be less likely and it increases the asymptotic error rate slope as a function of SNR, i.e., $\eta \to \infty$ [3]. Space time codes and beamforming techniques [4] are well-known techniques achieving high diversity order. These techniques are more suited for the application which require high reliability [5].

(ii) Multiplexing gain: Given the spatial dimension in MIMO systems exploits another degree of freedom by spatially multiplexing of different data streams such as V-BLAST. Consequently, data rate is increased proportionally to the minimum number of transmitter and receiver without increasing the spectrum or transmit power.

1.2. Spatial Modulation

Spatial modulation (SM) [6, 7] is an emerging multiple-input multiple-output (MIMO) technology, where the information is conveyed simultaneously over both the signal and the antenna spaces. In SM, part of the incoming bits is used to choose a transmit antenna to be activated while the rest is to select the modulation symbol to be sent. Then the detector makes a joint estimate of the indices of both the activated antenna and the transmitted signal. As shown extensively in the SM literature, this approach provides better multiplexing gains and error performances than conventional methods. Furthermore, because only one antenna is active during each signaling period, the transmit chain is simplified and the inter-channel interference (ICI) is completely avoided. From a broader perspective, conventional SM (C-SM) scheme, where only one antenna is activated, can be seen as a special case of the generalized SM (G-SM) presented in [8–11]. In G-SM each index mapped by the antenna bits addresses a group of simultaneously activated antennas. The active antennas may transmit the same symbol and thus benefit from repetition diversity as proposed in [8–10] or each active antenna may transmit different symbols and thus achieving multiplexing gains as presented in [11]. A special case of this type of G-SM is also presented in [12], where the advantages of G-SM are combined with the Alamouti space-time block coding (STBC) for improved error performance over conventional SM and other spatial multiplexing techniques. At the other extreme, space shift keying (SSK) [13] has also emerged as a special form of SM, where only the transmitting antenna index is used to bear information, making the receiver to only detect which antenna was emitting power.

In general, because of their implementation simplicity and performance and rate improvements, both conventional and also generalized SM/SSK based wireless communications systems have created a significant research interest in recent years spanning a wide range of application areas (We refer the reader to [14] for a thorough review).

1.3. MIMO with Dual Polarized Antennas

Several works have focused on the modeling and performance of channel with uni-polarized antennas, which require a large inter-antenna separation in the base-station to reduce the correlation effect. However, using dual-polarized antennas can be an alternative solution and offer more compact implementation. While less space is feasible due to the co-located antennas with different polarizations, multi-polarized structure in turn represents another correlation, known as cross-polar discrimination (XPD), as a result of polarization mismatch. Several measurements have shown the relationship between XPD and distance between transmitter and receiver [15] - [16]. Although aforementioned works have shed a light to the improvement obtained by using dual-polarized antennas, they are limited to the measured data. Theoretical and practical results of [17] show the degradation of two vertically polarized antennas, in terms of capacity, compared to dual polarized when XPD is almost 0 dB and 0.2 dB, respectively. Effects of various antenna configurations and propagation environments have been also investigated in [18] and [19], where dual-polarized antennas provide uncorrelated branches, which improve the performance. Experimental results of [20], conducted in an indoor environment at 3.6 GHz, indicate the sensitivity of XPD on spatial characteristics. Experimental results of some of previous works are as below, which are useful to characterize polarization matrices as described in detail in Chapter 3. In [21], XPD is measured to be between 5 dB- 11 dB for indoor propagation environment. Small/ micro cells are considered at a frequency of 1800 MHz in [22], where XPD is from 5 dB to 15 dB and it is shown that horizontal/ vertical antenna configuration works around 1 dB worse than horizontal diversity. Indoor MIMO channel for wireless local area is addressed for 5.25 GHz in [23]. In [24], XPD is obtained to be between -3 dB and -4 dB for handheld mobiles and between -8 dB and -10 dB for antenna on top of a car. The results are consistent with the observations of other works regarding the independence of XPD to transmitter- receiver distance, unless there is a strong constant path, where approximately 3 dB degradation in XPD is observed within 100 meters. For other channels, XPD is shown to vary from 4 dB to 10 dB. Sensitivity of XPD to delay multi-path in NLOS channels has been studied in [25]. That is, the less delay in channel (LOS channel) the higher XPD.

Moreover, [26] and [27] propose geometrical XPD models, independent of measurement. Impact of XPD on the achieved antenna selection gain is also addressed in [28]. Further theoretical channel models have been reported in the literature [29]-[30]. [29] - [31] propose geometrical scattering models for dual-polarized MIMO fixed wireless channels and statistical model is presented in [32]. A more generalized statistical model is also presented incorporating channel characterizations such as line of sight (LOS), shadowing and temporal correlations characterizing dual-polarized MIMO land mobile satellite [33]. It is also shown that hybrid polarization systems offer independent propagation paths for the two polarizations and thus have better performance in terms of capacity [34]. Capacity of dual-polarized systems is further investigated and compared with uni-polarized MIMO channel and the results are used to show that dual-polarized channels outperform in presence of non-ideal conditions [30], [31], and [35]. Moreover, performance enhancement due to the use of dual-polarized antenna is considered for spatial multiplexing [36] and space-time block coding (STBC) using a hybrid scheme in [37].

1.4. Scope Of The Thesis

Thus, the main contribution of the presented work is to combine the SM and dual-polarized antenna to achieve higher data rate as well as space and energy efficiency. This scheme provide additional dimension, namely polarization selection and increase the data rate by one bit compared to the system equipped with uni-polarized antennas with the same number of transmit antennas. The performance analysis is derived in perfect channel estimation and in terms of transmit and receive correlation matrices for the general $M \times N$ Rician channel. Channel is modeled with the well-known Kronecker model and the equilibrium points, where dual-polarized and uni-polarized channels achieve the same performance, is derived and it is compared with the equilibrium points, where dual-polarized and uni-polarized systems have the same ergodic mutual information. Furthermore, it is shown that the equilibrium points obtained by performance and ergodic mutual information is the same in Rayleigh channel, when the number of transmit and receive antennas are the same. Simulation is also conducted

for the Rician channel to show the effect of Rician factor. Furthermore, the equilibrium points are derived in presence of channel estimation error to evaluate the impact of estimation error. Finally, G-SM is considered as general case of SM.

1.5. Thesis Outline

The dissertation is organized as follows: We review some background information in Chapter 1 such as MIMO communication, spatial modulation and dual-polarized channels. Chapter 2, represents MIMO communication systems with emphasis on different channel realizations. Spatial modulation is also introduced as a method, which can be implemented over MIMO systems. Chapter 3, illustrates dual-polarized channel and its model in both SISO and MIMO. The main contribution of this work is presented in Chapter 4, where equilibrium points are derived in terms of mutual information and Chernoff bound and they are compared by equilibrium points of exact error performance analysis. Considering the importance of channel estimation error, Chapter 5 addresses the performance and equilibrium points under imperfect channel estimation. Finally, Chapter 6 shows the results for generalized spatial modulation.

2. MIMO COMMUNICATION SYSTEMS

During the past decades, MIMO systems have become the cornerstone of wireless communication to provide higher data rates as well as more reliable communication. MIMO systems are well investigated in the literature and their advantages such as array gain, spatial diversity, and spatial multiplexing result in significant performance gain. Advantages of MIMO systems are briefly shown in Figure 2.1. While taking benefits from time and frequency dimensions proposed by the conventional SISO communication, this technology offers an extra dimension known as spatial dimension due to the multiple antennas at both transmitter and receiver. In other words, multi antennas provide several channels either piping multiple RF streams and increasing the data rate or piping the same RF stream and improving the reliability of the communication.

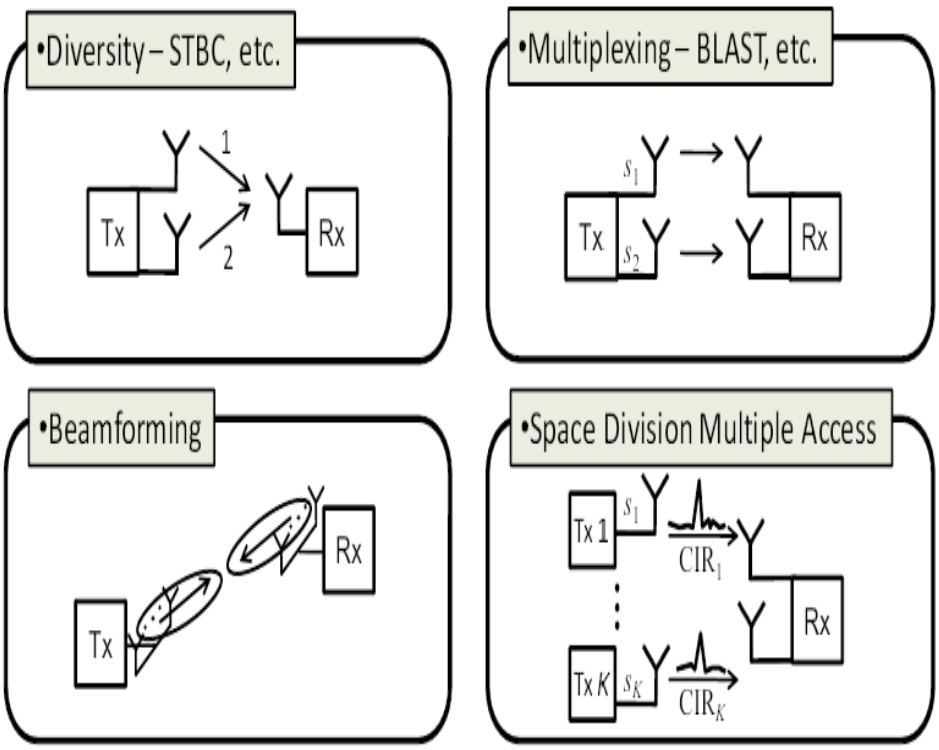

Figure 2.1: Advantages of a MIMO system.

2.1. MIMO Channel Models

Different channels with M transmit antennas and N receive antennas can be shown by channel matrix as below.

$$\mathbf{H} = \begin{bmatrix} h_{1,1} & h_{1,2} & \cdots & h_{1,(M)} \\ h_{2,1} & h_{2,2} & \cdots & h_{2,(M)} \\ h_{3,1} & h_{3,2} & \cdots & h_{3,(M)} \\ h_{4,1} & h_{4,2} & \cdots & h_{4,(M)} \\ \vdots & \vdots & \vdots & \vdots \\ h_{(N-1),1} & h_{(N-1),2} & \cdots & h_{(N-1),(M)} \\ h_{(N),1} & h_{(N),2} & \cdots & h_{(N),(M)} \end{bmatrix} \tag{2.1}$$

where $h_{i,j}$ represents the channel coefficient between jth transmit and ith receive antenna, for $i = 0, \ldots, N$ and $j = 0, \ldots, M$. The amplitude of received signal is randomly changed. Assuming the large number of independent and identically distributed (i.i.d) paths from transmitter to the receiver, the received amplitude is following the complex Gaussian distribution due to the central limit theorem. Consequently, its envelope becomes Rayleigh distribution if the channel has zero mean. Alternatively, if the channel has non-zero mean, then the channel is known as Rician fading characterized by Rician factor, K. Rayleigh and Rician fading channels are explained in more detailed in the following sections.

2.1.1. Correlated Rayleigh Fading Channels

Assume M transmit and N receive antennas creating MN paths. Rayleigh fading is a model used to describe a multipath channel, where the paths are i.i.d complex Gaussian and none of the paths is dominant. In other words, mean of the channel is zero. Moreover, spacing between antennas causes correlations between them. To put it mathematically, assume r_I and r_Q are both zero mean Gaussian random variables with variance σ^2, i.e., $\mathcal{N}(0, \sigma^2)$. r_I and r_Q stand for in-phase (real) and quadrate (imaginary) components of received signal. Therefore, the envelope of signal, $z = |r| = \sqrt{r_I + r_Q}$,

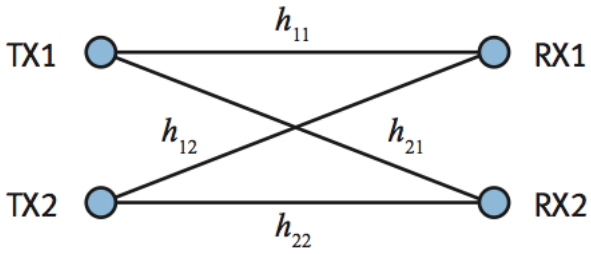

Figure 2.2: A 2×2 channel.

follows the Rayleigh distribution as below

$$p_Z(z) = \frac{z}{\sigma^2} \exp(-z^2/2\sigma^2) \tag{2.2}$$

For simplicity, assume a 2×2 channel as shown in Figure 2.2 with the channel matrix defined as

$$\mathbf{H} = \begin{bmatrix} h_{1,1} & h_{1,2} \\ h_{2,1} & h_{2,2} \end{bmatrix} \tag{2.3}$$

In practice, signals at transmitter and receiver are correlated and the correlation is effected by

(i) Signal angular spread (AS),
(ii) Angle of arrival (AoA),
(iii) Subscriber direction of travel (DoT).

Let us define transmit and receive spatial correlation coefficient as

$$E\left\{h_{1,1}h_{1,2}^*\right\} = E\left\{h_{2,1}^*h_{2,2}\right\} = \alpha_t \tag{2.4}$$

$$E\left\{h_{1,1}h_{2,1}^*\right\} = E\left\{h_{1,2}^*h_{2,2}\right\} = \alpha_r \tag{2.5}$$

Transmit and receive spatial correlation impact by spatial correlation matrices, $\mathbf{\Sigma}_t$ and $\mathbf{\Sigma}_r$.

$$\mathbf{\Sigma}_{\mathrm{t}} = \begin{bmatrix} 1 & \alpha_t \\ \alpha_t^* & 1 \end{bmatrix}, \qquad \mathbf{\Sigma}_{\mathrm{r}} = \begin{bmatrix} 1 & \alpha_r \\ \alpha_r^* & 1 \end{bmatrix} \tag{2.6}$$

This model can be furthermore extended to the $M \times N$ system, such that $\mathbf{\Sigma}_t$ and $\mathbf{\Sigma}_r$ are $M \times M$ transmit and $N \times N$ receive correlation matrices, respectively due to the inter- antenna spacing and they can be defined as

$$E\left\{\mathbf{H}\mathbf{H}^H\right\} = \mathbf{\Sigma}_r \tag{2.7}$$

$$E\left\{\mathbf{H}\mathbf{H}^H\right\} = \mathbf{\Sigma}_t \tag{2.8}$$

where each element of spatial matrices can be shown by

$$E\left\{\sum\nolimits_k \mathbf{H}_{i,k}\mathbf{H}_{j,k}^*\right\} = [\mathbf{\Sigma}_r]_{i,j} = \sigma_{i,j}^r \tag{2.9}$$

$$E\left\{\sum\nolimits_k \mathbf{H}_{k,i}\mathbf{H}_{k,j}^*\right\} = [\mathbf{\Sigma}_t]_{i,j} = \sigma_{i,j}^t \tag{2.10}$$

Various kinds of models are proposed to model transmit and receive spatial correlations, i.e., $\mathbf{\Sigma}_t$ and $\mathbf{\Sigma}_r$, such as uniform model and exponential model. In practice, it is reasonable to have more correlation for the nearest antennas and as the distance between antennas increases, the correlation decreases. Thus, comparing with uniform correlation matrices, exponential model defined as below is more realistic.

$$\alpha_{i,j} = \begin{cases} \alpha^{j-i}, i \leq j \\ \alpha_{j,i}^*, i > j \end{cases}, |\alpha| \leq 1 \tag{2.11}$$

It is also shown in [38] that increasing the correlation is equivalent to decreasing SNR.

Channel matrix can be shown using the well known Kronecker model [39] as

$$\mathbf{H} = \mathbf{\Sigma}_r^{\frac{1}{2}} \mathbf{H}_w \mathbf{\Sigma}_t^{\frac{1}{2}T} \tag{2.12}$$

where $\mathbf{H}_w$ is an $N \times M$ matrix whose elements are formed by Rayleigh distribution.

2.1.2. Correlated Rician Fading Channels

In the previous section, if the channel is non- zero, then channel known as Rician fading channel, where the non- zero mean is defined as LOS component and it is well characterized by Rician factor, K. In this scenario, channel elements have Rician distribution as

$$p_Z(z) = \frac{2z\,(K+1)}{P_r} \exp(-K - \frac{(K+1)\,z^2}{P_r}) I_0 \left(2z \sqrt{\frac{K\,(K+1)}{P_r}} \right) \tag{2.13}$$

where P_r is the average received power and I_0 represents the modified Bessel function of first kind. K is ratio of power received over LOS to the power of scattered signals and thus it has different values for each channel, however, throughout this work, K is assumed to be constant. The Rician channel matrix can be modeled by

$$\mathbf{H} = \sqrt{\frac{K}{K+1}} \bar{\mathbf{H}} + \sqrt{\frac{1}{K+1}} \tilde{\mathbf{H}} \tag{2.14}$$

where the fix part, $\bar{\mathbf{H}}$, is a deterministic matrix representing the Rician component of the channel whereas variable part, $\tilde{\mathbf{H}}$, is the Rayleigh component and thus defined as

$$\tilde{\mathbf{H}} = \mathbf{\Sigma}_r^{\frac{1}{2}} \mathbf{H}_w \mathbf{\Sigma}_t^{\frac{1}{2}T} \tag{2.15}$$

Notice that when $K = 0$, the channel is equivalent to the Rayleigh fading channel. On the other hand, when K is large enough there is only LOS.

2.2. Spatial Modulation

As it is known, modulation is a method to transmit the signal by changing one or more properties of the carrier signal. Commonly used modulations are frequency modulation (FM) and amplitude modulation (AM). Recently, a novel modulation technique is proposed by Mesleh *et al.* [6] known as spatial modulation (SM).

The main idea of SM is to transmit an RF stream not only using the constellation symbols but also over antenna space. Figure 2.3a illustrates SM methodology. As has been shown some parts of input (S2) is used to switch between antennas, i.e., if S2 is 0, first antenna will be used and if it is 1, second antenna will be activated. The second part of data stream (S1) is mapped to the constellation symbols and transmitted via activated antenna. Figure 2.3b is an example of SM with 4 transmit antennas conveying signal over QPSK constellation. Let assume the input bits of a transmission instant is 1110. The first part (11) is assigned to the antenna constellation. Thus, the corresponding antenna is the forth antenna, which is shown by red color. Second part (10) is also mapped to the constellation diagram and is represents by yellow. Alternatively, assume 0001 is transmitted at second transmission instant (as has been shown in Figure 2.3c). Mapping strategy is tabulated in Table 2.1.

As can be seen, there is only one activated antenna at each transmission, which eliminates the ICI and has a considerable reduction of complexity at receiver end.

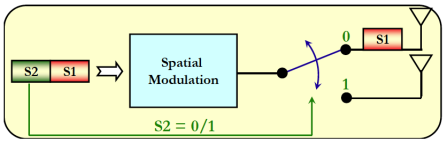

(a) Using an RF input stream to switch between transmit antennas.

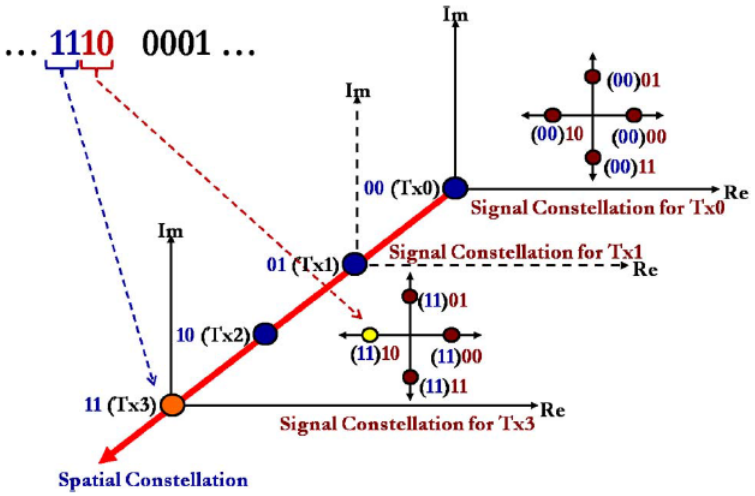

(b) Constellation symbols transmitted over different antennas at first transmission instant.

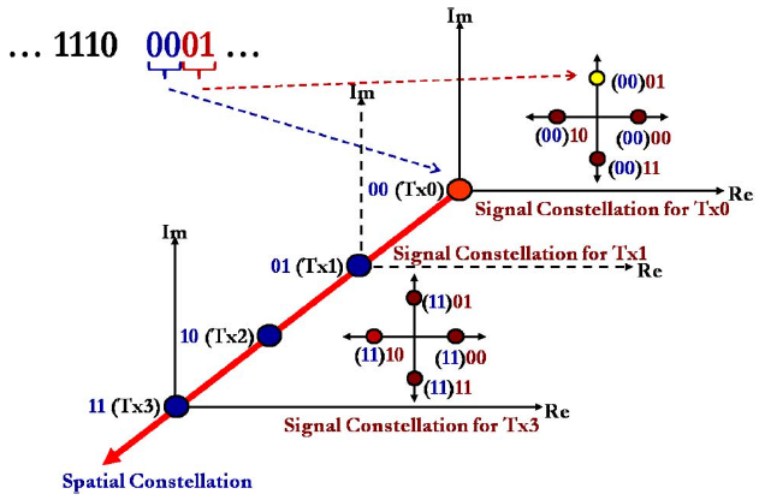

(c) Constellation symbols transmitted over different antennas at second transmission instant.

Figure 2.3: SM technique [14].

Table 2.1: Mapping input bits to corresponding constellation symbols and antenna space.

Incoming bits	Symbol bits	Antenna	$\mathbf{x^T}$	X_s
$\overbrace{0\ 0}^{symbol\ bits}\ \overbrace{0}^{antenna}\ \overbrace{0}^{polarization}$	00	1	$\begin{bmatrix} 0 & 0 & 0 & 1 \end{bmatrix}$	1
0001	00	2	$\begin{bmatrix} 0 & 0 & 1 & 0 \end{bmatrix}$	1
0010	00	3	$\begin{bmatrix} 0 & 1 & 0 & 0 \end{bmatrix}$	1
0011	00	4	$\begin{bmatrix} 1 & 0 & 0 & 0 \end{bmatrix}$	1
0100	01	1	$\begin{bmatrix} 0 & 0 & 0 & j \end{bmatrix}$	j
0101	01	2	$\begin{bmatrix} 0 & 0 & j & 0 \end{bmatrix}$	j
0110	01	3	$\begin{bmatrix} 0 & j & 0 & 0 \end{bmatrix}$	j
0111	01	4	$\begin{bmatrix} j & 0 & 0 & 0 \end{bmatrix}$	j
1000	10	1	$\begin{bmatrix} 0 & 0 & 0 & -1 \end{bmatrix}$	-1
1001	10	2	$\begin{bmatrix} 0 & 0 & -1 & 0 \end{bmatrix}$	-1
1010	10	3	$\begin{bmatrix} 0 & -1 & 0 & 0 \end{bmatrix}$	-1
1011	10	4	$\begin{bmatrix} -1 & 0 & 0 & 0 \end{bmatrix}$	-1
1100	11	1	$\begin{bmatrix} 0 & 0 & 0 & -j \end{bmatrix}$	-j
1101	11	2	$\begin{bmatrix} 0 & 0 & -j & 0 \end{bmatrix}$	-j
1110	11	3	$\begin{bmatrix} 0 & -j & 0 & 0 \end{bmatrix}$	-j
1111	11	4	$\begin{bmatrix} -j & 0 & 0 & 0 \end{bmatrix}$	-j

3. DUAL-POLARIZED MIMO SYSTEM

3.1. SISO Channel with Dual-Polarized Antennas

Suppose an 1×1 system equipped with two co-located antennas, which have orthogonal polarizations (either horizontal and vertical or alternatively slanted polarizations), as shown in Figure 3.1.

Figure 3.1: 1×1 dual- polarized channel [36].

The 1×1 dual-polarized configuration as shown in Figure 3.1 create a 2×2 channel as

$$\mathbf{H}_p = \begin{bmatrix} \varrho_{1_p,1_p} & \varrho_{1_p,1_{p'}} \\ \varrho_{1_{p'},1_p} & \varrho_{1_{p'},1_{p'}} \end{bmatrix} \tag{3.1}$$

As it turns out, dual- polarized antennas pose polarization correlations in terms of XPD, including cross- polar isolation (XPI) and cross- polar ratio (XPR). Each of transmit and receive antennas has an antenna pattern, one of which is shown in Figure 3.2, where solid line represents co-polar and dashed line shows cross-polar radiation of

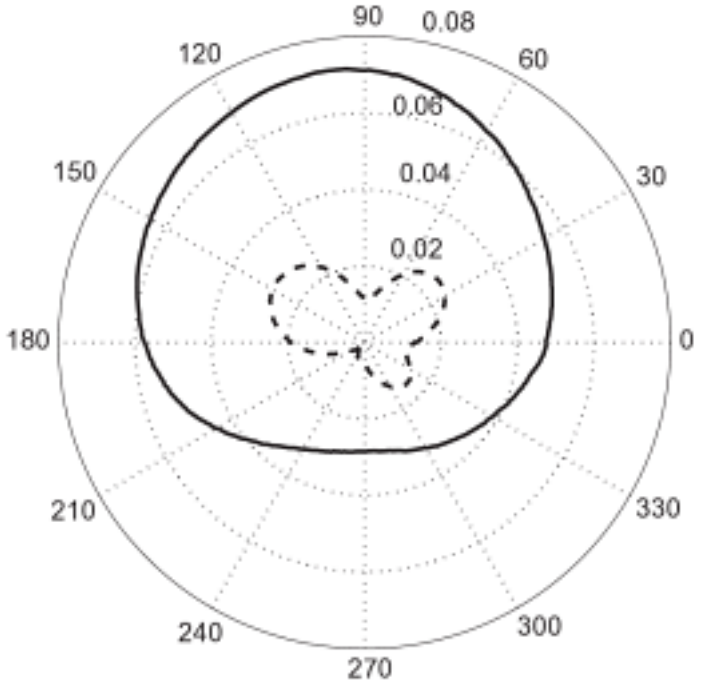

Figure 3.2: Antenna-pattern.

an antenna.

XPI is an antenna characteristic and denotes the effects of cross-polar antenna pattern. For an ideal antenna, designed with a specific polarization (either linear or circular), received cross-polar signal has to be zero. Nevertheless, in practice, it is not the case and there is some received signal, whose polarization is orthogonal to the desired polarization. The ratio of power of co-polar signal to the power of cross-polar signal is defined by XPI. In other words, effects of XPI can be shown by coupling matrices at the transmitter and receiver sides as

$$\mathbf{Q}_{\mathrm{t}} = \begin{bmatrix} 1 & \sqrt{q_t} \\ \sqrt{q_t} & 1 \end{bmatrix}, \qquad \mathbf{Q}_{\mathrm{r}} = \begin{bmatrix} 1 & \sqrt{q_r} \\ \sqrt{q_r} & 1 \end{bmatrix} \tag{3.2}$$

in which ${q_r}^{-1}$ and ${q_t}^{-1}$ represent the XPI at receive and transmit antennas, respectively. By definition $0 \leq q_r \leq 1$ and $0 \leq q_t \leq 1$. Notice that, transmission over LOS preserves the polarization of transmitted signal and thus; the polarization of the signal received by the receiver through LOS path is only affected by XPI.

On the other hand, XPR is an effect of channel. That is to say, polarization of the transmitted signal is changed through the channel as a result of reflection or diffraction. So, XPR= $\cot^2\theta = \frac{1-\mu}{\mu}$, in which θ is a polarization rotation of transmitted signal caused as the signal goes trough the channel. μ is the power of signal with orthogonal polarization and $1-\mu$ is the power of signal with desired polarization. Consequently, polarization correlation coefficient at each 1×1 dual-polarized channel, can be defined as

$$\begin{aligned}\gamma_t &= \frac{E\left\{\tilde{\varrho}_{ip,ip}\tilde{\varrho}^*_{ip,ip'}\right\}}{\sqrt{\mu(1-\mu)}} = \frac{E\left\{\tilde{\varrho}_{ip',ip}\tilde{\varrho}^*_{ip',ip'}\right\}}{\sqrt{\mu(1-\mu)}} \\ \gamma_r &= \frac{E\left\{\tilde{\varrho}_{ip,ip}\tilde{\varrho}^*_{ip',ip}\right\}}{\sqrt{\mu(1-\mu)}} = \frac{E\left\{\tilde{\varrho}_{ip,ip'}\tilde{\varrho}^*_{ip',ip'}\right\}}{\sqrt{\mu(1-\mu)}}\end{aligned} \tag{3.3}$$

where subscripts p and p' are two orthogonal polarizations. As defined in (3.3), γ_t and γ_r are by definition between 0 and 1, i.e., $0 \le \gamma_t \le 1$ and $0 \le \gamma_r \le 1$. The aforementioned correlation coefficients are assumed to be the same for all dual-polarized antennas.

Accordingly, polarization correlation matrices, are shown by $\mathbf{\Pi_t}$ and $\mathbf{\Pi_r}$, at transmitter and receiver, respectively. $\mathbf{\Pi_t}$ and $\mathbf{\Pi_r}$ are 2×2 matrices, which can be modeled as

$$\mathbf{\Pi}_{\mathrm{t}} = \begin{bmatrix} 1 & \gamma_t \\ \gamma_t^* & 1 \end{bmatrix}, \qquad \mathbf{\Pi}_{\mathrm{r}} = \begin{bmatrix} 1 & \gamma_r \\ \gamma_r^* & 1 \end{bmatrix} \tag{3.4}$$

Considering the effects of XPI and XPR, XPD can be defined as the combination of XPI and XPR. Consequently, the Rayleigh channel for Fig. 3.1 can be shown using transmit and receive polarization coefficient as

$$\breve{\mathbf{H}} = \mathbf{Q}_r \mathbf{\Pi}_r^{\frac{1}{2}} \breve{\mathbf{H}}_w \mathbf{\Pi}_t^{\frac{1}{2}T} \mathbf{Q}_t \tag{3.5}$$

where $\breve{\mathbf{H}}_w$ is a 2×2 matrix, whose elements are independent circularly symmetric complex exponentials of unit amplitude and uniformly distributed phase over $[0, 2\pi)$.

Channel can be also modeled for the Rician case as

$$\mathbf{H} = \sqrt{\frac{K}{1+K}}\mathbf{Q}_{\mathrm{r}}\overline{\overline{\mathbf{H}}}\mathbf{Q}_{\mathrm{t}} + \sqrt{\frac{1}{1+K}}\mathbf{Q}_r\mathbf{\Pi}_r^{\frac{1}{2}}\breve{\mathbf{H}}_w\mathbf{\Pi}_t^{\frac{1}{2}T}\mathbf{Q}_t \tag{3.6}$$

where $\overline{\overline{\mathbf{H}}}$ is a 2×2 deterministic matrix representing LOS coefficients and K is the Rician factor.

3.2. MIMO Channel with Dual-Polarized Antennas

Assuming spatially separated dual-polarized antennas, adds spatial correlation coefficient by spatial matrices. Transmit and receive spatial correlation matrices can be modeled exponentially as defined in Equation 2.11.

Having $M \times N$ MIMO channel with dual polarized antennas results in $2N \times 2M$ dimensional channel matrix as

$$\mathbf{H}_p = \begin{bmatrix} \varrho_{1_p,1_p} & \varrho_{1_p,1_{p'}} & \varrho_{1_p,2_p} & \cdots & \varrho_{1_p,M_{p'}} \\ \varrho_{1_{p'},1_p} & \varrho_{1_{p'},1_{p'}} & \varrho_{1_{p'}h,2_p} & \cdots & \varrho_{1_{p'},M_{p'}} \\ \varrho_{2_p,1_p} & \varrho_{2_p,1_{p'}} & \varrho_{2_p,2_p} & \cdots & \varrho_{2_p,M_{p'}} \\ \varrho_{2_{p'},1_p} & \varrho_{2_{p'},1_{p'}} & \varrho_{2_{p'},2_p} & \cdots & \varrho_{2_{p'},M_{p'}} \\ \vdots & \vdots & \vdots & \vdots & \vdots \\ \varrho_{N_p,1_p} & \varrho_{N_p,1_{p'}} & \varrho_{N_p,2_p} & \cdots & \varrho_{N_p,M_{p'}} \\ \varrho_{N_{p'},1_p} & \varrho_{N_{p'},1_{p'}} & \varrho_{N_{p'},2_p} & \cdots & \varrho_{N_{p'},M_{p'}} \end{bmatrix} \tag{3.7}$$

each of $\varrho_{i_p,j_{p'}}$, for $i = 1 \ldots N$ and $j = 1 \ldots M$, represents the channel coefficient observed between the pth polarization direction of the ith receive antenna and the p'th polarization of the jth transmit antenna. For the sake of simplicity, subscripts of elements of $\mathbf{H}_p$ can be written in numerous format. Thus; the equivalent channel becomes as

$$\mathbf{H} = \begin{bmatrix} h_{1,1} & h_{1,2} & \cdots & h_{1,(2M)} \\ h_{2,1} & h_{2,2} & \cdots & h_{2,(2M)} \\ h_{3,1} & h_{3,2} & \cdots & h_{3,(2M)} \\ h_{4,1} & h_{4,2} & \cdots & h_{4,(2M)} \\ \vdots & \vdots & \vdots & \vdots \\ h_{(2N-1),1} & h_{(2N-1),2} & \cdots & h_{(2N-1),(2M)} \\ h_{(2N),1} & h_{(2N),2} & \cdots & h_{(2N),(2M)} \end{bmatrix} \tag{3.8}$$

We assume a slow fading MIMO channel including an average component and variable component. We also assume the scattering environment is identical for all antennas at both sides. Channel can be modeled using Equation 2.14.

There is also spatial correlation matrices, $\mathbf{\Sigma}_t$ and $\mathbf{\Sigma}_r$, due to the MIMO channel with spatially separated dual polarized antennas as described in Chapter 2.

Considering the effects of coupling matrices and assuming identical orientation for all sub-arrays, $\overline{\mathrm{H}}$ can be written as [3]

$$\overline{\mathrm{H}} = 1_{N\times M} \otimes \mathbf{Q}_{\mathrm{r}}\overline{\overline{\mathbf{H}}}\mathbf{Q}_{\mathrm{t}} \tag{3.9}$$

where $\overline{\overline{\mathbf{H}}}$ is a 2×2 deterministic matrix as defined before. $\overline{\mathrm{H}}$ is such that $[\overline{\mathrm{H}}]_{p,q} = \bar{h}_{p,q}$, for $p = 1, \ldots, 2N$ and $q = 1, \ldots, 2M$. Variable part of the channel, $\widetilde{\mathbf{H}}$, however, is $[\widetilde{\mathbf{H}}]_{p,q} = \tilde{h}_{p,q}$. We assume that

$$\mathrm{E}\left[\tilde{h}^R_{p,q}\tilde{h}^R_{\hat{p},\hat{q}}\right] = \mathrm{E}\left[\tilde{h}^I_{p,q}\tilde{h}^I_{\hat{p},\hat{q}}\right], \tag{3.10}$$

$$\mathrm{E}\left[\tilde{h}^R_{p,q}\tilde{h}^I_{\hat{p},\hat{q}}\right] = \mathrm{E}\left[\tilde{h}^I_{p,q}\tilde{h}^R_{\hat{p},\hat{q}}\right] = 0 \tag{3.11}$$

for all channel coefficient pairs $(\tilde{h}_{p,q}, \tilde{h}_{\hat{p},\hat{q}})$ $(p, \hat{p} = 1, \ldots, 2N$ and $q, \hat{q} = 1, \ldots, 2M)$.

$\widetilde{\mathbf{H}}$ can be defined as

$$\widetilde{\mathbf{H}} = \widehat{\mathbf{H}} \otimes \breve{\mathbf{H}} \tag{3.12}$$

where $\widehat{\mathbf{H}}$ is an $N \times M$ matrix, whose elements are possibly correlated defined as $[\widehat{\mathbf{H}}]_{p,q} = re^{j\theta}$ and its covariance implies spatial covariance. $\breve{\mathbf{H}}$ is a 2×2 matrix defined as $[\breve{\mathbf{H}}]_{p,q} = e^{j\varphi}$ [3], which models the rotation of the polarization and correlated phase between the four channels created by 1×1 dual-polarized antenna. Each term of Equation 3.12 can be calculated using [33] and [3] as

$$\widehat{\mathbf{H}} = \mathbf{\Sigma}_r^{\frac{1}{2}} \widehat{\mathbf{H}}_w \mathbf{\Sigma}_t^{\frac{1}{2}T} \tag{3.13}$$

$\widehat{\mathbf{H}}_w$ is $N \times M$ independent Rayleigh fading channel matrix, whose elements are described as i.i.d complex Gaussian random variables, i.e., $\mathcal{CN}(0, 1)$.

Using Equation 3.5 and Equation 3.12, the variable part becomes as

$$\widetilde{\mathbf{H}} = \mathbf{\Psi}_r^{\frac{1}{2}} \widetilde{\mathbf{H}}_w \mathbf{\Psi}_t^{\frac{1}{2}T} \tag{3.14}$$

where $\mathbf{\Psi}_r = \mathbf{\Sigma}_r \otimes (\mathbf{Q}_r \mathbf{\Pi}_r \mathbf{Q}_r)$, $\mathbf{\Psi}_t = \mathbf{\Sigma}_t \otimes (\mathbf{Q}_t \mathbf{\Pi}_t \mathbf{Q}_t)$ and $\widetilde{\mathbf{H}}_w = \widehat{\mathbf{H}}_w \otimes \breve{\mathbf{H}}_w$, as shown in the appendix. $\mathbf{\Psi}_t$ and $\mathbf{\Psi}_r$ are $2M \times 2M$ and $2N \times 2N$ real valued and Hermitian symmetric transmit and receive correlation matrices, respectively.

It can be easily seen that after the Kronecker product, $\widetilde{\mathbf{H}}_w$ becomes an independent Rayleigh fading channel matrix, whose elements are described as i.i.d complex Gaussian random variables, i.e., $[\widetilde{\mathbf{H}}_w]_{p,q} = \widetilde{h}_{w_{p,q}} \sim \mathcal{CN}(0, 1)$ for $p = 1, \ldots, 2N$ and $q = 1, \ldots, 2M$.

Notice that as Equation 3.8 shows, the equivalent uni-polarized system is $2M \times 2N$ channel defined as

$$\mathbf{H}' = \sqrt{\frac{K}{1+K}}\overline{\mathbf{H}}' + \sqrt{\frac{1}{1+K}}\widetilde{\mathbf{H}}' \tag{3.15}$$

where $\overline{\mathbf{H}}'$ is a $2N \times 2M$ deterministic matrix and $\widetilde{\mathbf{H}}' = \mathbf{\Psi}'^{\frac{1}{2}}_{r}\widetilde{\mathbf{H}}'_{w}\mathbf{\Psi}'^{\frac{1}{2}T}_{t}$. $\mathbf{\Psi}'_{r} = \mathbf{\Sigma}'_{r}$, $\mathbf{\Psi}'_{t} = \mathbf{\Sigma}'_{t}$ are $2N \times 2N$ and $2M \times 2M$ receive and transmit spatial correlation matrices as there is no polarization correlations. $\widetilde{\mathbf{H}}'_{w}$ is also $2N \times 2M$ independent Rayleigh fading channel matrix, whose elements are described as i.i.d complex Gaussian random variables, i.e., $[\widetilde{\mathbf{H}}'_{w}]_{p,q} = \widetilde{h}'_{w_{p,q}} \sim \mathcal{CN}(0,1)$ for $p = 1, \ldots, 2N$ and $q = 1, \ldots, 2M$.

4. DUAL-POLARIZED SPATIAL MODULATION

4.1. System Model

In this dissertation, we consider a MIMO system employing M transmit and N receive antennas, each of which are dual polarized. As in [40], we assume that the number of transmit antennas is an integer power of 2, i.e., $M = 2^m$, mapping ℓ bits to L-ary digital modulation, where $L = 2^\ell$ and $\boldsymbol{\mathcal{X}} = \left\{ X_1, \ \ldots \ X_k, \ \ldots \ X_L \right\}$ represents the set of constellation symbols. In this scheme, spectral efficiency is $R = m + 1 + \ell = \log_2(2ML)$ bits/s/Hz. At each transmission instant, $m+1+\ell$ bits of incoming stream is chosen. $m+1$ bits are used to select one of the transmit antennas and its polarization. In other words, m bits are used to select one of the M dual-polarized antennas and depending on the value of the $(m+1)$-st bit, vertical or horizontal polarization, or alternatively one of the slanted polarizations, will be chosen. Later on, ℓ bits are mapped to the L-ary symbol space. Throughout this work, we assume bit-to-antenna index and bit-to-symbol mapping to be uniform. The received signal is modeled as

$$\mathbf{y} = \mathbf{H}\mathbf{x} + \boldsymbol{\nu} \tag{4.1}$$

where all of the entries of transmitted signal, $\mathbf{x}$, are zero except one of them. The position of non-zero element represents the index of activated antenna as well as its polarization and its value denotes the transmitted symbol. Table 4.1 shows the mapping strategy. We assume a power constraint of unity, as in [40], i.e., $E_{\mathbf{x}}\left[\mathbf{x}^H\mathbf{x} = 1\right]$.

Suppose X_s is the sth element of modulation alphabet, for $s = 1, \ldots, L$ and if we assume that u denotes the index of activated antenna together with its polarization, for $u = 1, \ldots, 2M$, then Equation 4.1 can be written as

$$\mathbf{y} = \mathbf{h}_u X_s + \boldsymbol{\nu} \tag{4.2}$$

Table 4.1: Adapting SM for dual-polarized antenna configuration.

Incoming bits	Symbol bits	Antenna	Polarization	$\mathbf{x^T}$	X_s
$\overbrace{0\ 0}^{symbol\ bits}\ \overbrace{0}^{antenna}\ \overbrace{0}^{polarization}$	00	I	p	$\begin{bmatrix} 0 & 0 & 0 & 1 \end{bmatrix}$	1
0001	00	I	p'	$\begin{bmatrix} 0 & 0 & 1 & 0 \end{bmatrix}$	1
0010	00	II	p	$\begin{bmatrix} 0 & 1 & 0 & 0 \end{bmatrix}$	1
0011	00	II	p'	$\begin{bmatrix} 1 & 0 & 0 & 0 \end{bmatrix}$	1
0100	01	I	p	$\begin{bmatrix} 0 & 0 & 0 & j \end{bmatrix}$	j
0101	01	I	p'	$\begin{bmatrix} 0 & 0 & j & 0 \end{bmatrix}$	j
0110	01	II	p	$\begin{bmatrix} 0 & j & 0 & 0 \end{bmatrix}$	j
0111	01	II	p'	$\begin{bmatrix} j & 0 & 0 & 0 \end{bmatrix}$	j
1000	10	I	p	$\begin{bmatrix} 0 & 0 & 0 & -1 \end{bmatrix}$	-1
1001	10	I	p'	$\begin{bmatrix} 0 & 0 & -1 & 0 \end{bmatrix}$	-1
1010	10	II	p	$\begin{bmatrix} 0 & -1 & 0 & 0 \end{bmatrix}$	-1
1011	10	II	p'	$\begin{bmatrix} -1 & 0 & 0 & 0 \end{bmatrix}$	-1
1100	11	I	p	$\begin{bmatrix} 0 & 0 & 0 & -j \end{bmatrix}$	-j
1101	11	I	p'	$\begin{bmatrix} 0 & 0 & -j & 0 \end{bmatrix}$	-j
1110	11	II	p	$\begin{bmatrix} 0 & -j & 0 & 0 \end{bmatrix}$	-j
1111	11	II	p'	$\begin{bmatrix} -j & 0 & 0 & 0 \end{bmatrix}$	-j

where $\mathbf{y}$ and $\boldsymbol{\nu}$ are the $2N \times 1$ received signal and channel noise vectors, respectively. The elements of $\boldsymbol{\nu}$ are independent identically distributed (i.i.d.) complex Gaussian variables with zero mean and variance N_0, i.e., $\nu_k \sim \mathcal{CN}(0, N_0)$ for $k = 1, \ldots, 2N$, thus signal to noise ratio (SNR) is $SNR = \eta = \frac{\bar{E}_s}{N_0} = \frac{1}{N_0}$. $\mathbf{h}_u$ also represents the uth column of $\mathbf{H}$. Since there exists a dual- polarized MIMO system, $\mathbf{H}$ is defined as in Section 3.2.

4.2. Mutual Information

In the following section, we investigate the ergodic mutual information to compare $M \times N$ dual-polarized with $2M \times 2N$ uni-polarized channel and finally, equilibrium point, where the uni-polarized system achieves the same ergodic mutual information as dual-polarized scheme, is derived with respect to the polarization coefficient, spatial coefficients and inverse of XPI. According to the equilibrium point, one can decide to use uni-polar or dual-polar system to achieve higher ergodic mutual information and consequently, higher capacity.

The channel is assumed to be Rayleigh, i.e., $K = 0$, where the channel model in Equation 2.14 reduces to the variable component as defined in Equation 3.14. The mutual information of a MIMO system can be calculated using. Notice that the difference between mutual information in this section and the one achieved in is that here we assign all the energy to the activated antenna and so there is no need for normalization. Moreover, in this part, numbers of transmitter and receiver are not limited to be the same as it was assumed in the aforementioned work.

$$I_{DP} = \log_2|\mathbf{I} + \eta\mathbf{H}\mathbf{H}^H| \tag{4.3}$$

Assuming high SNR, Equation 4.3 reduces to

$$I_{DP} \approx \log_2|\eta\mathbf{H}\mathbf{H}^H| \tag{4.4}$$

Putting Equation 3.14 in Equation 4.4, Equation 4.4 can be further simplified to

$$I_{DP} \approx 2N\log_2(\eta) + \log_2|\mathbf{\Psi}_t| + \log_2|\mathbf{\Psi}_r| + \log_2|\tilde{\mathbf{H}}_w\tilde{\mathbf{H}}_w^H| \tag{4.5}$$

where $\mathbf{\Psi}_r$,$\mathbf{\Psi}_t$ and $\tilde{\mathbf{H}}_w$ are defined as before. Now, taking the expectation of Equation

4.5, the ergodic mutual information becomes

$$\begin{aligned}\bar{I}_{DP} &= E[I_{DP}] \\ &\approx 2N\log_2(\eta) + \log_2|\mathbf{\Psi}_t| + \log_2|\mathbf{\Psi}_r| \\ &+ \frac{1}{\log 2}\left(\sum_{k=0}^{2M-1}\sum_{a=1}^{2N-k-1}\frac{1}{a} - 2M\zeta\right) \end{aligned} \tag{4.6}$$

where $\zeta \approx 0.57721566$ is Euler's constant. Equation 4.6 can be more simplified to

$$\begin{aligned}\bar{I}_{DP} &= E[I_{DP}] \\ &\approx 2N\log_2(\eta) + \log_2|\mathbf{\Sigma}_r \otimes (\mathbf{Q}_r\mathbf{\Pi}_r\mathbf{Q}_r)| + \log_2|\mathbf{\Sigma}_t \otimes (\mathbf{Q}_t\mathbf{\Pi}_t\mathbf{Q}_t)| \\ &+ \frac{1}{\log 2}\left(\sum_{k=0}^{2M-1}\sum_{a=1}^{2N-k-1}\frac{1}{a} - 2M\zeta\right) \\ &\approx 2N\log_2(\eta) + 2\log_2|\mathbf{\Sigma}_r| + 2N\log_2|\mathbf{Q}_r| + N\log_2|\mathbf{\Pi}_r| \\ &+ 2\log_2|\mathbf{\Sigma}_t| + 2M\log_2|\mathbf{Q}_t| + M\log_2|\mathbf{\Pi}_t| \\ &+ \frac{1}{\log 2}\left(\sum_{k=0}^{2M-1}\sum_{a=1}^{2N-k-1}\frac{1}{a} - 2M\zeta\right) \end{aligned} \tag{4.7}$$

Notice that using the exponential model for spatial correlation and polarization correlation matrices, as defined before, determinant of correlation matrices for $2M \times 2N$ uni-polarized and $M \times N$ dual-polarized system, can be calculated as follow

$$|\mathbf{\Psi}_t| = |\mathbf{\Sigma}_t|^2|\mathbf{Q}_t|^{2M}|\mathbf{\Pi}_t|^M = \left(1-\alpha_t^2\right)^{2M-2}\left(1-\gamma_t^2\right)^M(1-q_t)^{2M} \tag{4.8}$$

$$|\mathbf{\Psi}_r| = |\mathbf{\Sigma}_r|^2|\mathbf{Q}_r|^{2N}|\mathbf{\Pi}_r|^N = \left(1-\alpha_r^2\right)^{2N-2}\left(1-\gamma_r^2\right)^N(1-q_r)^{2N} \tag{4.9}$$

$$|\mathbf{\Psi'}_t| = |\mathbf{\Sigma'}_t|^2 = \left(1-\alpha_t^2\right)^{2M-1} \tag{4.10}$$

$$|\mathbf{\Psi'}_r| = |\mathbf{\Sigma'}_r|^2 = \left(1-\alpha_r^2\right)^{2N-1} \tag{4.11}$$

Considering the uni-polarized channel given in Equation 3.15, ergodic mutual information of $2M \times 2N$ uni-polarized and $M \times N$ dual-polarized system can be compared

over their hypothesis, H_{DP} and H_{UP}, as below

$$
\begin{aligned}
& \bar{I}_{DP} \gtrless_{H_{UP}}^{H_{DP}} \bar{I}_{UP} \\
\Longrightarrow \quad & 2N\log_2(\eta) + 2\log_2(1-\alpha_r^2)^{N-1} + N\log_2(1-\gamma_r^2) + 2\log_2(1-\alpha_t^2)^{M-1} \\
+ \quad & M\log_2(1-\gamma_t^2) + 2N\log_2|\mathbf{Q}_r| + 2M\log_2|\mathbf{Q}_t| + \frac{1}{\log 2}\left(\sum_{k=0}^{2M-1}\sum_{a=1}^{2N-k-1}\frac{1}{a} - 2M\zeta\right) \\
\gtrless_{H_{UP}}^{H_{DP}} \quad & 2N\log_2(\eta) + \log_2(1-\alpha_r^2)^{2N-1} + \log_2(1-\alpha_t^2)^{2M-1} \\
+ \quad & \frac{1}{\log 2}\left(\sum_{k=0}^{2M-1}\sum_{a=1}^{2N-k-1}\frac{1}{a} - 2M\zeta\right) \\
\Longrightarrow \quad & (2N-2)\log_2(1-\alpha_r^2) + N\log_2(1-\gamma_r^2) + (2M-2)\log_2(1-\alpha_t^2) \\
+ \quad & M\log_2(1-\gamma_t^2) + 2N\log_2(1-q_r) + 2M\log_2(1-q_t) \\
\gtrless_{H_{UP}}^{H_{DP}} \quad & (2N-1)\log_2(1-\alpha_r^2) + (2M-1)\log_2(1-\alpha_t^2)
\end{aligned}
\tag{4.12}
$$

which after some manipulation results in

$$
(1-\gamma_r^2)^N(1-\gamma_t^2)^M \gtrless_{H_{UP}}^{H_{DP}} \frac{(1-\alpha_r^2)(1-\alpha_t^2)}{(1-q_r)^{2N}(1-q_t)^{2M}} \tag{4.13}
$$

The above Equation shows that for a given channel and antenna parameters (i.e., $\alpha_r, \alpha_t, q_r, q_t, \gamma_r,$ and γ_t) there may exists an equilibrium point, γ_e, where $2M \times 2N$ uni-polar channel has the same performance as $M \times N$ dual-polarized system. It is worthy to mention that for completely uncorrelated channel, i.e., $\alpha_r = \alpha_t = 0$, assuming infinite XPI, i.e., $q_r = q_t = 0$, there is no situation that dual-polarized results in better performance. In other words, in the best case, dual-polarized can achieve the performance of uni-polarized system. While dual-polarized channel outperforms in the region, where $\gamma < \gamma_e$, uni-polarized system has higher ergodic mutual information in $\gamma > \gamma_e$. More generally, for a certain α_r and α_t, if the equilibrium point achieve by γ_r^e, γ_t^e, q_r^e, and q_t^e, then, for each and every value less than γ_r^e, γ_t^e, q_r^e, and q_t^e, dual-polarized antenna has higher mutual information. Also, notice that equilibrium point is independent of SNR. There are different combinations of aforementioned parameters, nevertheless, for the sake of illustration, following curves are provided for certain values.

Following curves are shown the equilibrium points for 2×2 dual and 4×4 uni-polarized channel. SNR is set to be 20 dB. Lines without markers represent ergodic mutual information of dual-polarized system while lines with marker denote uni-polarized scheme. Simulation is conducted for different spatial correlation coefficients and the curves with $\alpha_r = \alpha_t = 0$ represent spatially uncorrelated channels. Notice that $\alpha_r = \alpha_t$, $q_r = q_t$, and $\gamma_r = \gamma_t$ are assumed for the sake of simplicity and other unequal values do not change the general conclusion.

As has been explained, in uncorrelated channel, and when $q_r = q_t = 0$, i.e., Figure 4.1a, two system has the same performance in term of mutual information only when $\gamma_r = \gamma_t = 0$. As the spatial correlation coefficient increases, the equilibrium point becomes larger. Therefore, the region, in which dual-polarized outperforms get larger. Furthermore, comparing Figure 4.1a and Figure 4.1b illustrates that increasing q_r and q_t decreases the threshold points. That is why in low spatial correlation coefficient such as 0 and 0.3, which have low equilibrium points in infinite XPI, there are no equilibriums.

Going through the same steps as before, the equilibrium point can be achieved for $M \times N$ uni-polar and $M \times N$ dual-polarized channel as

$$
\begin{aligned}
& \bar{I}_{DP} \gtrless^{\mathbf{H}_{DP}}_{\mathbf{H}_{UP}} \bar{I}_{UP} \\
\Longrightarrow \quad & 2N\log_2(\eta) + 2\log_2(1-\alpha_r^2)^{N-1} + N\log_2(1-\gamma_r^2) + 2\log_2(1-\alpha_t^2)^{M-1} \\
+ \quad & M\log_2(1-\gamma_t^2) + 2N\log_2|\mathbf{Q}_r| + 2M\log_2|\mathbf{Q}_t| + \frac{1}{\log 2}\left(\sum_{k=0}^{2M-1}\sum_{a=1}^{2N-k-1}\frac{1}{a} - 2M\zeta\right) \\
\gtrless^{\mathbf{H}_{DP}}_{\mathbf{H}_{UP}} \quad & N\log_2(\eta) + \log_2(1-\alpha_r^2)^{N-1} + \log_2(1-\alpha_t^2)^{M-1} + \frac{1}{\log 2}\left(\sum_{k=0}^{M-1}\sum_{a=1}^{N-k-1}\frac{1}{a} - M\zeta\right)
\end{aligned}
\tag{4.14}
$$

$$
\begin{aligned}
& \log_2\left((1-\gamma_r^2)^N(1-\gamma_t^2)^M\right) \gtrless^{\mathbf{H}_{DP}}_{\mathbf{H}_{UP}} \log_2\left(\frac{(1-\alpha_r^2)^{1-N}(1-\alpha_t^2)^{1-M}}{(1-q_r)^{2N}(1-q_t)^{2M}\,(\eta)^N}\right) \\
- \quad & \frac{1}{\log 2}\left(\sum_{k=0}^{2M-1}\sum_{a=1}^{2N-k-1}\frac{1}{a} - \sum_{k=0}^{M-1}\sum_{a=1}^{N-k-1}\frac{1}{a} - M\zeta\right)
\end{aligned}
\tag{4.15}
$$

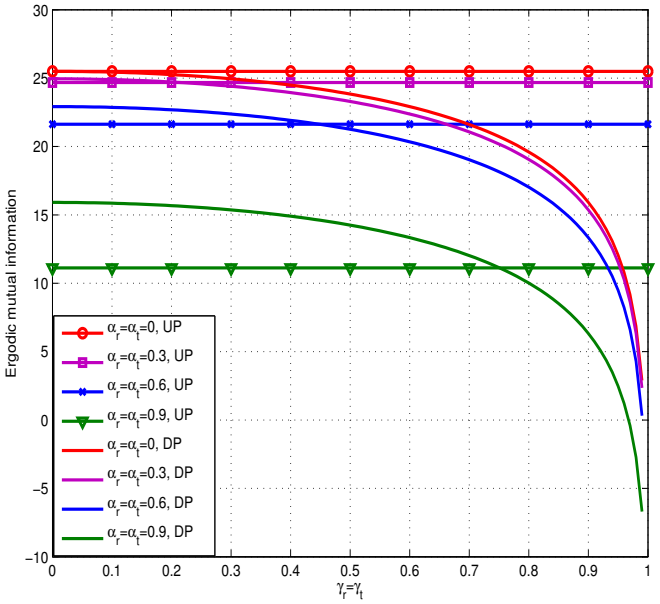

(a) $q_r = q_t = 0$.

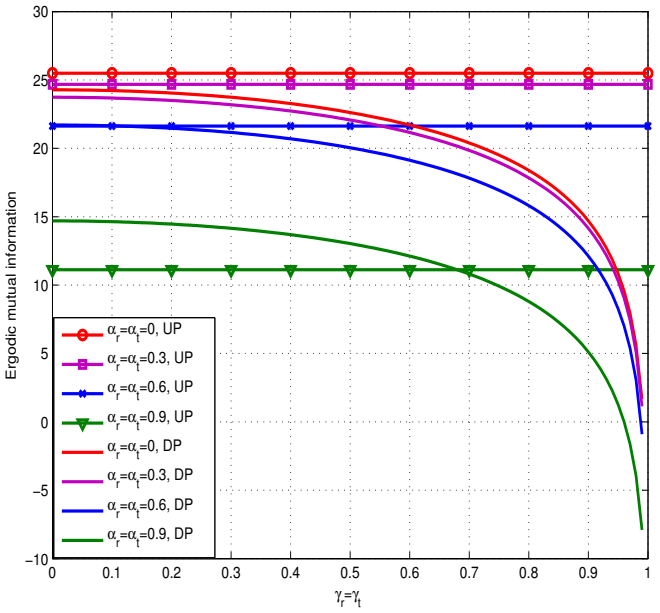

(b) $q_r = q_t = 0.1$.

Figure 4.1: Equilibrium points using ergodic mutual information for 4×4 uni-polar and 2×2 dual-polarized Rayleigh channel vs. polarization correlation coefficient in fixed $SNR = 20$ dB, and different XPI values for DP channels.

In this situation, equilibrium point depends on SNR. However, in high enough SNR, left hand side would be always greater than right hand side and so dual-polarized channel is preferable.

4.3. ABEP Analysis in Perfect Channel Estimation

In this section, we have considered the pairwise error probability (PEP) to find the average pairwise error probability (APEP) of dual-polarized system under SM. Having APEP, the average bit error probability (ABEP) can be approximated by using the well-known upper bound as

$$\bar{P}_b \leq \frac{1}{2ML} \sum_{u=1}^{2M} \sum_{\hat{u}=1}^{2M} \sum_{s=1}^{L} \sum_{\hat{s}=1}^{L} \frac{N(u, \hat{u}, s, \hat{s})}{\log_2(2ML)} \bar{P}_s(u, \hat{u}, s, \hat{s}) \tag{4.16}$$

where, $N(u, \hat{u}, s, \hat{s})$ is the number of bits in error between the respective channel and symbol pairs, $(\mathbf{h}_u, X_s)$ and $(\mathbf{h}_{\hat{u}}, X_{\hat{s}})$. The term $\log_2(2ML)$ denotes the total number of antenna and symbol bits. Division with this term indicates the summation weight for the corresponding PEP. $\bar{P}_s(u, \hat{u}, s, s)$ is the average pairwise symbol error probability (APEP). In the following sections, exact APEP is calculated and its Chernoff bound is also derived for further evaluation.

4.3.1. Exact APEP

PEP can be calculated by

$$P_s(u, \hat{u}, s, \hat{s}) = Q\left(\sqrt{\frac{\| \mathbf{z} \|^2}{2}}\right) \tag{4.17}$$

where $\mathbf{z}$, is given as [7]

$$\mathbf{z} = \sqrt{\eta}(\mathbf{h}_u X_s - \mathbf{h}_{\hat{u}} X_{\hat{s}}) \tag{4.18}$$

It can be easily shown that $\mathbf{z}$ as defined in Equation 4.18 is a proper complex Gaussian vector with joint PDF given by

$$f_{\mathbf{Z}}(\mathbf{z} \mid \mathbf{h}_u, \mathbf{h}_{\hat{u}}, X_s, X_{\hat{s}}) = \frac{e^{-(\mathbf{z}-\mathbf{m_z})^H \mathbf{\Lambda_z}^{-1}(\mathbf{z}-\mathbf{m_z})}}{\pi^{2N}|\mathbf{\Lambda_z}|} \tag{4.19}$$

where the mean and covariance of $\mathbf{z}$ are [40]

$$\mathbf{m_z} = \mathrm{E}[\mathbf{z}] = \sqrt{\frac{\eta K}{(K+1)}}(\bar{\mathbf{h}}_u X_s - \bar{\mathbf{h}}_{\hat{u}} X_{\hat{s}}) \tag{4.20}$$

$$\begin{aligned} \mathbf{\Lambda_z} &= \mathrm{E}\left[(\mathbf{z}-\mathbf{m_z})(\mathbf{z}-\mathbf{m_z})^H\right] \\ &= \frac{\psi^t_{u,u}|\ X_s|^2 + \psi^t_{\hat{u},\hat{u}} \mid X_{\hat{s}}|^2 - 2\,\mathrm{Re}\{\psi^t_{u,\hat{u}} X_s X^*_{\hat{s}}\}}{(K+1)}\eta\Psi_r \end{aligned} \tag{4.21}$$

Using PEP expression for each constellation, APEP can be calculated using MGF approach as

$$\begin{aligned} \bar{P}_s(u,\hat{u},s,\hat{s}) &= \int_{\mathbf{z}} Q\left(\sqrt{\frac{\|\ \mathbf{z}\ \|^2}{2}}\right) f_{\mathbf{Z}}(\mathbf{z} \mid \mathbf{h}_u, \mathbf{h}_{\hat{u}}, X_s, X_{\hat{s}}) d\mathbf{z} \\ &= \frac{1}{\pi}\int_0^{\frac{\pi}{2}} \frac{\exp\left(-\frac{1}{4}\mathbf{m}_{\mathbf{z}}^H\left[\frac{\mathbf{\Lambda_z}}{4} + \sin^2\theta\mathbf{I}\right]^{-1}\tilde{\mathbf{m}}_{\mathbf{z}}\right)}{\left|\frac{\tilde{\mathbf{\Lambda}}_{\mathbf{z}}}{4\sin^2\theta} + \mathbf{I}\right|} d\theta \end{aligned} \tag{4.22}$$

where $\mathbf{m_z}$ and $\mathbf{\Lambda_z}$ are as given in Equation 4.20 and Equation 4.21. Notice that, this integral cannot be simplified any further and can be calculated numerically, however, in a special case when $K = 0$, i.e., Rayleigh channel, the results of this integral has a closed form [41].

4.3.2. APEP Using Chernoff Bound

According to Equation 4.17, PEP can be upper bounded using Chernoff bound as

$$P_s(u,\hat{u},s,\hat{s}) = Q\left(\sqrt{\frac{\| \mathbf{z} \|^2}{2}}\right) = Q\left(\sqrt{\frac{\eta}{2}\|\mathbf{H}\mathbf{x}_{u,s} - \mathbf{H}\mathbf{x}_{\hat{u},\hat{s}}\|_F^2}\right) \quad (4.23)$$

$$\leqslant \frac{1}{2}\exp\left(-\frac{\eta}{4}\|\mathbf{H}\mathbf{x}_{u,s} - \mathbf{H}\mathbf{x}_{\hat{u},\hat{s}}\|_F^2\right) \quad (4.24)$$

$$= \frac{1}{2}\exp\left(-\frac{\eta}{4}\|\mathbf{H}(\mathbf{x}_{u,s} - \mathbf{x}_{\hat{u},\hat{s}})\|_F^2\right) \quad (4.25)$$

where $\mathbf{x}_{u,s}$ denotes the input vector, where all entries are zero expect uth element, whose value is sth symbol from the constellation alphabets.

Another way to calculate the mean and covariance matrix of $\mathbf{z}$ is to look at the alternative model of the channel, which is equivalent to the previous model, and it is given by

$$\mathbf{y} = (\mathbf{x}^T \otimes \mathbf{I}_N)vec(\mathbf{H}) + \boldsymbol{\nu} \quad (4.26)$$

where

$$vec(\mathbf{H}) = \sqrt{\frac{K}{1+K}}vec(\bar{\mathbf{H}}) + \sqrt{\frac{1}{1+K}}\boldsymbol{\Psi}^{\frac{1}{2}}vec(\tilde{\mathbf{H}}_w) \quad (4.27)$$

and

$$\boldsymbol{\Psi} = \boldsymbol{\Psi}_t^T \otimes \boldsymbol{\Psi}_r \quad (4.28)$$

Accordingly, Equation 4.25 can be rewritten as

$$P_s(u,\hat{u},s,\hat{s}) \leqslant \frac{1}{2}\exp\left(-\frac{\eta}{4}\left\|\left((\mathbf{x}_{u,s}^T - \mathbf{x}_{\hat{u},\hat{s}}^T) \otimes \mathbf{I}_N\right) vec(\mathbf{H})\right\|_F^2\right) \quad (4.29)$$

Defining $\mathbf{z}$ as

$$\begin{aligned}\mathbf{z} &= \sqrt{\eta}(\mathbf{x}_{u,s}^T \otimes \mathbf{I}_N - \mathbf{x}_{\hat{u},\hat{s}}^T \otimes \mathbf{I}_N) vec(\mathbf{H}) \qquad (4.30)\\ &= \sqrt{\eta}(\mathbf{x}_{u,s}^T \otimes \mathbf{I}_N - \mathbf{x}_{\hat{u},\hat{s}}^T \otimes \mathbf{I}_N)\left(\sqrt{\frac{K}{1+K}} vec(\bar{\mathbf{H}}) + \sqrt{\frac{1}{1+K}}\boldsymbol{\Psi}^{\frac{1}{2}} vec(\tilde{\mathbf{H}}_w)\right)\\ &= \sqrt{\frac{K\eta}{(1+K)}}\left((\mathbf{x}_{u,s}^T - \mathbf{x}_{\hat{u},\hat{s}}^T) \otimes \mathbf{I}_N\right) vec(\bar{\mathbf{H}})\\ &+ \sqrt{\frac{\eta}{(1+K)}}\left((\mathbf{x}_{u,s}^T - \mathbf{x}_{\hat{u},\hat{s}}^T) \otimes \mathbf{I}_N\right) \boldsymbol{\Psi}^{\frac{1}{2}} vec(\tilde{\mathbf{H}}_w) \qquad (4.31)\end{aligned}$$

mean and covariance matrix are given by

$$\mathbf{m}_z = \sqrt{\frac{K\eta}{(1+K)}}\left((\mathbf{x}_{u,s}^T - \mathbf{x}_{\hat{u},\hat{s}}^T) \otimes \mathbf{I}_N\right) vec(\bar{\mathbf{H}}) \qquad (4.32)$$

$$\begin{aligned}\boldsymbol{\Lambda}_z &= E\left\{\frac{\eta}{(1+K)}\left((\mathbf{x}_{u,s}^T - \mathbf{x}_{\hat{u},\hat{s}}^T) \otimes \mathbf{I}_N\right) \boldsymbol{\Psi}^{\frac{1}{2}} vec(\tilde{\mathbf{H}}_w) vec(\tilde{\mathbf{H}}_w)^H \boldsymbol{\Psi}^{\frac{H}{2}} \left((\mathbf{x}_{u,s} - \mathbf{x}_{\hat{u},\hat{s}})^* \otimes \mathbf{I}_N\right)\right\}\\ &= \eta\frac{\left((\mathbf{x}_{u,s}^T - \mathbf{x}_{\hat{u},\hat{s}}^T) \otimes \mathbf{I}_N\right) \boldsymbol{\Psi} \left((\mathbf{x}_{u,s} - \mathbf{x}_{\hat{u},\hat{s}})^* \otimes \mathbf{I}_N\right)}{(1+K)} \qquad (4.33)\end{aligned}$$

Taking the expectation of Equation 4.29 over proper complex Gaussian distribution results in

$$\bar{P}_s(u,\hat{u},s,\hat{s}) \leqslant \frac{1}{2}\frac{1}{|\mathbf{A}|}\exp\left(-tr\left(\frac{\eta K}{4(1+K)}\left((\mathbf{x}_{u,s}^T - \mathbf{x}_{\hat{u},\hat{s}}^T) \otimes \mathbf{I}_N\right) vec(\bar{\mathbf{H}}) vec(\bar{\mathbf{H}})^H \left((\mathbf{x}_{u,s} - \mathbf{x}_{\hat{u},\hat{s}})^* \otimes \mathbf{I}_N\right)[\mathbf{A}]^{-1}\right)\right) \qquad (4.34)$$

where

$$\mathbf{A} = \mathbf{I} + \eta\frac{\left((\mathbf{x}_{u,s}^T - \mathbf{x}_{\hat{u},\hat{s}}^T) \otimes \mathbf{I}_N\right) \boldsymbol{\Psi} \left((\mathbf{x}_{u,s} - \mathbf{x}_{\hat{u},\hat{s}})^* \otimes \mathbf{I}_N\right)}{4(1+K)} \qquad (4.35)$$

Having APEP, either exact calculation or Chernoff bound, there may be an equilibrium point, γ_e, with respect to polarization coefficient, which results in the same performance for $2M \times 2N$ uni-polarized and $M \times N$ dual-polarized channel, i.e., $\gamma_e : \bar{P}_{b_{DP}}(u,\hat{u},s,\hat{s}) = \bar{P}_{b_{UP}}(u,\hat{u},s,\hat{s})$.

An special case of Equation 4.35 is Rayleigh channel, i.e., $K = 0$, where Equation 4.35 reduces to [42]

$$\begin{aligned} \bar{P}_s\left(u, \hat{u}, s, \hat{s}\right) \leq \frac{1}{2}|\mathbf{A}|^{-1} &= \frac{1}{2}\left|\mathbf{I} + \eta\frac{\boldsymbol{\Upsilon}\left(u, \hat{u}, s, \hat{s}\right)\boldsymbol{\Psi}\boldsymbol{\Upsilon}\left(u, \hat{u}, s, \hat{s}\right)^H}{4}\right|^{-1} \\ &= \frac{1}{2}\left|\mathbf{I} + \eta\frac{\boldsymbol{\Psi}\boldsymbol{\Upsilon}\left(u, \hat{u}, s, \hat{s}\right)^H\boldsymbol{\Upsilon}\left(u, \hat{u}, s, \hat{s}\right)}{4}\right|^{-1} \end{aligned} \tag{4.36}$$

where

$$\boldsymbol{\Upsilon}\left(u, \hat{u}, s, \hat{s}\right) = \left((\mathbf{x}_{u,s}^T - \mathbf{x}_{\hat{u},\hat{s}}^T) \otimes \mathbf{I}_N\right) \tag{4.37}$$

Equation 4.36 can be further written as

$$\bar{P}_s\left(u, \hat{u}, s, \hat{s}\right) \leq \frac{1}{2}\left|\mathbf{I} + \eta\frac{\boldsymbol{\Psi}\left(\boldsymbol{\Upsilon}\left(u, \hat{u}, s, \hat{s}\right)^H\boldsymbol{\Upsilon}\left(u, \hat{u}, s, \hat{s}\right) - \epsilon\mathbf{I}\right)}{4}\right|^{-1} \tag{4.38}$$

when $\epsilon \to 0$. The added extra term makes the second term inside the determinant to be full rank, which is helpful in the following steps.

In high enough SNR Equation 4.38 can be written as

$$\begin{aligned} \bar{P}_s\left(u, \hat{u}, s, \hat{s}\right) &\leq \frac{1}{2}\left|\eta\frac{\boldsymbol{\Psi}\left(\boldsymbol{\Upsilon}\left(u, \hat{u}, s, \hat{s}\right)^H\boldsymbol{\Upsilon}\left(u, \hat{u}, s, \hat{s}\right) - \epsilon\mathbf{I}\right)}{4}\right|^{-1} \\ &= \frac{1}{2\left(\frac{\eta}{4}\right)^{NM}}|\boldsymbol{\Psi}|^{-1}\left|\boldsymbol{\Upsilon}\left(u, \hat{u}, s, \hat{s}\right)^H\boldsymbol{\Upsilon}\left(u, \hat{u}, s, \hat{s}\right) - \epsilon\mathbf{I}\right|^{-1} \end{aligned} \tag{4.39}$$

Considering Equation 4.39 enables us to compare $M \times N$ dual-polarized with $2M \times 2N$ uni-polarized channel. Notice that $\left|\boldsymbol{\Upsilon}\left(u, \hat{u}, s, \hat{s}\right)^H\boldsymbol{\Upsilon}\left(u, \hat{u}, s, \hat{s}\right) - \epsilon\mathbf{I}\right|$ is the same for both cases and thus, they cancel each other out. As a result, APEP depends on $|\boldsymbol{\Psi}|$, which is independent of transmitted symbol and activated antenna and so, it can go out from all the summations of Equation 4.16. Therefore, using Equations 4.8 - (4.11), Equation 4.28 and after some manipulation, we have

$$\begin{aligned} \bar{P}_{b_{DP}} &\lessgtr_{H_{UP}}^{H_{DP}} \bar{P}_{b_{UP}} \\ &\Longrightarrow \quad |\boldsymbol{\Psi}| \gtrless_{H_{UP}}^{H_{DP}} \left|\boldsymbol{\Psi}'\right| \\ &\Longrightarrow \quad \left(1-\gamma_r^2\right)^{NM}\left(1-\gamma_t^2\right)^{NM} \gtrless_{H_{UP}}^{H_{DP}} \frac{\left(1-\alpha_r^2\right)^M\left(1-\alpha_t^2\right)^N}{\left(1-q_r\right)^{2NM}\left(1-q_t\right)^{2NM}} \end{aligned} \tag{4.40}$$

Notice that the equilibrium point achieved by ergodic mutual information, Equation 4.13, and APEP, Equation 4.40, will be exactly the same, when $N = M$.

In order to make the results more visible, assume 2×2 dual-polarized and 4×4 uni-polarized system. following 3-D curves illustrate the performance of two aforementioned scenarios in terms of average bit error probability vs. transmit spatial correlation coefficient and polarization correlation coefficient for fixed receive spatial correlation coefficients of 0 and 0.8. Red surfaces of Figures 4.2 and blue surfaces of Figure 4.3 represent uni-polarized channels and they are independent of γ_r and γ_t, as expected. As can be seen, in all curves, for fixed amount of α_r and α_t, when $\gamma_r = \gamma_t < \gamma_e$, dual-polarized system outperforms and for a fixed $\gamma_r = \gamma_t$, when $\alpha_t > \alpha_e$, dual-polarized scheme offers better bit error performance.

Intersection lines between two surfaces in Figure 4.2 and Figure 4.3 denote equilibrium points. To make the intersection points more clear, Rayleigh curves for a certain parameters are reflected to the 2-D curves as shown in Figure 4.4. Notice that the intersection points achieved by exact performance and Chernoff bound are the same.

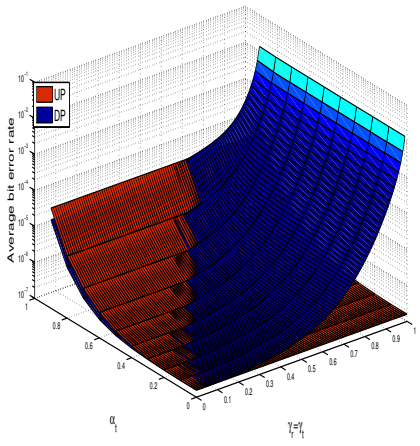

(a) $K = 0$, $\alpha_r = 0$.

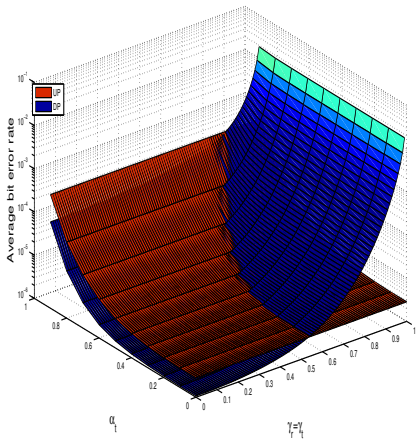

(b) $K = 0$, $\alpha_r = 0.8$.

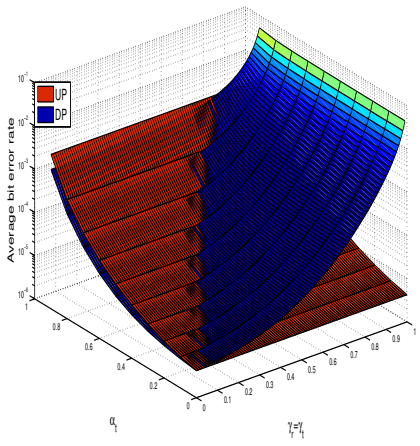

(c) $K = 3$, $\alpha_r = 0$.

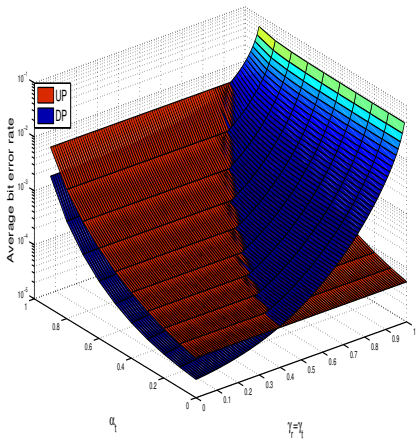

(d) $K = 3$, $\alpha_r = 0.8$.

Figure 4.2: Exact performance for 4×4 uni-polar and 2×2 dual-polarized channel in fixed $SNR = 20$ dB, $q_r = q_t = 0$, using QPSK.

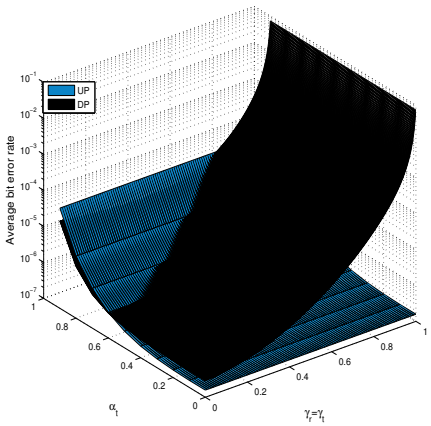

(a) $K = 0$, $\alpha_r = 0$.

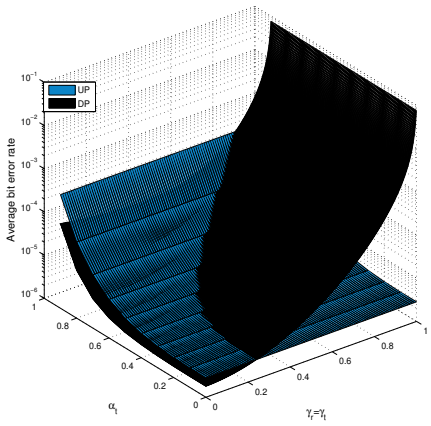

(b) $K = 0$, $\alpha_r = 0.8$.

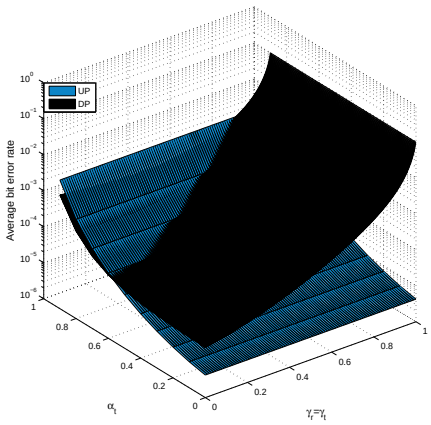

(c) $K = 3$, $\alpha_r = 0$.

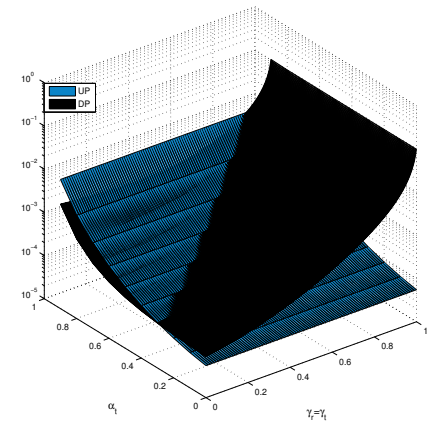

(d) $K = 3$, $\alpha_r = 0.8$.

Figure 4.3: Exact performance for 4×4 uni-polar and 2×2 dual-polarized channel in fixed $SNR = 20$ dB, $q_r = q_t = 0.1$, using QPSK.

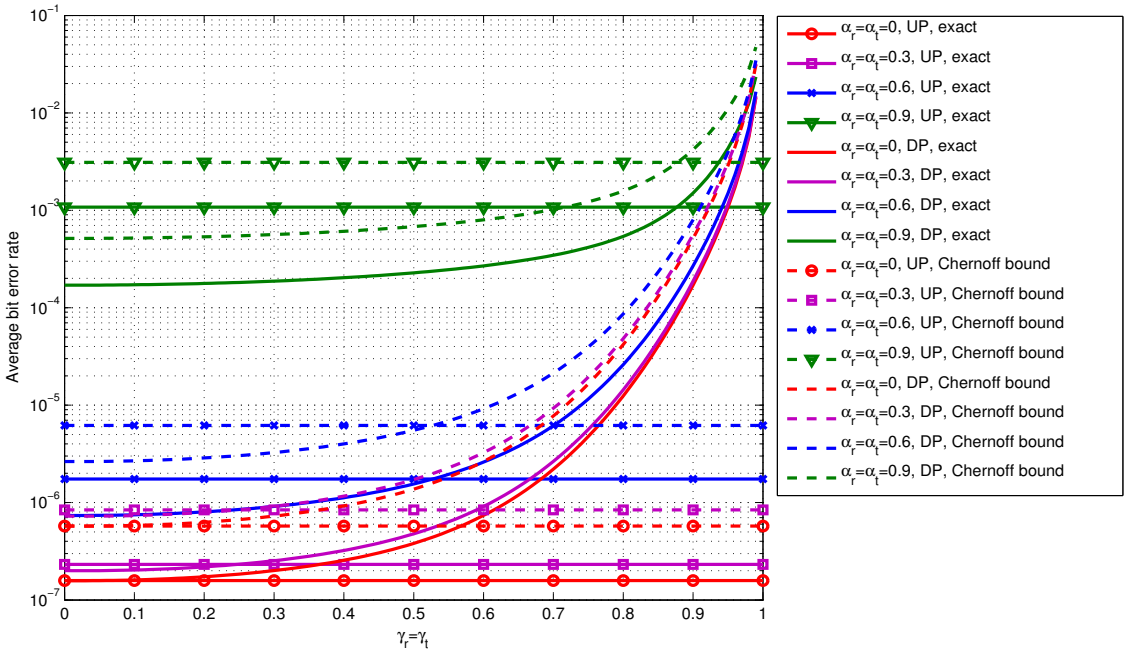

(a) $q_r = q_t = 0$.

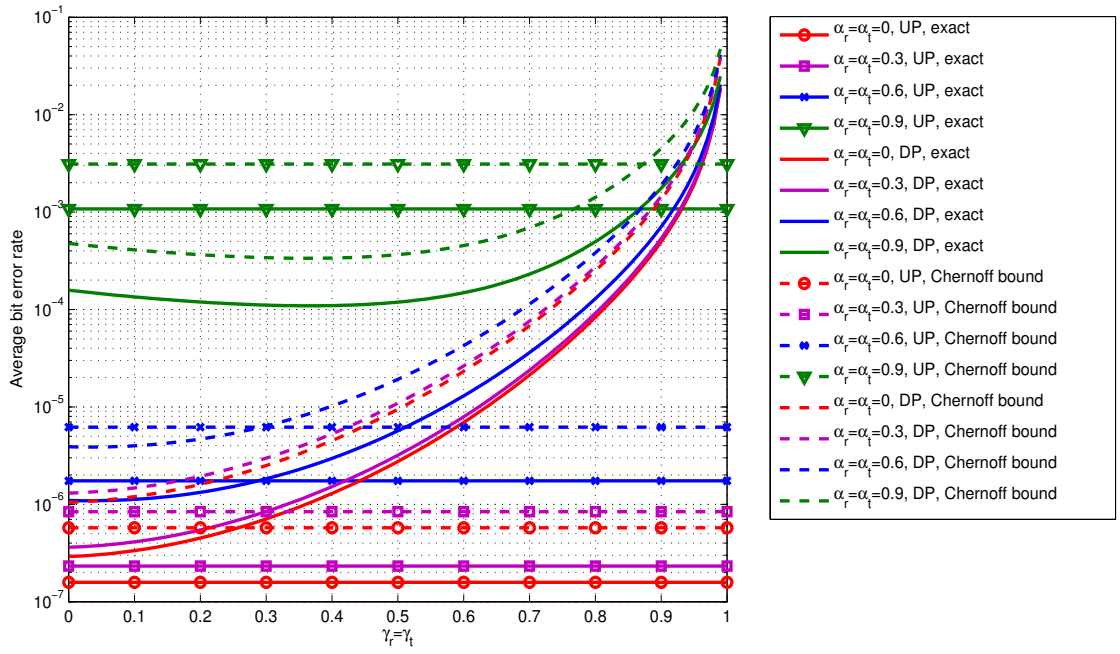

(b) $q_r = q_t = 0.1$.

Figure 4.4: Equilibrium points using exact error performance and Chernoff bound for 4×4 uni-polar and 2×2 dual-polarized Rayleigh channel in fixed $SNR = 20$ dB.

Comparing the equilibrium points of Figure 4.4 and Figure 4.1 there are some gaps between them. These gaps between results of error performance and ergodic mutual information stems from dropping of $\mathbf{I}$ in mutual information in high SNR. In other words, $SNR = 20$ dB is not high enough such that the effect of $\mathbf{I}$ in Equation 4.3 and Equation 4.38 can be ignored.

Table 4.2 and Table 4.3 compare the 2×2 dual-polarized and 4×4 uni-polarized system, transmitting QPSK, i.e., $R = 4$. The aforementioned Tables provide γ_es for Rayleigh and Rician channel, respectively, for different values of α_r and α_t. SNR is assumed to be fixed, i.e., $SNR = 30$ dB, and $q_r = 0$ and $q_t = 0$, i.e., orthogonally polarized antennas are completely isolated. In a system, where γ is less than γ_e, it is worthy to use dual-polarized antennas and alternatively, if γ is greater than γ_e, uni-polarized antenna outperforms.

As can be seen from Table 4.2 and Table 4.3, transmit and receive spatial correlation coefficients do not impact the equilibrium points with the same weight. In other words, the thresholds in Rician channels are more sensitive to transmit spatial correlation coefficients rather than receive spatial correlation coefficient. Furthermore, the results obtained from exact performance and Chernoff bound are closely match to each other.

Table 4.4 and Table 4.5 are provided to evaluate the impact of XPI on the equilibrium points. To address this problem, all of the parameters of channel are remained the same as those of Table 4.2 and Table 4.3 and the only changes are in the values of q_r and q_t, i.e., $q_r = q_t = 0.1$. Notice that for the values of α_r and α_t corresponding to those cells of Tables, in which no value is provided, uni-polarized antenna outperforms for all values of γs.

Table 4.6 and Table 4.8 show the results for different Rician factors. $SNR = 30$ dB and different values of α_ts in perfect channel estimation for $\alpha_r = 0$, $\alpha_r = 0.5$, and $\alpha_r = 0.8$, respectively. XPI is assumed to be infinite. It has been shown that variation of equilibrium points is limited and it is more influenced by correlation coefficients rather than Rician factor.

Table 4.2: Performance equilibrium points for Rayleigh channel. First and second values are obtained from exact performance and Chernoff bound, respectively, $SNR = 30$ dB, $q_r = q_t = 0$.

α_r, α_t	0	0.1	0.2	0.3	0.4	0.5	0.6	0.7	0.8	0.9
0	0.0335	0.0337	0.0381	0.0521	0.296	0.352	0.409	0.465	0.502	0.505
	0.0335	0.0337	0.0385	0.0542	0.292	0.35	0.409	0.467	0.504	0.508
0.1	0.0361	0.0363	0.0409	0.18	0.301	0.355	0.412	0.468	0.505	0.508
	0.0363	0.0365	0.0416	0.18	0.297	0.353	0.412	0.469	0.507	0.511
0.2	0.045	0.0452	0.0513	0.269	0.314	0.364	0.419	0.476	0.514	0.517
	0.0461	0.0464	0.0533	0.263	0.311	0.362	0.419	0.477	0.517	0.52
0.3	0.261	0.264	0.277	0.3	0.334	0.378	0.432	0.489	0.53	0.533
	0.255	0.257	0.272	0.297	0.332	0.377	0.432	0.491	0.533	0.537
0.4	0.309	0.31	0.317	0.332	0.359	0.398	0.45	0.509	0.556	0.561
	0.305	0.307	0.314	0.33	0.357	0.398	0.451	0.511	0.559	0.566
0.5	0.349	0.35	0.355	0.366	0.389	0.425	0.475	0.536	0.593	0.617
	0.347	0.348	0.353	0.365	0.388	0.425	0.476	0.538	0.597	0.624
0.6	0.391	0.392	0.396	0.405	0.425	0.458	0.508	0.571	0.642	0.71
	0.391	0.391	0.395	0.405	0.425	0.459	0.509	0.573	0.643	0.71
0.7	0.44	0.441	0.444	0.452	0.47	0.501	0.55	0.616	0.691	0.763
	0.441	0.441	0.444	0.453	0.471	0.502	0.552	0.617	0.691	0.763
0.8	0.503	0.503	0.506	0.514	0.53	0.559	0.606	0.669	0.738	0.805
	0.504	0.504	0.507	0.515	0.531	0.561	0.607	0.669	0.738	0.805
0.9	0.596	0.596	0.598	0.605	0.619	0.644	0.684	0.735	0.793	0.852
	0.598	0.597	0.6	0.606	0.62	0.645	0.684	0.735	0.793	0.853

Table 4.3: Performance equilibrium points for Rician channel, $K = 3$. First and second values are obtained from exact performance and Chernoff bound, respectively, $SNR = 30$ dB, $q_r = q_t = 0$.

α_r, α_t	0	0.1	0.2	0.3	0.4	0.5	0.6	0.7	0.8	0.9
0	0.0232	0.0585	0.147	0.249	0.32	0.382	0.441	0.497	0.538	0.555
	0.0224	0.0606	0.149	0.247	0.319	0.382	0.442	0.499	0.543	0.565
0.1	0.0257	0.0624	0.154	0.252	0.323	0.385	0.443	0.499	0.541	0.559
	0.025	0.0649	0.156	0.25	0.321	0.384	0.444	0.502	0.546	0.569
0.2	0.0338	0.076	0.174	0.263	0.33	0.391	0.45	0.507	0.551	0.573
	0.0339	0.0793	0.174	0.261	0.329	0.391	0.451	0.509	0.555	0.583
0.3	0.0508	0.106	0.203	0.28	0.343	0.403	0.462	0.52	0.568	0.597
	0.0523	0.11	0.202	0.278	0.342	0.403	0.463	0.522	0.572	0.609
0.4	0.0866	0.159	0.237	0.302	0.361	0.419	0.478	0.538	0.592	0.639
	0.0903	0.16	0.235	0.3	0.36	0.419	0.479	0.54	0.595	0.65
0.5	0.16	0.217	0.274	0.329	0.384	0.44	0.5	0.562	0.622	0.693
	0.161	0.216	0.272	0.328	0.383	0.441	0.501	0.564	0.625	0.699
0.6	0.234	0.271	0.314	0.362	0.413	0.468	0.527	0.591	0.659	0.741
	0.233	0.269	0.313	0.361	0.413	0.469	0.529	0.593	0.66	0.745
0.7	0.3	0.326	0.361	0.403	0.45	0.504	0.563	0.628	0.699	0.782
	0.298	0.325	0.36	0.403	0.451	0.505	0.564	0.629	0.7	0.785
0.8	0.37	0.391	0.42	0.457	0.501	0.553	0.611	0.675	0.745	0.822
	0.37	0.391	0.42	0.458	0.502	0.554	0.612	0.676	0.746	0.824
0.9	0.468	0.486	0.511	0.544	0.584	0.632	0.686	0.743	0.803	0.867
	0.47	0.488	0.513	0.546	0.586	0.634	0.687	0.744	0.804	0.869

Table 4.4: Performance equilibrium points for Rayleigh channel. First and second values are obtained from exact performance and Chernoff bound, respectively, $SNR = 30$ dB, $q_r = q_t = 0.1$.

α_r, α_t	0	0.1	0.2	0.3	0.4	0.5	0.6	0.7	0.8	0.9
0	-	-	-	-	-	-	0.0416	0.321	0.485	0.685
	-	-	-	-	-	-	0.0424	0.32	0.486	0.685
0.1	-	-	-	-	-	-	0.0459	0.323	0.487	0.686
	-	-	-	-	-	-	0.0471	0.323	0.488	0.686
0.2	-	-	-	-	-	-	0.0614	0.329	0.491	0.689
	-	-	-	-	-	-	0.0639	0.329	0.492	0.69
0.3	-	-	-	-	-	-	0.1	0.34	0.498	0.694
	-	-	-	-	-	-	0.105	0.34	0.499	0.695
0.4	-	-	-	-	-	0.00153	0.166	0.355	0.509	0.702
	-	-	-	-	-	-	0.167	0.355	0.51	0.703
0.5	-	-	-	-	-	0.0278	0.22	0.374	0.523	0.713
	-	-	-	-	-	0.0277	0.219	0.374	0.525	0.714
0.6	-	-	-	-	0.0156	0.0898	0.266	0.398	0.543	0.728
	-	-	-	-	0.015	0.0927	0.266	0.399	0.544	0.729
0.7	0.0249	0.0247	0.0294	0.0439	0.0881	0.202	0.315	0.43	0.569	0.747
	0.0249	0.0247	0.0297	0.0449	0.0908	0.202	0.315	0.43	0.57	0.748
0.8	0.151	0.15	0.16	0.184	0.228	0.291	0.372	0.474	0.607	0.774
	0.153	0.153	0.162	0.186	0.229	0.291	0.372	0.475	0.609	0.776
0.9	0.315	0.315	0.319	0.331	0.354	0.395	0.458	0.55	0.675	0.818
	0.316	0.316	0.32	0.332	0.356	0.396	0.46	0.553	0.678	0.82

Table 4.5: Performance equilibrium points for Rician channel, $K = 3$. First and second values are obtained from exact performance and Chernoff bound, respectively, $SNR = 30$ dB, $q_r = q_t = 0.1$.

α_r, α_t	0	0.1	0.2	0.3	0.4	0.5	0.6	0.7	0.8	0.9
0	-	-	-	-	-	-	0.0426	0.322	0.496	0.709
	-	-	-	-	-	-	0.0434	0.323	0.498	0.713
0.1	-	-	-	-	-	-	0.0462	0.324	0.497	0.71
	-	-	-	-	-	-	0.0472	0.325	0.499	0.714
0.2	-	-	-	-	-	-	0.0585	0.33	0.502	0.714
	-	-	-	-	-	-	0.0598	0.331	0.504	0.718
0.3	-	-	-	-	-	-	0.0841	0.341	0.51	0.72
	-	-	-	-	-	-	0.0861	0.342	0.512	0.724
0.4	-	-	-	-	-	-	0.13	0.356	0.521	0.729
	-	-	-	-	-	-	0.132	0.357	0.523	0.733
0.5	-	-	-	-	-	-	0.186	0.376	0.537	0.741
	-	-	-	-	-	-	0.188	0.377	0.539	0.745
0.6	-	-	-	-	-	0.0291	0.24	0.402	0.559	0.757
	-	-	-	-	-	0.0295	0.241	0.404	0.561	0.761
0.7	-	-	-	-	-	0.102	0.295	0.437	0.589	0.778
	-	-	-	-	-	0.105	0.296	0.439	0.592	0.782
0.8	-	-	-	-	0.0615	0.225	0.361	0.488	0.635	0.806
	-	-	-	-	0.0641	0.228	0.363	0.491	0.639	0.81
0.9	-	0.00879	0.0592	0.155	0.266	0.366	0.468	0.581	0.712	0.847
	-	0.0104	0.0644	0.161	0.27	0.37	0.473	0.587	0.717	0.851

Table 4.6: Effect of different Rician factors on equilibrium points, $q_r = q_t = 0$, $\alpha_r = 0$, $SNR = 30$ dB.

α_t , K	0	3	5	10	100
0.1	0.0337	0.0585	0.0616	0.0649	0.0739
0.3	0.0521	0.249	0.246	0.244	0.244
0.5	0.352	0.382	0.383	0.384	0.397
0.7	0.465	0.497	0.502	0.51	0.57
0.9	0.505	0.555	0.587	0.663	0.834

Table 4.7: Effect of different Rician factors on equilibrium points, $q_r = q_t = 0$, $\alpha_r = 0.5$, $SNR = 30$ dB.

α_t , K	0	3	5	10	100
0.1	0.35	0.217	0.213	0.211	0.204
0.3	0.366	0.329	0.327	0.326	0.321
0.5	0.425	0.44	0.442	0.443	0.449
0.7	0.536	0.562	0.565	0.571	0.608
0.9	0.617	0.693	0.717	0.753	0.842

Table 4.8: Effect of different Rician factors on equilibrium points, $q_r = q_t = 0$, $\alpha_r = 0.8$, $SNR = 30$ dB.

α_t , K	0	3	5	10	100
0.1	0.503	0.391	0.384	0.385	0.405
0.3	0.514	0.457	0.455	0.458	0.473
0.5	0.559	0.553	0.555	0.559	0.568
0.7	0.669	0.675	0.678	0.683	0.693
0.9	0.805	0.822	0.829	0.839	0.864

To evaluate the impact K factor in presence of finite XPI, Figure 4.9 and Figure 4.10 are presented as below

Table 4.9: Effect of different Rician factors on equilibrium points, $q_r = q_t = 0.1$, $\alpha_r = 0.5$, $SNR = 30$ dB.

α_t , K	0	3	5	10	100
0.1	-	-	-	-	-
0.3	-	-	-	-	-
0.5	0.0278	-	-	-	0.0525
0.7	0.374	0.376	0.382	0.395	0.539
0.9	0.713	0.741	0.756	0.784	0.894

Table 4.10: Effect of different Rician factors on equilibrium points, $q_r = q_t = 0.1$, $\alpha_r = 0.8$, $SNR = 30$ dB.

α_t , K	0	3	5	10	100
0.1	0.15	-	-	-	-
0.3	0.184	-	-	-	0.0727
0.5	0.291	0.225	0.233	0.253	0.391
0.7	0.474	0.488	0.498	0.52	0.656
0.9	0.774	0.806	0.818	0.837	0.911

4.3.3. Simulation Results

In this section, we provide the results of simulation and theoretical analysis for spatial modulation over dual-polarized MIMO channel. XPI for both transmit and receive antennas are such that $q_r = q_t = 0.1$, without loss of generality.

To justify the theoretical derivations, assume the case where $\alpha_t = 0.1$ and $\alpha_r = 0.9$. The equilibrium point obtained by Equation 4.40 is 0.4324 and the point achieved from exact

performance analysis and Chernoff bound are 0.43 and 0.444, respectively in $SNR = 20$ dB. Notice that as α_t increases, the effect of dropped $\mathbf{I}$ in Equation 4.39, becomes more and more significant and the gap between theoretical results and exact performance becomes larger.

In Figures 4.5- 4.8, we consider $\alpha_t = \alpha_r = 0.8$ for correlated channels. We have simulated the average bit error rate for $\gamma_t = \gamma_r = \gamma = 0.2, 0.5$ and 0.8. The results are compared with uni-polarized system with the same number of antennas as well as the situation, where the number of antennas is doubled. Rician factor is 3, i.e., K=3. The fixed channel matrix $\overline{\mathbf{H}}$ is set to be an all one matrix as in [40] but other fixed matrix choices are also valid. In other words, Figures 4.5- 4.8 includes:

(i) 4×4 uni-polarized MIMO system employing QPSK($R = 2 + 2 = 4$);

(ii) 2×2 uni-polarized MIMO system employing 8-PSK($R = 1 + 3 = 4$);

(iii) 2×2 dual-polarized MIMO system employing QPSK for different XPD factors ($R = 1 + 2 + 1 = 4$).

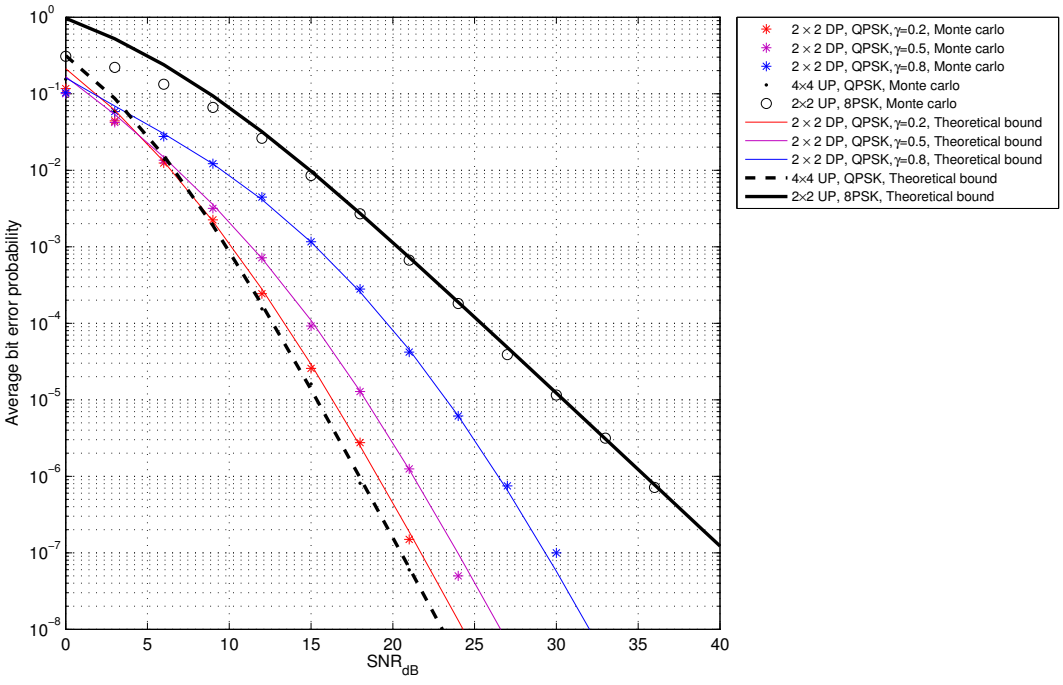

Figure 4.5: Uncorrelated Rayleigh channel, $R = 4$.

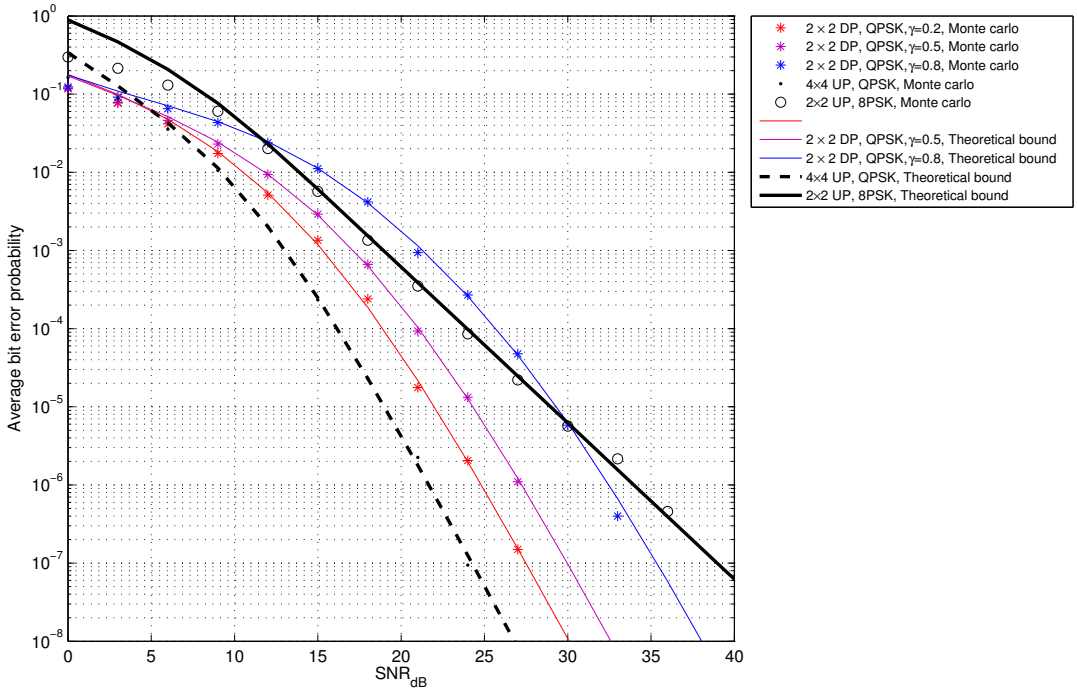

Figure 4.6: Uncorrelated Rician channel, $R = 4$.

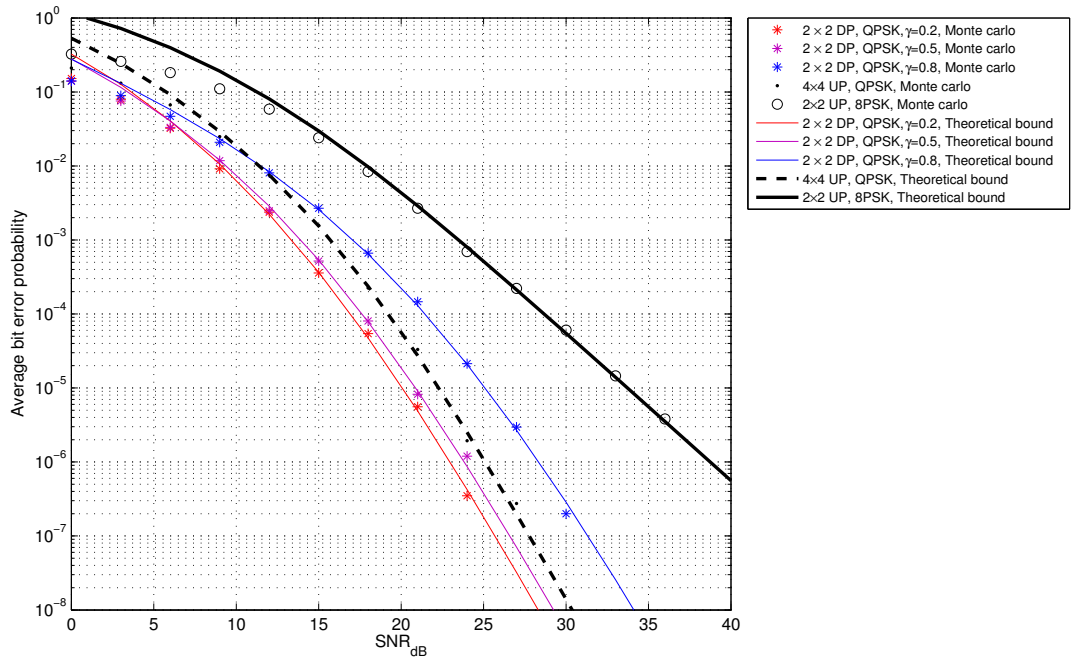

Figure 4.7: Correlated Rayleigh channel, $R = 4$.

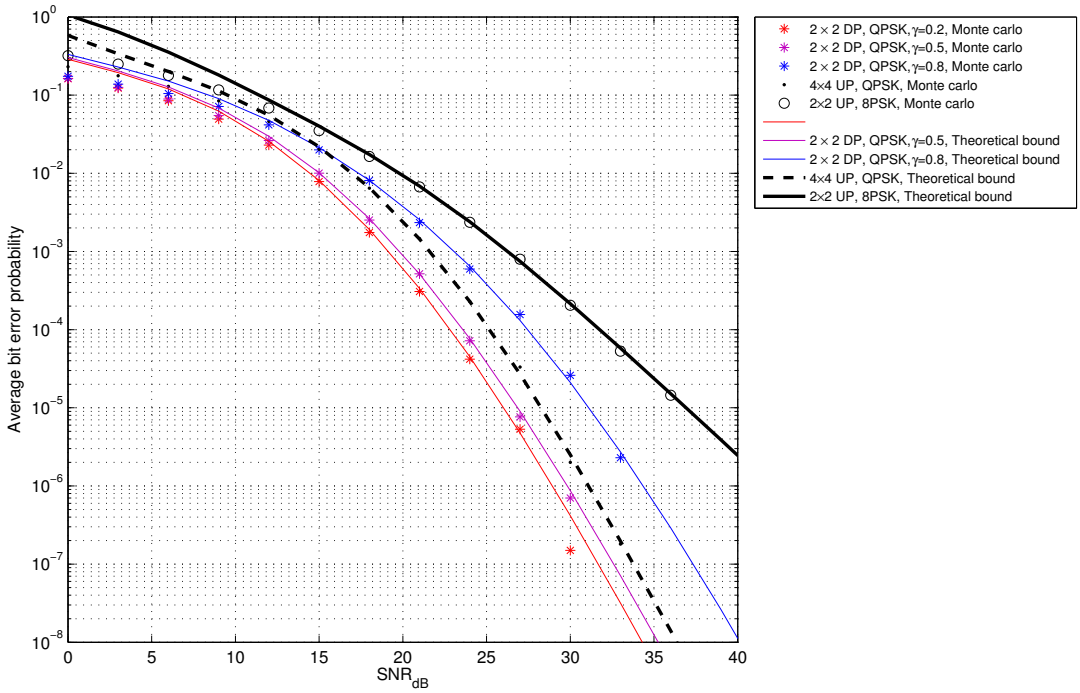

Figure 4.8: Correlated Rician channel, $R = 4$.

As can be seen, in all curves, theoretical results are closely matched to the simulation results. Moreover, in all uncorrelated fading channels, performance of 2×2 dual-polarized system is worse than 4×4 uni-polarized MIMO channel which can be easily justified using Table 4.4 and Table 4.5. Moreover, all of the dual-polarized channels achieved the diversity of double order, which in turn represents that in high enough SNR, they will outperform the uni-polarized channel with the same number of antennas, regardless of channel realization. In correlated fading channel, however, existence of XPD deteriorates transmit and receive correlation matrices, $\mathbf{\Psi_t}$ and $\mathbf{\Psi_r}$. As a result, performance of 2×2 dual-polarized system in low polarization correlation coefficient, γ, is even better than 4×4 uni-polarized MIMO system. According to previous works, γ is practically very small and close to zero [43].

5. DUAL-POLARIZED SPATIAL MODULATION IN CHANNEL ESTIMATION ERROR

5.1. Average Error Analysis in Presence of Channel Estimation Error

The results of the previous section can be extended to the case where there is channel estimation error. In this section, we have considered the PEP and extended the results for the case of L-QAM and L-PSK to find APEP. Having APEP, ABEP can be approximated using Equation 4.16.

Note that in practice, receiver cannot estimate channel perfectly and there is channel estimation error. In other words, receiver estimates channel as $\mathbf{G}$ [40] instead of $\mathbf{H}$

$$\mathbf{G}=\sqrt{\frac{K}{K+1}}\bar{\mathbf{H}}+\sqrt{\frac{1}{K+1}}\left(\mathbf{\Psi}_r^{\frac{1}{2}}\tilde{\mathbf{H}}_w\mathbf{\Psi}_t^{\frac{1}{2}T}+\mathbf{\Xi}_r^{\frac{1}{2}}\mathbf{\Delta}\mathbf{\Xi}_t^{\frac{1}{2}T}\right) \tag{5.1}$$

where $\mathbf{\Xi}_r$ and $\mathbf{\Xi}_t$ are $2N\times 2N$ and $2M\times 2M$ matrices, respectively, representing receive and transmit error correlation matrices due to the imperfect estimation of space correlation matrices or estimation error in polarization correlation or both. $\mathbf{\Delta}$ is a $2N\times 2M$ error matrix and its elements, $\delta_{i,j}$, are i.i.d zero mean complex Gaussian with variance σ_e^2, i.e., $\delta_{i,j}\sim\mathcal{C}N(0,\sigma_e^2)$.

Considering this model for imperfect channel estimation, mean and covariance matrix of received signal conditioned on erroneous channel and transmitted symbol can be calculated as in [40]

$$\begin{aligned}\mathbf{m}_{u,s} &= \mathrm{E}\left[\mathbf{y}\mid\mathbf{g}_u,X_s\right]\\ &= \sqrt{\frac{K}{(K+1)}}\left(\mathbf{I}-\mathbf{\Gamma}_r\right)\bar{\mathbf{h}}_uX_s+\mathbf{\Gamma}_r\mathbf{g}_uX_s \end{aligned}\tag{5.2}$$

$$\begin{aligned}\mathbf{\Lambda}_{u,s} &= \mathrm{E}\left[(\mathbf{y}-\mathbf{m}_{u,s})(\mathbf{y}-\mathbf{m}_{u,s})^H\mid\mathbf{g}_u,X_s\right]\\ &= \frac{1}{\eta}\mathbf{I}+\frac{\Psi_{u,u}^t|X_s|^2}{K+1}\mathbf{\Psi}_r\left(\mathbf{I}-\mathbf{\Gamma}_r\right)\end{aligned}\tag{5.3}$$

where

$$\mathbf{\Gamma}_r=\left(\mathbf{I}+\sigma_e^2\mathbf{\Psi}_r^{-1}\mathbf{\Xi}_r\right)^{-1} \tag{5.4}$$

$\mathbf{h}_u$, $\bar{\mathbf{h}}_u$ and $\mathbf{g}_u$ are the uth columns of $\mathbf{H}$, $\overline{\mathbf{H}}$ and $\mathbf{G}$, respectively, for $u = 1, \ldots, 2N$.

In the case where $\mathbf{\Xi}_r = \mathbf{\Psi}_r$, $\mathbf{\Gamma}_r$ becomes $\mathbf{\Gamma}_r = \frac{1}{1+\sigma_e^2}\mathbf{I}$, as a result, mean and covariance matrices reduces to

$$\mathbf{m}_{u,s} = \sqrt{\frac{K}{(K+1)}}(1-\rho^2)\bar{\mathbf{h}}_u X_s + \rho^2 \mathbf{g}_u X_s \tag{5.5}$$

$$\mathbf{\Lambda}_{u,s} = \frac{1}{\eta}\mathbf{I} + \frac{(1-\rho^2)\Psi^t_{u,u}|X_s|^2}{K+1}\mathbf{\Psi}_r \tag{5.6}$$

where $\rho = 1/\sqrt{1+\sigma_e^2}$.

Using ML detection, the receiver has an erroneous decision if the probability of having $(\hat{u}, \hat{s})$ is more than (u, s) and thus distance metric $D(u, s)$ and PEP are defined as

$$D(u,s) = (\mathbf{y} - \mathbf{m}_{u,s})^H \mathbf{\Lambda}_{u,s}^{-1} (\mathbf{y} - \mathbf{m}_{u,s}) + \log|\mathbf{\Lambda}_{u,s}| \tag{5.7}$$

$$\begin{aligned} P_s(u,\hat{u},s,\hat{s}) &= Pr.\Big\{ (\mathbf{y} - \mathbf{m}_{u,s})^H \mathbf{\Lambda}_{u,s}^{-1} (\mathbf{y} - \mathbf{m}_{u,s}) + \log|\mathbf{\Lambda}_{u,s}| \\ &> (\mathbf{y} - \mathbf{m}_{\hat{u},\hat{s}})^H \mathbf{\Lambda}_{\hat{u},\hat{s}}^{-1} (\mathbf{y} - \mathbf{m}_{\hat{u},\hat{s}}) + \log|\mathbf{\Lambda}_{\hat{u},\hat{s}}| \Big\} \end{aligned} \tag{5.8}$$

5.1.1. PEP for L-QAM

As long as in L-QAM, different amounts of energies are assigned to different symbols, conditional covariance matrix, $\mathbf{\Lambda}_{u,s}$, as defined in Equation 5.3 is not identical for all symbols. Nevertheless, there are reasons as mentioned in [40], which enable us to assume them as if they are the same. As a result, we can suppose that $|X_s| = |X_{\hat{s}}|$ and consequently $\mathbf{\Lambda}_{u,s} = \mathbf{\Lambda}_{\hat{u},\hat{s}}$. This approximation simplifies the PEP in Equation 5.8 as

$$\begin{aligned} P_s(u,\hat{u},s,\hat{s}) &\approx Pr.\Big\{ (\mathbf{y} - \mathbf{m}_{u,s})^H \mathbf{\Lambda}_{u,s}^{-1} (\mathbf{y} - \mathbf{m}_{u,s}) \\ &> (\mathbf{y} - \mathbf{m}_{\hat{u},\hat{s}})^H \mathbf{\Lambda}_{u,s}^{-1} (\mathbf{y} - \mathbf{m}_{\hat{u},\hat{s}}) \Big\} \end{aligned} \tag{5.9}$$

Furthermore, $P_s(u, \hat{u}, s, \hat{s})$ can be calculated using Equation 4.17, where $\mathbf{z}$ is the $2N \times 1$ vector defined as [7]

$$\mathbf{z} = \mathbf{\Lambda}_{u,s}^{-\frac{1}{2}} (\mathbf{m}_{u,s} - \mathbf{m}_{\hat{u},\hat{s}}) \tag{5.10}$$

Mean and covariance matrix can be calculated using

$$\mathbf{m_z} = \sqrt{\frac{K}{1+K}}\mathbf{\Lambda}_{u,s}^{-\frac{1}{2}}\left(\left(\mathbf{x}_{u,s}^T - \mathbf{x}_{\hat{u},\hat{s}}^T\right)\otimes\mathbf{I}\right)vec\left(\bar{\mathbf{H}}\right) \tag{5.11}$$

and

$$\begin{aligned}\mathbf{\Lambda_z} &= \mathrm{E}\left[(\mathbf{z}-\mathbf{m_z})(\mathbf{z}-\mathbf{m_z})^H\right] \\ &= \left[\mathbf{\Lambda}_{u,s}^{-\frac{1}{2}}\mathbf{\Gamma}_r\right]\left(\mathbf{\Theta}_1+\mathbf{\Theta}_2\right)\left[\mathbf{\Lambda}_{u,s}^{-\frac{1}{2}}\mathbf{\Gamma}_r\right]^H\end{aligned} \tag{5.12}$$

where $\mathbf{\Theta}_1$ and $\mathbf{\Theta}_2$ in Equation 5.12 are given as

$$\begin{aligned}\mathbf{\Theta}_1 &= \frac{\left(\mathbf{x}_{u,s}^T-\mathbf{x}_{\hat{u},\hat{s}}^T\right)\mathbf{\Psi}_t^T\left(\mathbf{x}_{u,s}^T-\mathbf{x}_{\hat{u},\hat{s}}^T\right)^H}{K+1}\mathbf{\Psi}_r = \frac{\left(\left(\mathbf{x}_{u,s}^T-\mathbf{x}_{\hat{u},\hat{s}}^T\right)\otimes\mathbf{I}\right)\mathbf{\Psi}\left(\left(\mathbf{x}_{u,s}^T-\mathbf{x}_{\hat{u},\hat{s}}^T\right)\otimes\mathbf{I}\right)^H}{K+1} \\ \mathbf{\Theta}_2 &= \frac{\sigma_e^2\left[\left(\mathbf{x}_{u,s}^T-\mathbf{x}_{\hat{u},\hat{s}}^T\right)\mathbf{\Xi}_t^T\left(\mathbf{x}_{u,s}^T-\mathbf{x}_{\hat{u},\hat{s}}^T\right)^H\right]}{K+1}\mathbf{\Xi}_r = \frac{\sigma_e^2\left[\left(\left(\mathbf{x}_{u,s}^T-\mathbf{x}_{\hat{u},\hat{s}}^T\right)\otimes\mathbf{I}\right)\mathbf{\Xi}\left(\left(\mathbf{x}_{u,s}^T-\mathbf{x}_{\hat{u},\hat{s}}^T\right)\otimes\mathbf{I}\right)^H\right]}{K+1}\end{aligned} \tag{5.13}$$

where

$$\mathbf{\Psi} = \mathbf{\Psi}_t^T \otimes \mathbf{\Psi}_r \tag{5.14}$$

and

$$\mathbf{\Xi} = \mathbf{\Xi}_t^T \otimes \mathbf{\Xi}_r \tag{5.15}$$

5.1.2. PEP for L-PSK

In L-PSK, however, $|X_s| = |X_{\hat{s}}| = 1$ and $\mathbf{\Lambda}_{u,s} = \mathbf{\Lambda}_{\hat{u},\hat{s}}$ for all symbols and thus, there is no need for any approximation. Hence, $\mathbf{\Lambda}_{u,v}$ as defined in Equation 5.3 simplifies to

$$\mathbf{\Lambda}_{u,s} = \mathbf{\Lambda} = \frac{1}{\eta}\mathbf{I} + \frac{\psi_{u,u}^t}{K+1}\mathbf{\Psi}_r\left(\mathbf{I}-\mathbf{\Gamma}_r\right) \tag{5.16}$$

It can be easily seen that distance metric and PEP also changes as below

$$D_{\text{ PSK}}(u,s) = \left(\mathbf{y}-\mathbf{m}_{u,s}\right)^H\mathbf{\Lambda}^{-1}\left(\mathbf{y}-\mathbf{m}_{u,s}\right) \tag{5.17}$$

$$\begin{aligned}P_s(u,\hat{u},s,\hat{s}) &= Pr.\Big\{\left(\mathbf{y}-\mathbf{m}_{u,s}\right)^H\mathbf{\Lambda}^{-1}\left(\mathbf{y}-\mathbf{m}_{u,s}\right) \\ &> \left(\mathbf{y}-\mathbf{m}_{\hat{u},\hat{s}}\right)^H\mathbf{\Lambda}^{-1}\left(\mathbf{y}-\mathbf{m}_{\hat{u},\hat{s}}\right)\Big\}\end{aligned} \tag{5.18}$$

Consequently, $\mathbf{z}$ in PEP expression, Equation 4.17, is as

$$\mathbf{z} = \mathbf{\Lambda}^{-\frac{1}{2}}\left(\mathbf{m}_{u,s}-\mathbf{m}_{\hat{u},\hat{s}}\right) \tag{5.19}$$

Taking these changes into consideration, mean and covariance of vector $\mathbf{z}$ remains the same as Equation 5.11 and Equation 5.12 except the point that in L-PSK $\mathbf{\Lambda}_{u,s} = \mathbf{\Lambda}_{\hat{u},\hat{s}} = \mathbf{\Lambda}$.

5.1.3. Exact ABEP and Chernoff Bound

While exact APEP can be derived using Equation 4.22, Chernoff bound can be achieved setting $\sin^2\theta$ as 1 in Equation 4.22, where Equation 4.22 reduces to

$$\bar{P}_s(u,\hat{u},s,\hat{s}) < \frac{1}{2}\frac{\exp\left(-\frac{1}{4}\mathbf{m}_{\mathbf{z}}^H[\frac{\mathbf{\Lambda}_{\mathbf{z}}}{4}+\mathbf{I}]^{-1}\mathbf{m}_{\mathbf{z}}\right)}{\left|\frac{\mathbf{\Lambda}_{\mathbf{z}}}{4}+\mathbf{I}\right|} \tag{5.20}$$

Considering the Chernoff bound, an special case is Rayleigh channel, i.e., $K = 0$, where Equation 5.20 becomes [42]

$$\bar{P}_s\left(u,\hat{u},s,\hat{s}\right) \leq \frac{1}{2}\left|\frac{\mathbf{\Lambda}_z}{4}+\mathbf{I}\right|^{-1} \tag{5.21}$$

Assuming high SNR, i.e., $SNR >> 1$, and if eigenvalues of $\mathbf{\Lambda}_{u,s}^{-1}$ are greater than 1, Equation 5.21 reduces to

$$\bar{P}_s\left(u,\hat{u},s,\hat{s}\right) \leq \frac{1}{2}\left|\frac{\mathbf{\Lambda}_z}{4}\right|^{-1} \tag{5.22}$$

Also if, $\mathbf{\Psi}_r = \mathbf{\Xi}_r$ and $\mathbf{\Psi}_t = \mathbf{\Xi}_t$, then $\mathbf{\Theta}_1 + \mathbf{\Theta}_2 = \left(1+\sigma_e^2\right)\mathbf{\Theta}_1 = \left(1+\sigma_e^2\right)\left(\mathbf{\Theta}_1 - \epsilon\mathbf{I}\right)$, when $\epsilon \to 0$. Therefore,

$$\bar{P}_s\left(u,\hat{u},s,\hat{s}\right) \leq \frac{1}{2}\left(\frac{1}{4}\right)^{-2N}\left|\mathbf{\Lambda}_{u,s}^{-\frac{1}{2}}\mathbf{\Gamma}_r\right|^{-1}\left|\left(1+\sigma_e^2\right)\left(\mathbf{\Theta}_1-\epsilon\mathbf{I}\right)\right|^{-1}\left|\left(\mathbf{\Lambda}_{u,s}^{-\frac{1}{2}}\mathbf{\Gamma}_r\right)^H\right|^{-1} \tag{5.23}$$

$$= \frac{1}{2}\left(\frac{1}{4}\right)^{-2N}\left|\mathbf{\Lambda}_{u,s}^{-1}\mathbf{\Gamma}_r^2\right|^{-1}\left|\left(1+\sigma_e^2\right)\left(\mathbf{\Theta}_1-\epsilon\mathbf{I}\right)\right|^{-1} \tag{5.24}$$

$$= \frac{1}{2}\left(\frac{1}{4}\right)^{-2N}\left|\mathbf{\Lambda}_{u,s}\right|\left|\mathbf{\Gamma}_r^2\right|^{-1}\left|\left(1+\sigma_e^2\right)\left(\mathbf{\Theta}_1-\epsilon\mathbf{I}\right)\right|^{-1} \tag{5.25}$$

$$= \frac{1}{2}\left(\frac{1}{4}\right)^{-2N}\left(\frac{1}{\eta}\right)^{2N}\left|\mathbf{\Gamma}_r^2\right|^{-1}\left(1+\sigma_e^2\right)^{-2N}\left|\mathbf{\Theta}_1-\epsilon\mathbf{I}\right|^{-1} \tag{5.26}$$

$$= \frac{1}{2}\left(\frac{1}{4}\right)^{-2N}\left(\frac{1}{\eta}\right)^{2N}\left(\frac{1}{1+\sigma_e^2}\right)^{-2(2N)}\left(1+\sigma_e^2\right)^{-2N}|\mathbf{\Theta}_1-\epsilon\mathbf{I}|^{-1} \tag{5.27}$$

$$= \frac{1}{2}\left(\frac{1}{4}\right)^{-2N}\left(\frac{1}{\eta}\right)^{2N}\left(1+\sigma_e^2\right)^{4N}\left(1+\sigma_e^2\right)^{-2N}|\mathbf{\Theta}_1-\epsilon\mathbf{I}|^{-1} \tag{5.28}$$

$$= \frac{1}{2}\left(\frac{1}{4}\right)^{-2N}\left(\frac{1}{\eta}\right)^{2N}\left(1+\sigma_e^2\right)^{2N}|\mathbf{\Theta}_1-\epsilon\mathbf{I}|^{-1} \tag{5.29}$$

$$\bar{P}_{b_{DP}} \underset{H_{UP}}{\overset{H_{DP}}{\lesseqgtr}} \bar{P}_{b_{UP}} \tag{5.30}$$

$$\begin{aligned}\Longrightarrow \quad & \frac{1}{2ML}\sum_{u=1}^{2M}\sum_{\hat{u}=1}^{2M}\sum_{s=1}^{L}\sum_{\hat{s}=1}^{L}\frac{N(u,\hat{u},s,\hat{s})}{\log_2(2ML)}\left(\frac{1}{2}\left(\frac{1}{4}\right)^{-2N}\left(\frac{1}{\eta}\right)^{2N}\left(1+\sigma_e^2\right)^{2N}|\mathbf{\Theta}_1-\epsilon\mathbf{I}|^{-1}\right) \\ \underset{H_{UP}}{\overset{H_{DP}}{\lesseqgtr}} \quad & \frac{1}{2ML}\sum_{u=1}^{2M}\sum_{\hat{u}=1}^{2M}\sum_{s=1}^{L}\sum_{\hat{s}=1}^{L}\frac{N(u,\hat{u},s,\hat{s})}{\log_2(2ML)}\left(\frac{1}{2}\left(\frac{1}{4}\right)^{-2N}\left(\frac{1}{\eta}\right)^{2N}\left(1+\sigma_e^2\right)^{2N}\left|\mathbf{\Theta}_1'-\epsilon\mathbf{I}\right|^{-1}\right)\end{aligned} \tag{5.31}$$

and

$$\begin{aligned}|\mathbf{\Theta}_1-\epsilon\mathbf{I}|^{-1} &= \left|\mathbf{\Upsilon}\left(u,\hat{u},s,\hat{s}\right)\mathbf{\Psi}\mathbf{\Upsilon}\left(u,\hat{u},s,\hat{s}\right)^H-\epsilon\mathbf{I}\right|^{-1} \\ &= \left|\mathbf{\Psi}\left(\mathbf{\Upsilon}\left(u,\hat{u},s,\hat{s}\right)^H\mathbf{\Upsilon}\left(u,\hat{u},s,\hat{s}\right)-\epsilon'\mathbf{I}\right)\right|^{-1} \\ &= |\mathbf{\Psi}|^{-1}\left|\mathbf{\Upsilon}\left(u,\hat{u},s,\hat{s}\right)^H\mathbf{\Upsilon}\left(u,\hat{u},s,\hat{s}\right)-\epsilon'\mathbf{I}\right|^{-1}\end{aligned} \tag{5.32}$$

where $\mathbf{\Upsilon}\left(u,\hat{u},s,\hat{s}\right)$ is defined as Equation 4.37.

Notice that in Equation 5.31 all terms except $\mathbf{\Theta}_1$ and $\mathbf{\Theta'}_1$, are the same. Last term of Equation 5.32 is also the same for uni-polar and dual -polarized system and thus, they cancel each other out. Thus; ABEP depends on $|\mathbf{\Psi}|$, as in the case of perfect channel estimation. So, the equilibrium point achieved by

$$\begin{aligned}\bar{P}_{b_{DP}} &\underset{H_{UP}}{\overset{H_{DP}}{\lesseqgtr}} \bar{P}_{b_{UP}} \\ &\Longrightarrow \quad |\mathbf{\Psi}| \underset{H_{UP}}{\overset{H_{DP}}{\gtreqless}} \left|\mathbf{\Psi'}\right| \\ &\Longrightarrow \quad \left(1-\gamma_r^2\right)^{NM}\left(1-\gamma_t^2\right)^{NM} \underset{H_{UP}}{\overset{H_{DP}}{\gtreqless}} \frac{\left(1-\alpha_r^2\right)^M\left(1-\alpha_t^2\right)^N}{\left(1-q_r\right)^{2NM}\left(1-q_t\right)^{2NM}}\end{aligned} \tag{5.33}$$

Furthermore, in Equation 5.33, the effect of transmit and receive parameter are equal, nevertheless, considering the covariance of $\mathbf{z}$ as defined in Equation 5.12, shows that in practice, transmit and receive correlation coefficients have different impacts and equilibrium

point is more sensitive to the transmit correlation coefficient, as it can be seen in Table 5.3 and Table 5.4.

Equilibrium points are deployed in the following 3-D and 2-D Figures for infinite and finite XPI.

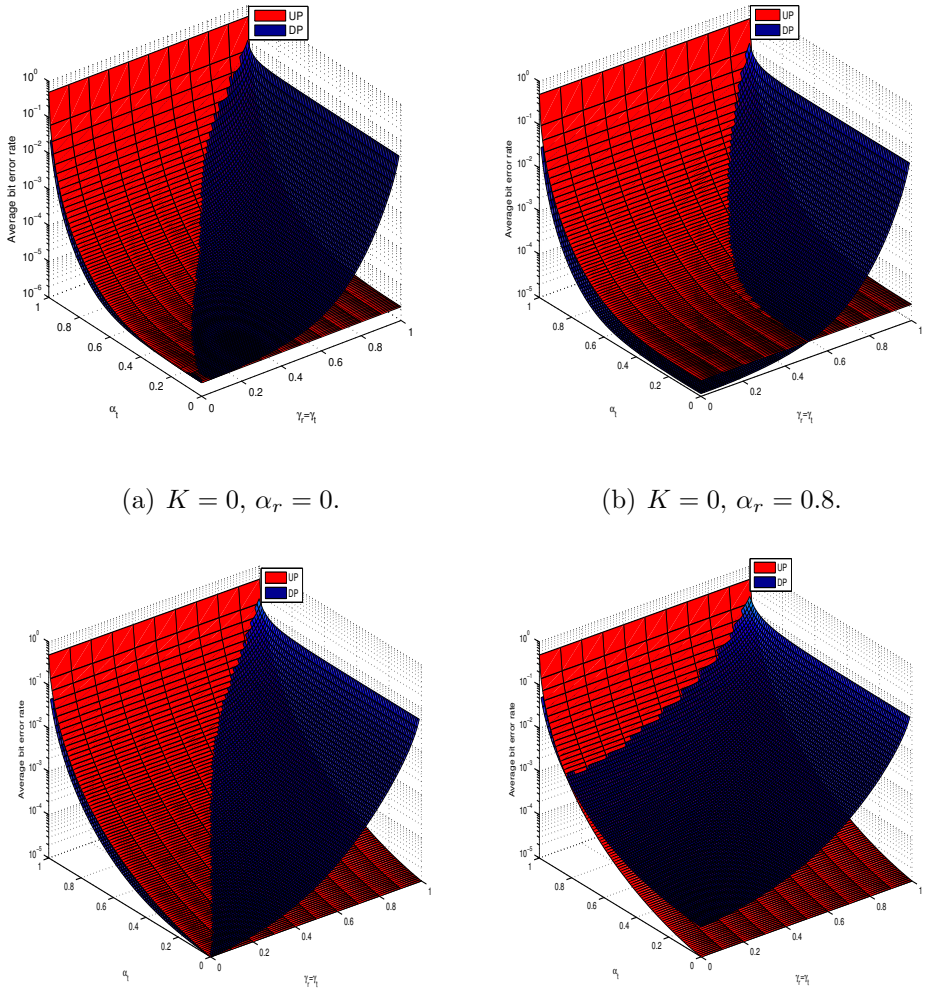

(a) $K = 0$, $\alpha_r = 0$.

(b) $K = 0$, $\alpha_r = 0.8$.

(c) $K = 3$, $\alpha_r = 0$.

(d) $K = 3$, $\alpha_r = 0.8$.

Figure 5.1: Exact performance for 4×4 uni-polar and 2×2 dual-polarized channel in fixed $SNR = 20$ dB, $q_r = q_t = 0$, using QPSK, $\sigma_e^2 = 0.01$.

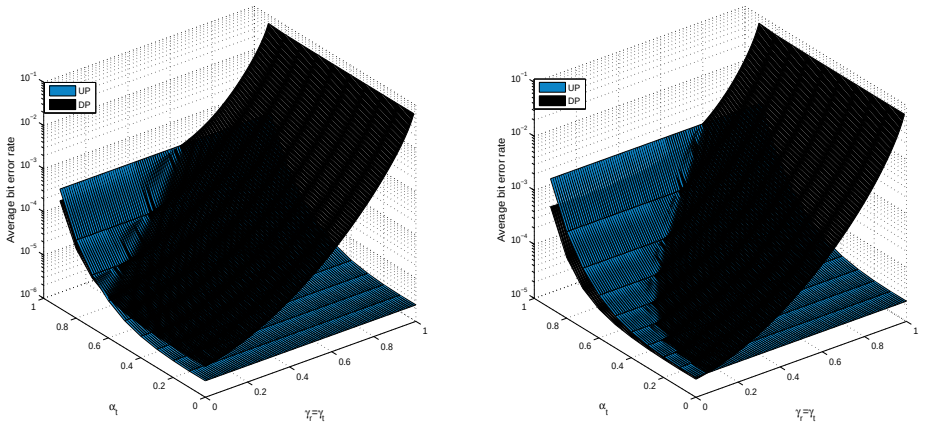

(a) $K = 0$, $\alpha_r = 0$.

(b) $K = 0$, $\alpha_r = 0.8$.

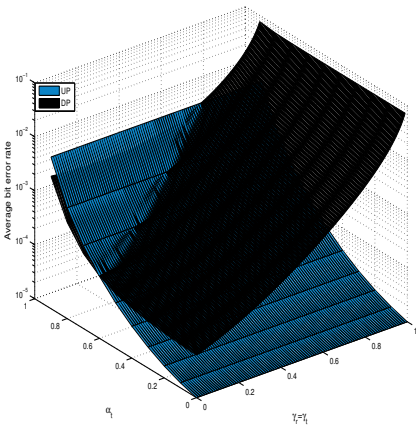

(c) $K = 3$, $\alpha_r = 0$.

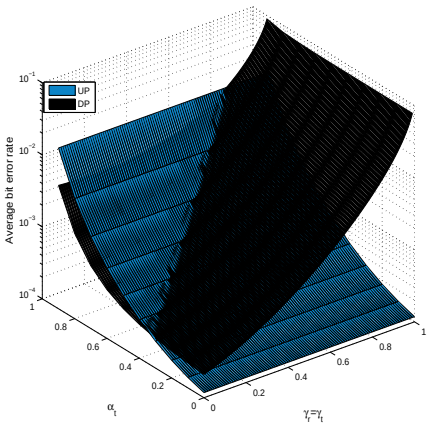

(d) $K = 3$, $\alpha_r = 0.8$.

Figure 5.2: Exact performance for 4×4 uni-polar and 2×2 dual-polarized channel in fixed $SNR = 20$ dB, $q_r = q_t = 0.1$, using QPSK, $\sigma_e^2 = 0.01$.

Tables 5.1 - 5.4 provide γ_es for the imperfect channel estimation error and other assumptions are the same as Table 4.2 and Table 4.5. Tables 5.5 - 5.9 also tabulate the effect of Rician factor for different values of α_r and α_t in a fixed SNR. It can be shown than in the presence of channel estimation error, as in the case of perfect channel estimation, the equilibrium points are less sensitive to the Rician factor and more sensitive to the transmit and receive spatial correlations.

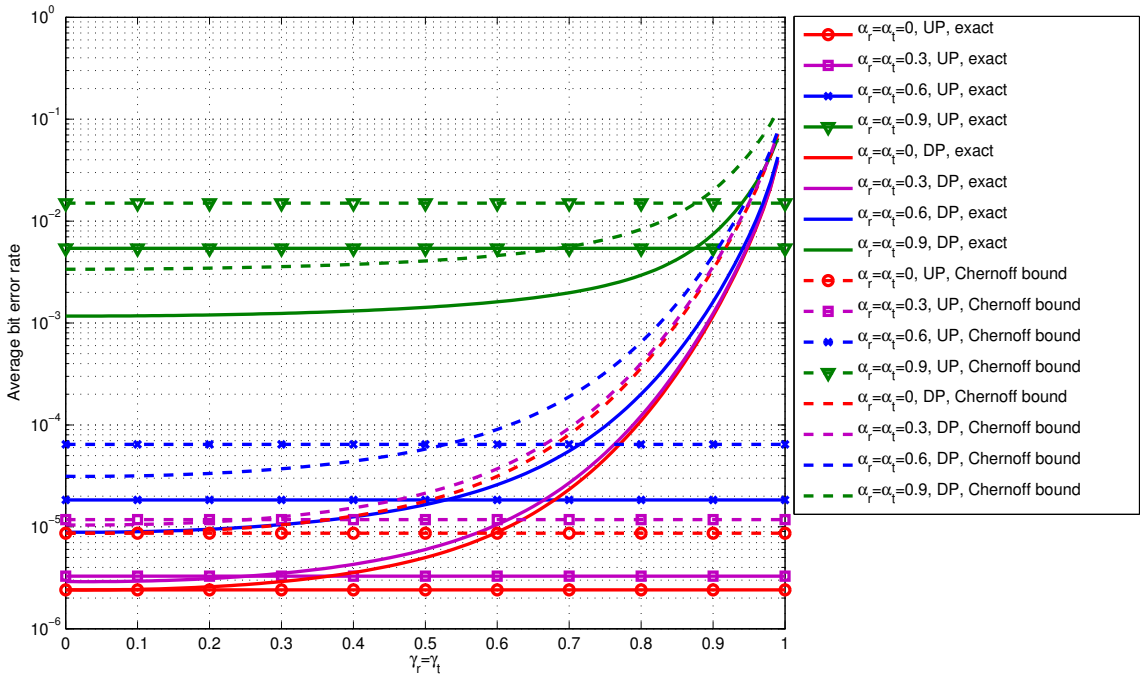

(a) $q_r = q_t = 0$, $\sigma_e^2 = 0.01$.

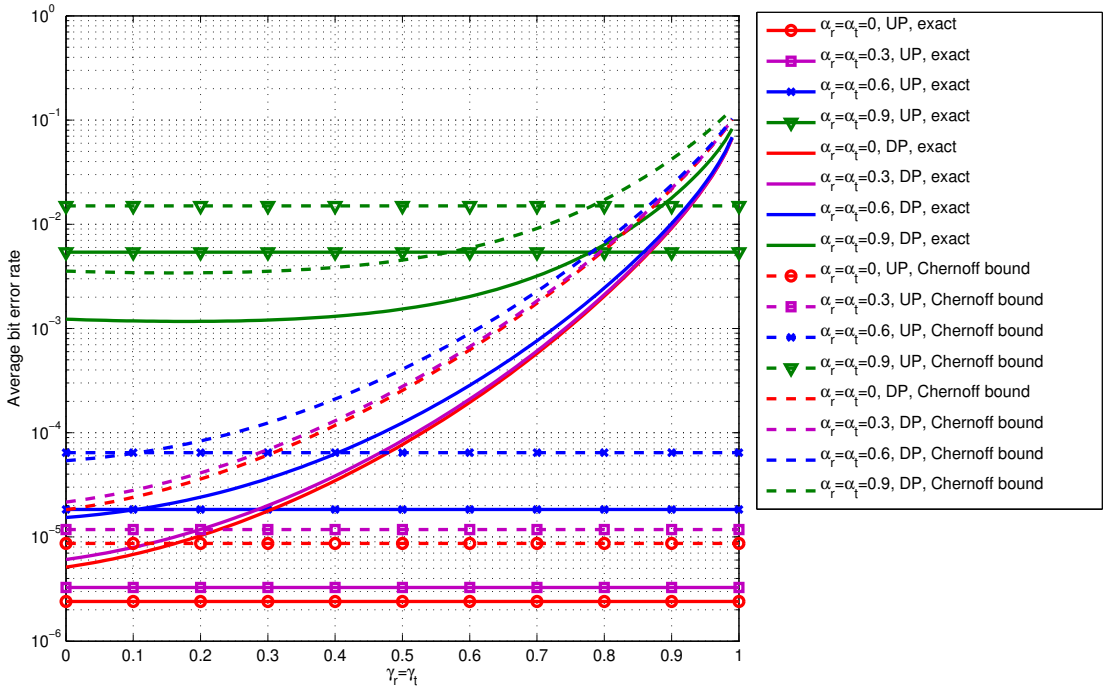

(b) $q_r = q_t = 0.1$, $\sigma_e^2 = 0.01$.

Figure 5.3: Equilibrium points using exact error performance and Chernoff bound for 4×4 uni-polar and 2×2 dual-polarized Rayleigh channel in fixed $SNR = 20$ dB.

Table 5.1: Performance equilibrium points for Rayleigh channel. First and second values are obtained from exact performance and Chernoff bound, respectively, $SNR = 30$ dB, $q_r = q_t = 0$, $\sigma_e^2 = 0.01$.

α_r, α_t	0	0.1	0.2	0.3	0.4	0.5	0.6	0.7	0.8	0.9
0	0.0344	0.0346	0.284	0.324	0.373	0.437	0.524	0.641	0.754	0.838
	0.0345	0.0348	0.262	0.314	0.368	0.438	0.529	0.643	0.751	0.837
0.1	0.0351	0.244	0.286	0.325	0.373	0.437	0.525	0.641	0.754	0.838
	0.0355	0.0358	0.265	0.315	0.369	0.438	0.529	0.643	0.751	0.837
0.2	0.14	0.15	0.292	0.328	0.375	0.439	0.526	0.641	0.753	0.838
	0.14	0.15	0.274	0.318	0.371	0.44	0.531	0.643	0.751	0.837
0.3	0.275	0.279	0.3	0.333	0.379	0.441	0.528	0.642	0.753	0.837
	0.248	0.255	0.285	0.324	0.375	0.443	0.533	0.643	0.75	0.836
0.4	0.292	0.295	0.311	0.34	0.384	0.445	0.531	0.643	0.752	0.836
	0.276	0.279	0.299	0.333	0.381	0.447	0.535	0.644	0.749	0.835
0.5	0.311	0.313	0.325	0.351	0.391	0.451	0.535	0.644	0.751	0.835
	0.299	0.301	0.316	0.345	0.389	0.453	0.54	0.645	0.748	0.834
0.6	0.331	0.333	0.343	0.365	0.403	0.46	0.542	0.646	0.75	0.834
	0.323	0.325	0.337	0.361	0.401	0.462	0.546	0.647	0.747	0.834
0.7	0.358	0.359	0.367	0.386	0.419	0.474	0.551	0.65	0.749	0.834
	0.353	0.355	0.363	0.383	0.42	0.476	0.555	0.65	0.747	0.833
0.8	0.395	0.396	0.402	0.417	0.447	0.496	0.568	0.658	0.752	0.836
	0.394	0.395	0.402	0.418	0.448	0.499	0.571	0.658	0.75	0.836
0.9	0.46	0.461	0.465	0.476	0.5	0.54	0.602	0.681	0.766	0.849
	0.463	0.463	0.468	0.479	0.503	0.544	0.604	0.681	0.765	0.85

Table 5.2: Performance equilibrium points for Rician channel, $K = 3$. First and second values are obtained from exact performance and Chernoff bound, respectively, $SNR = 30$ dB, $q_r = q_t = 0$, $\sigma_e^2 = 0.01$.

α_r, α_t	0	0.1	0.2	0.3	0.4	0.5	0.6	0.7	0.8	0.9
0	0.0193	0.0695	0.171	0.266	0.345	0.421	0.499	0.581	0.666	0.765
	0.016	0.076	0.172	0.262	0.343	0.421	0.502	0.584	0.667	0.765
0.1	0.021	0.0722	0.174	0.268	0.347	0.422	0.5	0.582	0.667	0.765
	0.0181	0.079	0.175	0.264	0.344	0.422	0.503	0.585	0.668	0.766
0.2	0.0265	0.0811	0.182	0.273	0.35	0.425	0.503	0.585	0.67	0.768
	0.0249	0.0885	0.183	0.269	0.348	0.426	0.506	0.588	0.671	0.768
0.3	0.0625	0.135	0.224	0.301	0.372	0.444	0.521	0.602	0.685	0.779
	0.0381	0.106	0.196	0.278	0.355	0.431	0.511	0.592	0.675	0.771
0.4	0.08	0.178	0.252	0.321	0.389	0.459	0.535	0.614	0.696	0.787
	0.0613	0.132	0.214	0.291	0.365	0.44	0.518	0.599	0.681	0.777
0.5	0.0926	0.164	0.241	0.312	0.381	0.451	0.526	0.605	0.689	0.784
	0.1	0.166	0.238	0.309	0.379	0.452	0.529	0.608	0.689	0.785
0.6	0.152	0.21	0.272	0.334	0.399	0.467	0.54	0.618	0.701	0.795
	0.155	0.209	0.269	0.332	0.398	0.468	0.543	0.62	0.701	0.795
0.7	0.221	0.261	0.31	0.364	0.424	0.489	0.56	0.637	0.718	0.809
	0.219	0.258	0.307	0.363	0.424	0.491	0.562	0.638	0.718	0.81
0.8	0.293	0.321	0.36	0.407	0.461	0.522	0.591	0.665	0.744	0.831
	0.291	0.32	0.359	0.407	0.462	0.524	0.593	0.665	0.743	0.832
0.9	0.389	0.41	0.44	0.48	0.528	0.585	0.649	0.717	0.79	0.865
	0.39	0.411	0.442	0.482	0.531	0.587	0.65	0.718	0.79	0.867

Table 5.3: Performance equilibrium points for Rayleigh channel. First and second values are obtained from exact performance and Chernoff bound, respectively, $SNR = 30$ dB, $q_r = q_t = 0.1$, $\sigma_e^2 = 0.01$.

α_r, α_t	0	0.1	0.2	0.3	0.4	0.5	0.6	0.7	0.8	0.9
0	-	-	-	-	-	-	0.00221	0.168	0.373	0.612
	-	-	-	-	-	-	-	0.169	0.371	0.6143
0.1	-	-	-	-	-	-	0.00259	0.168	0.373	0.613
	-	-	-	-	-	-	-	0.169	0.371	0.6143
0.2	-	-	-	-	-	-	0.0038	0.17	0.374	0.613
	-	-	-	-	-	-	-	0.171	0.372	0.6145
0.3	-	-	-	-	-	-	0.00602	0.172	0.375	0.613
	-	-	-	-	-	-	-	0.173	0.374	0.6148
0.4	-	-	-	-	-	-	0.00963	0.177	0.378	0.614
	-	-	-	-	-	-	0.00212	0.177	0.376	0.6153
0.5	-	-	-	-	-	-	0.0154	0.183	0.381	0.615
	-	-	-	-	-	-	0.0102	0.183	0.38	0.6165
0.6	-	-	-	-	-	-	0.0246	0.192	0.387	0.617
	-	-	-	-	-	-	0.0224	0.192	0.386	0.6188
0.7	-	-	-	-	-	-	0.0404	0.208	0.396	0.622
	-	-	-	-	-	-	0.0417	0.206	0.396	0.6237
0.8	-	-	-	-	-	-	0.0711	0.235	0.415	0.634
	-	-	-	-	-	-	0.0752	0.233	0.415	0.6356
0.9	-	-	-	-	-	0.0399	0.148	0.295	0.459	0.671
	-	-	-	-	-	0.042	0.151	0.293	0.461	0.672

Table 5.4: Performance equilibrium points for Rician channel, i.e.,$K = 3$. First and second values are obtained from exact performance and Chernoff bound, respectively, $SNR = 30$ dB, $q_r = q_t = 0.1$, $\sigma_e^2 = 0.01$.

α_r, α_t	0	0.1	0.2	0.3	0.4	0.5	0.6	0.7	0.8	0.9
0	-	-	-	-	-	-	-	0.136	0.338	0.5604
	-	-	-	-	-	-	-	0.138	0.3360	0.5641
0.1	-	-	-	-	-	-	-	0.138	0.339	0.5615
	-	-	-	-	-	-	-	0.14	0.3375	0.5652
0.2	-	-	-	-	-	-	-	0.144	0.343	0.5650
	-	-	-	-	-	-	-	0.146	0.3420	0.5686
0.3	-	-	-	-	-	-	-	0.153	0.351	0.571
	-	-	-	-	-	-	-	0.155	0.35	0.57
0.4	-	-	-	-	-	-	-	0.123	0.331	0.557
	-	-	-	-	-	-	-	0.169	0.3611	0.5835
0.5	-	-	-	-	-	-	0.0154	0.188	0.377	0.593
	-	-	-	-	-	-	0.0123	0.188	0.377	0.5961
0.6	-	-	-	-	-	-	0.0425	0.215	0.398	0.611
	-	-	-	-	-	-	0.0437	0.214	0.399	0.6138
0.7	-	-	-	-	-	-	0.0832	0.252	0.428	0.637
	-	-	-	-	-	-	0.0865	0.251	0.429	0.6392
0.8	-	-	-	-	-	0.00906	0.148	0.306	0.473	0.676
	-	-	-	-	-	0.00593	0.15	0.305	0.476	0.6777
0.9	-	-	-	-	0.0182	0.131	0.263	0.402	0.558	0.742
	-	-	-	-	0.0187	0.136	0.264	0.405	0.562	0.743

Table 5.5: Effect of different Rician factors on equilibrium points, $q_r = q_t = 0$, $\alpha_r = 0$, $\sigma_e^2 = 0.01$ $SNR = 30$ dB.

α_t , K	0	3	5	10	100
0.1	0.0346	0.0695	0.0728	0.0747	0.0755
0.3	0.324	0.266	0.257	0.248	0.243
0.5	0.437	0.421	0.41	0.397	0.395
0.7	0.641	0.581	0.563	0.543	0.566
0.9	0.838	0.765	0.741	0.726	0.824

Table 5.6: Effect of different Rician factors on equilibrium points, $q_r = q_t = 0$, $\alpha_r = 0.5$, $\sigma_e^2 = 0.01$ $SNR = 30$ dB.

α_t , K	0	3	5	10	100
0.1	0.313	0.164	0.175	0.19	0.205
0.3	0.351	0.312	0.313	0.316	0.32
0.5	0.451	0.451	0.449	0.447	0.449
0.7	0.644	0.605	0.597	0.588	0.606
0.9	0.835	0.784	0.774	0.773	0.834

Table 5.7: Effect of different Rician factors on equilibrium points, $q_r = q_t = 0$, $\alpha_r = 0.8$, $\sigma_e^2 = 0.01$ $SNR = 30$ dB.

α_t , K	0	3	5	10	100
0.1	0.396	0.321	0.328	0.352	0.406
0.3	0.417	0.407	0.417	0.436	0.474
0.5	0.496	0.522	0.532	0.546	0.569
0.7	0.658	0.665	0.67	0.678	0.692
0.9	0.836	0.831	0.834	0.84	0.861

Table 5.8: Effect of different Rician factors on equilibrium points, $q_r = q_t = 0.1$, $\alpha_r = 0.5$, $\sigma_e^2 = 0.01$ $SNR = 30$ dB.

α_t , K	0	3	5	10	100
0.1	-	-	-	-	-
0.3	-	-	-	-	-
0.5	-	-	-	-	-
0.7	0.183	0.188	0.2	0.23	0.451
0.9	0.615	0.593	0.601	0.63	0.838

Table 5.9: Effect of different Rician factors on equilibrium points, $q_r = q_t = 0.1$, $\alpha_r = 0.8$, $\sigma_e^2 = 0.01$ $SNR = 30$ dB.

α_t , K	0	3	5	10	100
0.1	-	-	-	-	-
0.3	-	-	-	-	0.0203
0.5	-	0.00906	0.0342	0.0842	0.314
0.7	0.235	0.306	0.335	0.381	0.572
0.9	0.634	0.676	0.696	0.727	0.86

5.1.4. Simulation Results

In this section, we provide the results of simulation and theoretical analysis for spatial modulation over dual-polarized MIMO channel in presence of channel estimation error. XPI for both transmit and receive antennas are such that $q_r = q_t = 0.1$, without loss of generality.

In Figures 5.4- 5.7, we consider $\alpha_t = \alpha_r = 0.8$ for correlated channels. We have simulated the average bit error rate for $\gamma_t = \gamma_r = \gamma = 0.2, 0.5$ and 0.8. The results are compared with uni-polarized system with the same number of antennas as well as the situation, where the number of antennas is doubled. Rician factor is 3, i.e., K=3. The fixed channel matrix $\overline{\mathbf{H}}$ is set to be an all one matrix as in [40] but other fixed matrix choices are also valid. In

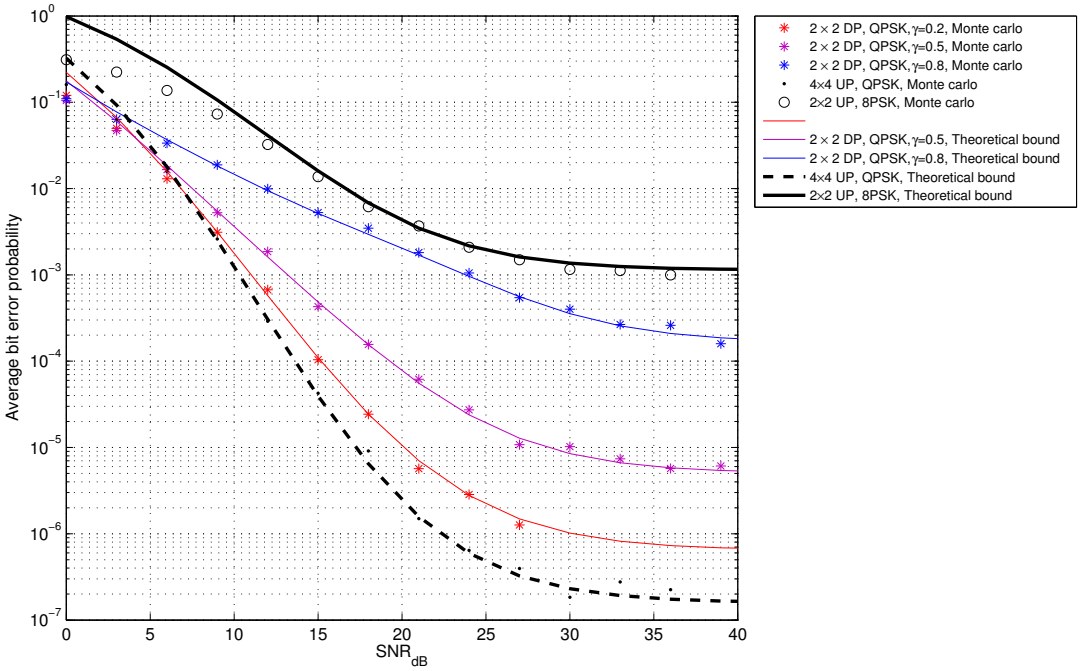

Figure 5.4: Uncorrelated Rayleigh channel, $R = 4$, $\sigma_e^2 = 0.01$.

other words, Figures 4.5- 4.8 includes:

(i) 4×4 uni-polarized MIMO system employing QPSK($R = 2 + 2 = 4$);

(ii) 2×2 uni-polarized MIMO system employing 8-PSK($R = 1 + 3 = 4$);

(iii) 2×2 dual-polarized MIMO system employing QPSK for different XPD factors ($R = 1 + 2 + 1 = 4$).

These observations are the results of Kronecker products of spatial correlation matrix and polarization correlation matrix, which ends up to the total correlation matrix. In uncorrelated channel employing dual-polarized antenna, correlation matrix achieving by Kronecker product, has more tendency to the correlation matrix of uni-polarized correlated fading channel, which has worse performance compared to uni-polarized uncorrelated fading channel. That is why, in a channel which is perfectly spatially uncorrelated, with polarization correlation, it is always worthy to use uni-polarized antenna, in terms of bit error performance (Although channel with dual-polarized antennas is still space efficient). However,

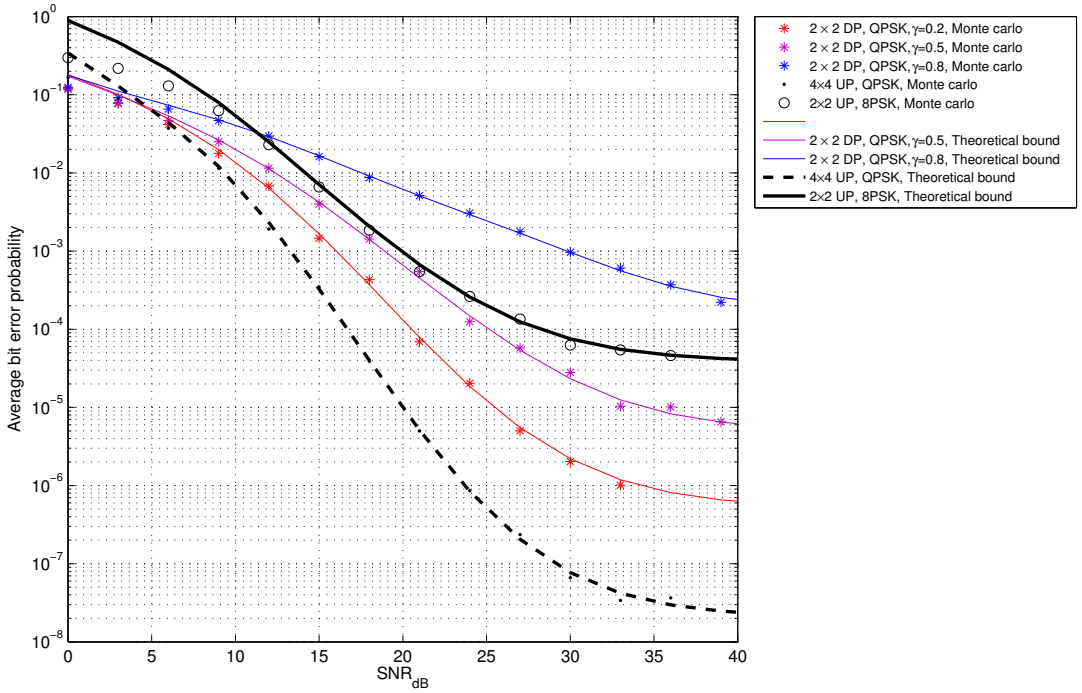

Figure 5.5: Uncorrelated Rician channel, $R = 4$, $\sigma_e^2 = 0.01$.

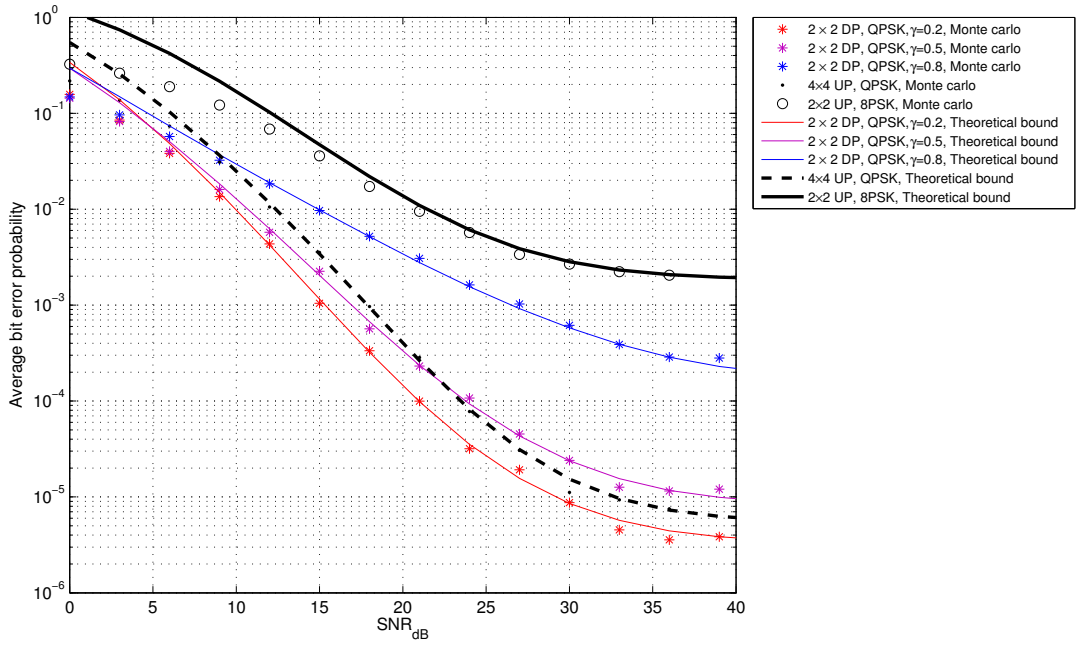

Figure 5.6: Correlated Rayleigh channel, $R = 4$, $\sigma_e^2 = 0.01$.

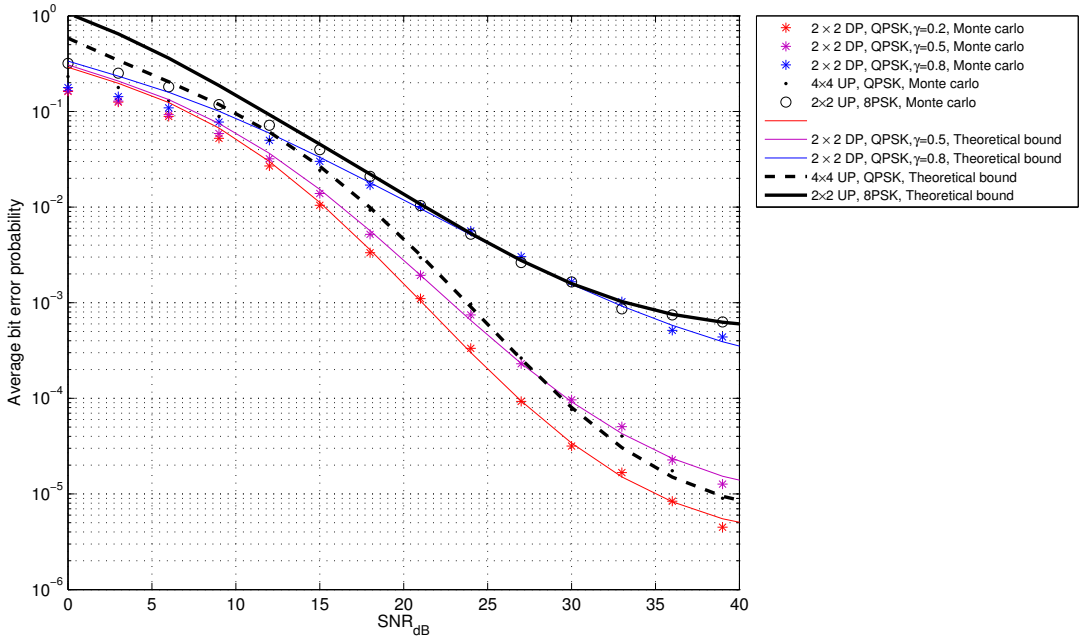

Figure 5.7: Correlated Rician channel, $R = 4$, $\sigma_e^2 = 0.01$.

when there is neither spatial correlation nor polarization correlation, two system have the same performance.

Comparing Figures 5.4- 5.7 and Figures 4.5- 4.8, shows that although channel estimation error deteriorate the performance of both uni-polarized and dual-polarized systems, dual-polarized system is more sensitive to the channel estimation error.

6. DUAL-POLARIZED GENERALIZED SPATIAL MODULATION IN CHANNEL ESTIMATION ERROR

6.1. Average Error Analysis in Generalized SM

The results of previous sections can be further extended to the case, where N_a antennas are active at each transmission instant and simultaneously transmit a constellation alphabet. Consequently, G-SM takes benefits of C-SM as well as diversity gain. To this purpose, there is $\begin{pmatrix} M \\ N_a \end{pmatrix}$ different combinations. As previous sections, assume m bits of input stream are assigned to select an N_a antennas. Therefore there are 2^m choices resulting in $\begin{pmatrix} \begin{pmatrix} M \\ N_a \end{pmatrix} \\ 2^m \end{pmatrix}$ combinations. As an example, suppose there is a system with 4 transmit antennas, 2 active antennas is desired and $m = 2$. Consequently, $\begin{pmatrix} 4 \\ 2 \end{pmatrix} = 6$ from which $2^2 = 4$ should be selected, which results in $\begin{pmatrix} 6 \\ 4 \end{pmatrix} = 15$ combinations. Obviously, large number of transmit antennas dramatically increases the number of combinations each of which has distinct error performance. Large amount of combinations highlights the importance of theoretical analysis to find the best antenna selection. To put mapping input bits to antennas and symbol more clearly, assume a 2×2 dual-polarized system, where 2 antennas are used simultaneously to transmit a signal and $m = 2$. Table 6.1 illustrates an example of transmitting QPSK using such a system and shows mapping strategy.

Notice that in this scenario, there is no need for number of transmit antennas to be power of two.

6.1.1. Channel Model

In the case of G-SM, received signal can be modeled as

$$\mathbf{y} = \mathbf{q}_u X_s + \boldsymbol{\nu} \tag{6.2}$$

Table 6.1: Mapping input bits to corresponding constellation symbols, antennas and their polarization for G-SM, $N_a = 2$, $m = 2$, QPSK.

Incoming bits	Symbol bits	Antennas	Polarizations	$\mathbf{x^T}$	X_s
$\overbrace{0\ \ 0}^{symbol\ bits}\ \overbrace{0\ \ 0}^{antenna\ index}$	00	I, I	p, p'	$\begin{bmatrix} 0 & 0 & 1 & 1 \end{bmatrix}$	1
0001	00	I, II	p, p	$\begin{bmatrix} 0 & 1 & 0 & 1 \end{bmatrix}$	1
0010	00	I, II	p', p'	$\begin{bmatrix} 1 & 0 & 1 & 0 \end{bmatrix}$	1
0011	00	II, II	p, p'	$\begin{bmatrix} 1 & 1 & 0 & 0 \end{bmatrix}$	1
0100	01	I, I	p, p'	$\begin{bmatrix} 0 & 0 & j & j \end{bmatrix}$	j
0101	01	I, II	p, p	$\begin{bmatrix} 0 & j & 0 & j \end{bmatrix}$	j
0110	01	I, II	p', p'	$\begin{bmatrix} j & 0 & j & 0 \end{bmatrix}$	j
0111	01	II, II	p, p'	$\begin{bmatrix} j & j & 0 & 0 \end{bmatrix}$	j
1000	10	I, I	p, p'	$\begin{bmatrix} 0 & 0 & -1 & -1 \end{bmatrix}$	-1
1001	10	I, II	p, p	$\begin{bmatrix} 0 & -1 & 0 & -1 \end{bmatrix}$	-1
1010	10	I, II	p', p'	$\begin{bmatrix} -1 & 0 & -1 & 0 \end{bmatrix}$	-1
1011	10	II, II	p, p'	$\begin{bmatrix} -1 & -1 & 0 & 0 \end{bmatrix}$	-1
1100	11	I, I	p, p'	$\begin{bmatrix} 0 & 0 & -j & -j \end{bmatrix}$	-j
1101	11	I,II	p, p	$\begin{bmatrix} 0 & -j & 0 & -j \end{bmatrix}$	-j
1110	11	I, II	p', p'	$\begin{bmatrix} -j & 0 & -j & 0 \end{bmatrix}$	-j
1111	11	II, II	p, p'	$\begin{bmatrix} -j & -j & 0 & 0 \end{bmatrix}$	-j

where $\mathbf{q}_u$ represents the uth aggregate channel vector written as

$$\mathbf{q}_u = \frac{1}{\sqrt{N_a}} \sum_{k=1}^{N_a} \mathbf{h}_{u_k} \tag{6.3}$$

u_k denotes the kth index in the set shown by u [44].

In presence of channel estimation error, however, q_u can be replaced by p_u defined as

$$\mathbf{p}_u = \frac{1}{\sqrt{N_a}} \sum_{k=1}^{N_a} \mathbf{g}_{u_k}. \tag{6.4}$$

Considering this model for imperfect channel estimation, mean and covariance matrix of received signal conditioned on erroneous channel and transmitted symbol can be calculated as

$$\begin{aligned}\mathbf{m}_{u,s} &= \mathrm{E}\left[\mathbf{y} \mid \mathbf{p}_u, X_s\right] \\ &= \sqrt{\frac{K}{(K+1)}}\left(\mathbf{I}-\mathbf{\Gamma}_r\right)\bar{\mathbf{p}}_u X_s + \mathbf{\Gamma}_r \mathbf{p}_u X_s \qquad (6.5)\\ \mathbf{\Lambda}_{u,s} &= \mathrm{E}\left[(\mathbf{y}-\mathbf{m}_{u,s})(\mathbf{y}-\mathbf{m}_{u,s})^H \mid \mathbf{p}_u, X_s\right] \\ &= \frac{\mathbf{I}}{\eta} + \frac{|X_s|^2\Phi_{u,u}}{K+1}\mathbf{\Psi}_r\left(\mathbf{I}-\mathbf{\Gamma}_r\right) \qquad (6.6)\end{aligned}$$

where

$$\mathbf{\Gamma}_r = \left(\mathbf{I} + \frac{\sigma_e^2\Omega_{u,u}}{\Phi_{u,u}}\mathbf{\Psi}_r^{-1}\mathbf{\Xi}_r\right)^{-1}. \qquad (6.7)$$

$\mathbf{q}_u$ and $\mathbf{p}_u$ are defined as before for $u = 1, \ldots, 2^n$. X_s is the sth element of the modulation alphabet $\boldsymbol{\mathcal{X}}$ for $s = 1, \ldots, L$. $\mathbf{I}$ is a $N \times N$ identity matrix and

$$\Phi_{i,j} = \frac{1}{N_a}\sum_{k=1}^{N_a}\sum_{\ell=1}^{N_a}\psi_{i_k,j_\ell}^t, \qquad \Omega_{i,j} = \frac{1}{N_a}\sum_{k=1}^{N_a}\sum_{\ell=1}^{N_a}\xi_{i_k,j_\ell}^t,$$

$\Phi_{i,j}$ and $\Omega_{i,j}$ denote the transmit correlations between the ith and jth aggregate perfect channels and the ith and jth aggregate channels in presence of error estimation, respectively.

Having mean and covariance, distance metric and PEP can be calculated using ML detection as was done in Equation 5.7 and Equation 5.8.

6.1.2. PEP for L-QAM and LPSK

In order to find PEP for G-SM employing L-QAM and L-PSK, same steps can be done as those of Section 5.1.1 and Section 5.1.2, where the only difference is mean and covariance matrix, which can be calculated as

$$\begin{aligned}\mathbf{m}_{\mathbf{z}} &= \sqrt{\frac{K}{K+1}}\mathbf{\Lambda}_{u,s}^{-\frac{1}{2}}\left(\bar{\mathbf{p}}_u X_s - \bar{\mathbf{p}}_{\hat{u}} X_{\hat{s}}\right) \\ \mathbf{\Lambda}_{\mathbf{z}} &= \left[\mathbf{\Sigma}_{u,s}^{-\frac{1}{2}}\mathbf{\Gamma}_r\right]\left(\chi_1\mathbf{\Psi}_r + \chi_2\mathbf{\Xi}_r\right)\left[\mathbf{\Sigma}_{u,s}^{-\frac{1}{2}}\mathbf{\Gamma}_r\right]^H. \qquad (6.8)\end{aligned}$$

	Uni-polarized	Dual-polarized
Nt	4	2
Na	2	2
R(QPSK)	4	4
Uncorrelated channel	$\{(1,2),(1,3),(2,4),(3,4)\}$ $\{(1,2),(1,4),(2,3),(3,4)\}$ $\{(1,3),(1,4),(2,3),(2,4)\}$	$\{(1,2),(1,3),(2,4),(3,4)\}$ $\{(1,2),(1,4),(2,3),(3,4)\}$
Correlated channel	$\{(1,2),(1,4),(2,3),(3,4)\}$	$\{(1,2),(1,3),(2,4),(3,4)\}$

Table 6.2: Best antenna configuration.

The scalar terms χ_1 and χ_2 in Equation 6.8 are given as [1]

$$\begin{aligned}\chi_1 &= \frac{\Phi_{u,u} \mid X_s \mid^2 + \Phi_{\hat{u},\hat{u}} \mid X_{\hat{s}} \mid^2 - 2\mathcal{R}\{\Phi_{u,\hat{u}} X_s X_{\hat{s}}^*\}}{K+1} \\ \chi_2 &= \frac{\sigma_e^2 \left[\Omega_{u,u} \mid X_s \mid^2 + \Omega_{\hat{u},\hat{u}} \mid X_{\hat{s}} \mid^2 - 2\mathcal{R}\{\Omega_{u,\hat{u}} X_s X_{\hat{s}}^*\}\right]}{K+1}.\end{aligned}$$

As it has mentioned, different antenna combinations result in different performance. Table 6.2 shows the combination which causes the best performance for 4×4 dual-polarized and 2×2 uni polarized channel, assuming $N_a = 2$ and $m = 2$.

Comparing 2×2 dual-polarized system and 4×4 uni-polarized channel there are equilibrium points, where the performance of two systems are equal. Tables 6.3 - 6.6 shows these points using exact error performance.

[1] In the special case, where $\mathbf{\Xi}_r = \mathbf{\Psi}_r$ and $\mathbf{\Xi}_t = \mathbf{\Psi}_t$, $\mathbf{\Lambda_z}$ becomes,

$$\mathbf{\Lambda_z} = \frac{\rho^2 \left[\Phi_{u,u} \mid X_s \mid^2 + \Phi_{\hat{u},\hat{u}} \mid X_{\hat{s}} \mid^2 - 2\mathcal{R}\{\Phi_{u,\hat{u}} X_s X_{\hat{s}}^*\}\right]}{K+1} \tilde{\mathbf{\Lambda}}_{u,s} \mathbf{\Psi}_r \tilde{\mathbf{\Lambda}}_{u,s}^H$$

where $\tilde{\mathbf{\Lambda}}_{u,s} = \mathbf{\Lambda}_{u,\hat{s}}^{-\frac{1}{2}}$ and $\rho = 1/\sqrt{1+\sigma_e^2}$.

Table 6.3: Performance equilibrium points for Rayleigh channel. Values are obtained from exact performance, $SNR = 30$ dB, $q_r = q_t = 0$, $\sigma_e^2 = 0$.

α_r, α_t	0	0.1	0.2	0.3	0.4	0.5	0.6	0.7	0.8	0.9
0	0.322	0.243	0.0467	0.287	0.34	0.393	0.453	0.534	0.663	0.791
0.1	0.327	0.261	0.241	0.292	0.342	0.394	0.454	0.536	0.665	0.792
0.2	0.34	0.289	0.272	0.304	0.349	0.399	0.459	0.54	0.669	0.793
0.3	0.36	0.318	0.302	0.322	0.361	0.408	0.466	0.548	0.676	0.796
0.4	0.385	0.35	0.334	0.346	0.378	0.421	0.478	0.56	0.685	0.801
0.5	0.416	0.386	0.369	0.375	0.4	0.439	0.494	0.577	0.698	0.807
0.6	0.454	0.429	0.411	0.411	0.43	0.465	0.518	0.602	0.715	0.815
0.7	0.501	0.483	0.465	0.46	0.472	0.503	0.555	0.639	0.737	0.826
0.8	0.562	0.553	0.542	0.535	0.541	0.566	0.617	0.692	0.767	0.843
0.9	0.648	0.651	0.653	0.657	0.667	0.689	0.723	0.766	0.812	0.872

Table 6.4: Performance equilibrium points for Rayleigh channel. Values are obtained from exact performance, $SNR = 30$ dB, $q_r = q_t = 0$, $\sigma_e^2 = 0.01$.

α_r, α_t	0	0.1	0.2	0.3	0.4	0.5	0.6	0.7	0.8	0.9
0	0.0244	0.0417	0.0928	0.277	0.359	0.434	0.524	0.664	0.791	0.879
0.1	0.0248	0.0422	0.0941	0.278	0.359	0.434	0.524	0.664	0.791	0.879
0.2	0.0262	0.0438	0.0986	0.279	0.36	0.434	0.524	0.664	0.791	0.878
0.3	0.0288	0.0469	0.108	0.282	0.361	0.435	0.525	0.664	0.79	0.878
0.4	0.0333	0.0522	0.128	0.286	0.363	0.437	0.526	0.665	0.789	0.877
0.5	0.0413	0.0619	0.167	0.292	0.366	0.439	0.529	0.665	0.788	0.877
0.6	0.0577	0.0828	0.208	0.301	0.371	0.443	0.532	0.665	0.786	0.875
0.7	0.109	0.154	0.244	0.315	0.38	0.449	0.537	0.666	0.784	0.874
0.8	0.25	0.254	0.289	0.338	0.395	0.461	0.547	0.67	0.783	0.873
0.9	0.38	0.362	0.367	0.392	0.434	0.492	0.573	0.684	0.786	0.876

Table 6.5: Performance equilibrium points for Rayleigh channel. Values are obtained from exact performance, $SNR = 30$ dB, $q_r = q_t = 0.1$, $\sigma_e^2 = 0$.

α_r, α_t	0	0.1	0.2	0.3	0.4	0.5	0.6	0.7	0.8	0.9
0	-	-	-	-	-	-	0.24	0.4	0.534	0.727
0.1	-	-	-	-	-	-	0.25	0.403	0.536	0.728
0.2	-	-	-	-	-	-	0.275	0.411	0.542	0.731
0.3	-	-	-	-	-	0.0107	0.305	0.425	0.552	0.737
0.4	0.00556	-	-	-	-	0.0353	0.34	0.445	0.568	0.746
0.5	0.0349	0.026	0.0145	0.0113	0.0242	0.293	0.378	0.471	0.591	0.758
0.6	0.105	0.13	0.177	0.241	0.298	0.355	0.422	0.507	0.621	0.773
0.7	0.209	0.245	0.283	0.323	0.365	0.413	0.474	0.554	0.662	0.794
0.8	0.293	0.323	0.356	0.392	0.431	0.479	0.539	0.616	0.714	0.822
0.9	0.394	0.42	0.45	0.484	0.525	0.575	0.637	0.707	0.784	0.864

Table 6.6: Performance equilibrium points for Rayleigh channel. Values are obtained from exact performance, $SNR = 30$ dB, $q_r = q_t = 0.1$, $\sigma_e^2 = 0.01$.

α_r, α_t	0	0.1	0.2	0.3	0.4	0.5	0.6	0.7	0.8	0.9
0	-	-	-	-	-	-	-	0.175	0.402	0.674
0.1	-	-	-	-	-	-	-	0.175	0.402	0.674
0.2	-	-	-	-	-	-	-	0.176	0.402	0.674
0.3	-	-	-	-	-	-	-	0.177	0.403	0.673
0.4	-	-	-	-	-	-	-	0.179	0.404	0.673
0.5	-	-	-	-	-	-	-	0.183	0.405	0.672
0.6	-	-	-	-	-	-	0.00317	0.188	0.408	0.672
0.7	-	-	-	-	-	-	0.0122	0.197	0.413	0.673
0.8	-	-	-	-	-	-	0.0313	0.215	0.423	0.676
0.9	-	-	-	-	-	-	0.0878	0.266	0.455	0.695

6.1.3. Simulation Results

In this section, performance of 2×2 dual-polarized antenna is compared with 4×4 uni-polarized channel with respect to SNR. Number of antennas in use is 2, i.e., $N_a = 2$. All of the curves are plotted for transmission of QPSK, i.e., $\ell = 2$. Moreover, number of bits assigned to select N_a antennas are 2 bits in uni-polarized and 1 in dual-polarized channel. In other words, $R = 4$ bits/sec/Hz. Polarization correlation coefficients are $0.2, 0.5$, and 0.8. In all dual-polarized curves XPI are set such that $q_r = q_t = 0.1$. Theoretical results are shown by solid lines while simulation results are represented by markers. As can be seen, theoretical curves closely match to the simulations and all results reach to 10^{-6}. Both dual-polarized channel and uni-polarized channels are plotted with combinations presented in Table 6.2 to have the best performance. Channel estimation error is 0, i.e., $\sigma_e^2 = 0$, in Figures 6.1 - 6.4 and 0.01, i.e., $\sigma_e^2 = 0.01$, in Figures 6.5 - 6.8. Rician factor is 3, i.e., $K = 3$ in Rician channels. In correlated channels, Figures 6.3 - 6.4 and Figures 6.7 - 6.8, $\alpha_r = \alpha_t = 0.8$, without loss of generality. As the Figures show, in uncorrelated channels, 4×4 uni-polarized system outperforms whereas in correlated channel, it is worthy to use 2×2 dual-polarized channel rather than 4×4 uni-polarized system.

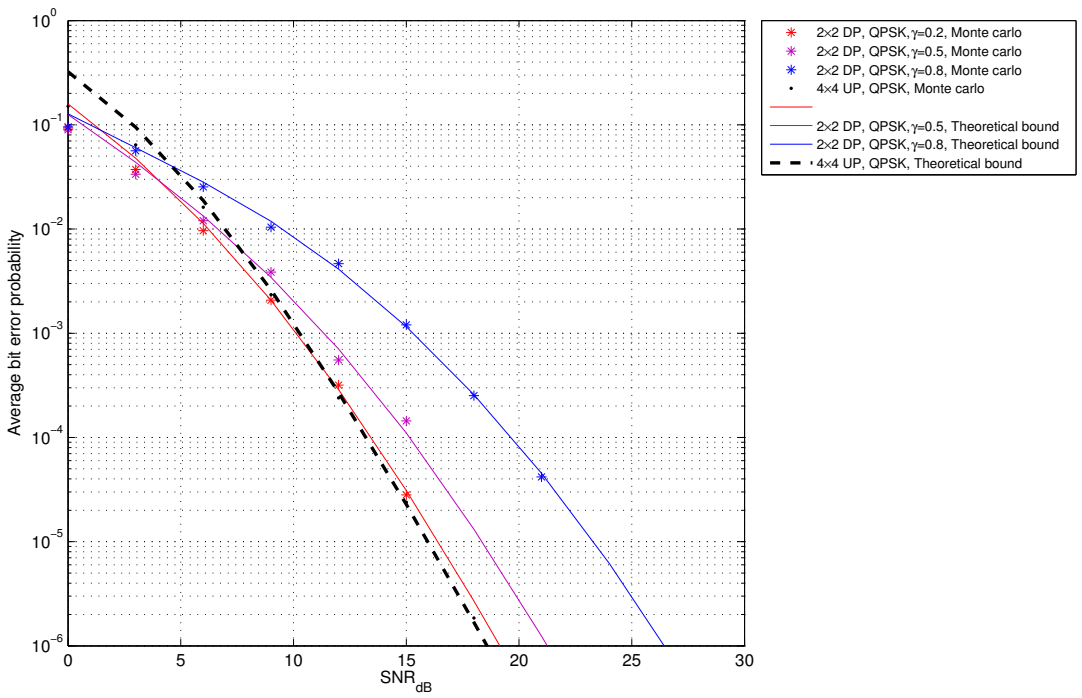

Figure 6.1: G-SM for uncorrelated Rayleigh channel, $R = 4$, $N_a = 2$, $m = 2$, QPSK.

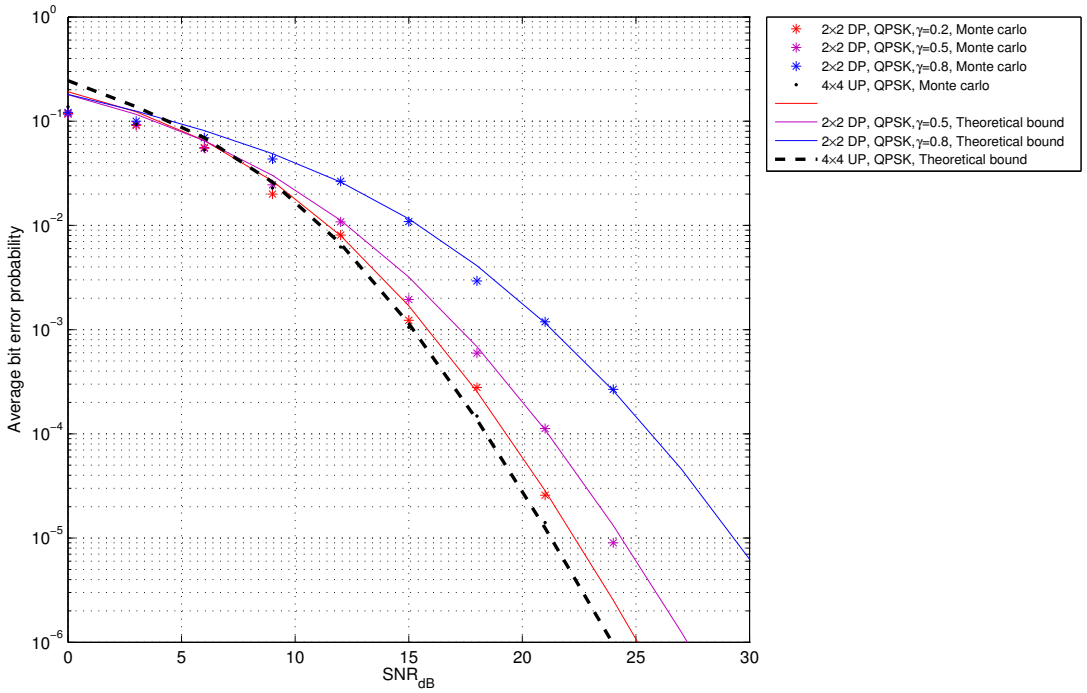

Figure 6.2: G-SM for uncorrelated Rician channel, $R = 4$, $N_a = 2$, $m = 2$, QPSK.

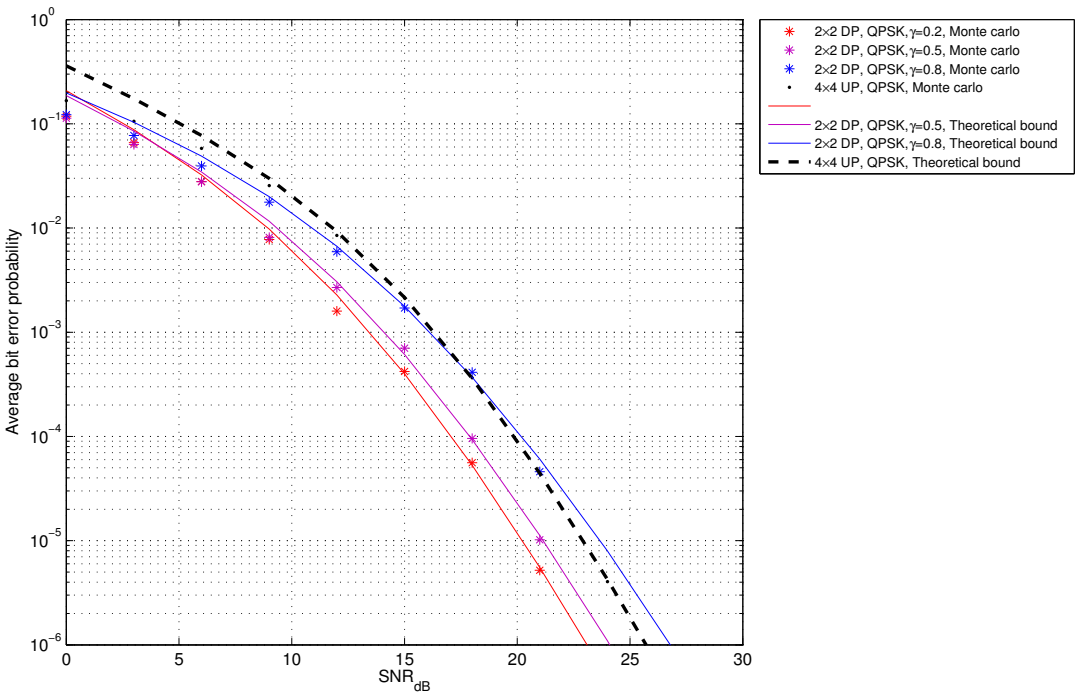

Figure 6.3: G-SM for correlated Rayleigh channel, $R = 4$, $N_a = 2$, $m = 2$, QPSK.

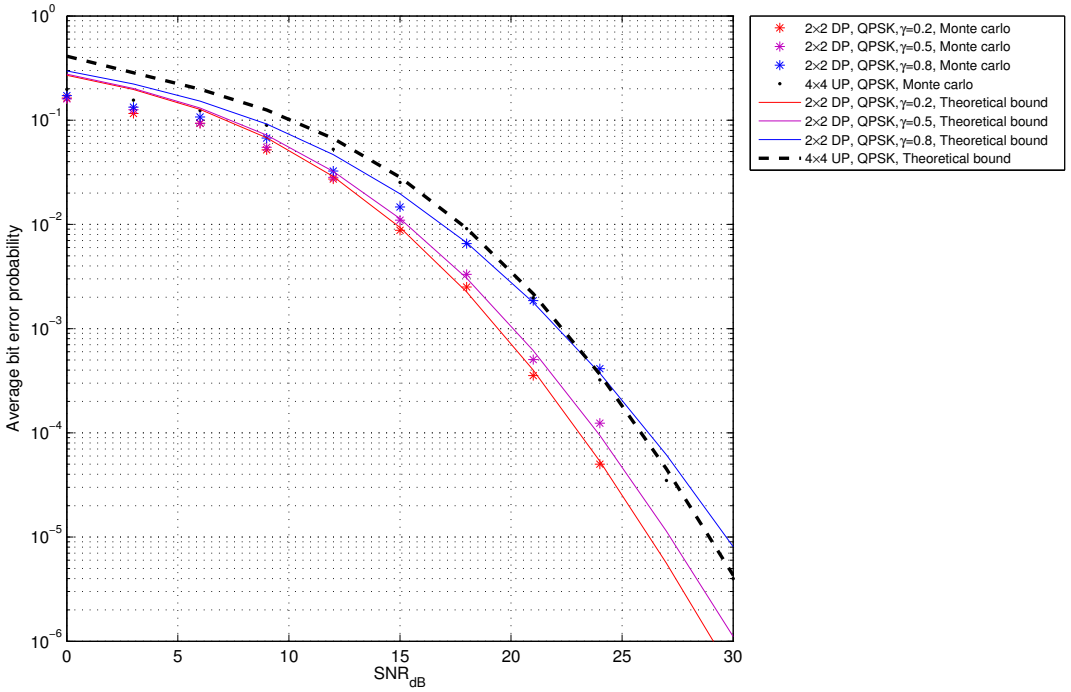

Figure 6.4: G-SM for correlated Rician channel, $R = 4$, $N_a = 2$, $m = 2$, QPSK.

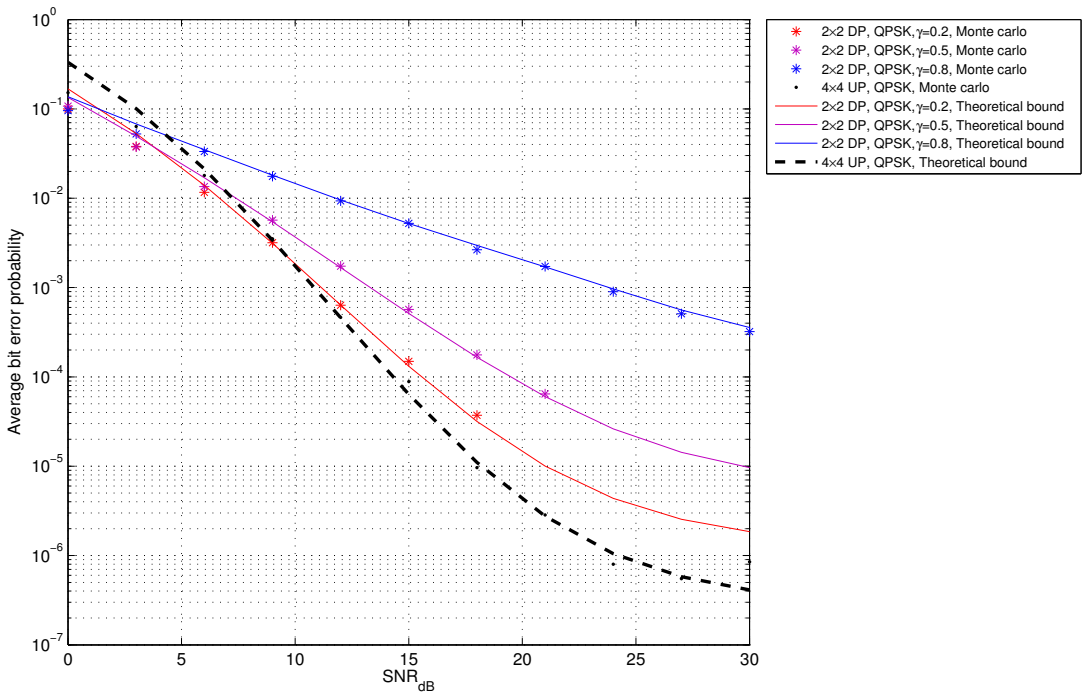

Figure 6.5: G-SM for uncorrelated Rayleigh channel, $R = 4$, QPSK, $\sigma_e^2 = 0.01$.

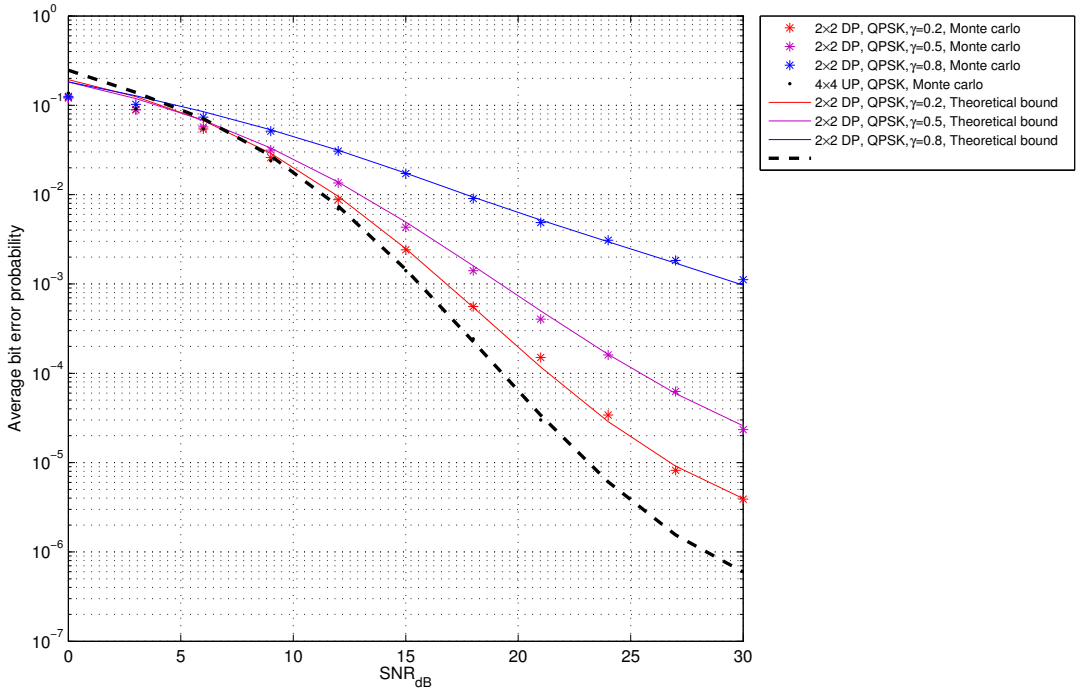

Figure 6.6: G-SM for uncorrelated Rician channel, $R = 4$, QPSK, $\sigma_e^2 = 0.01$.

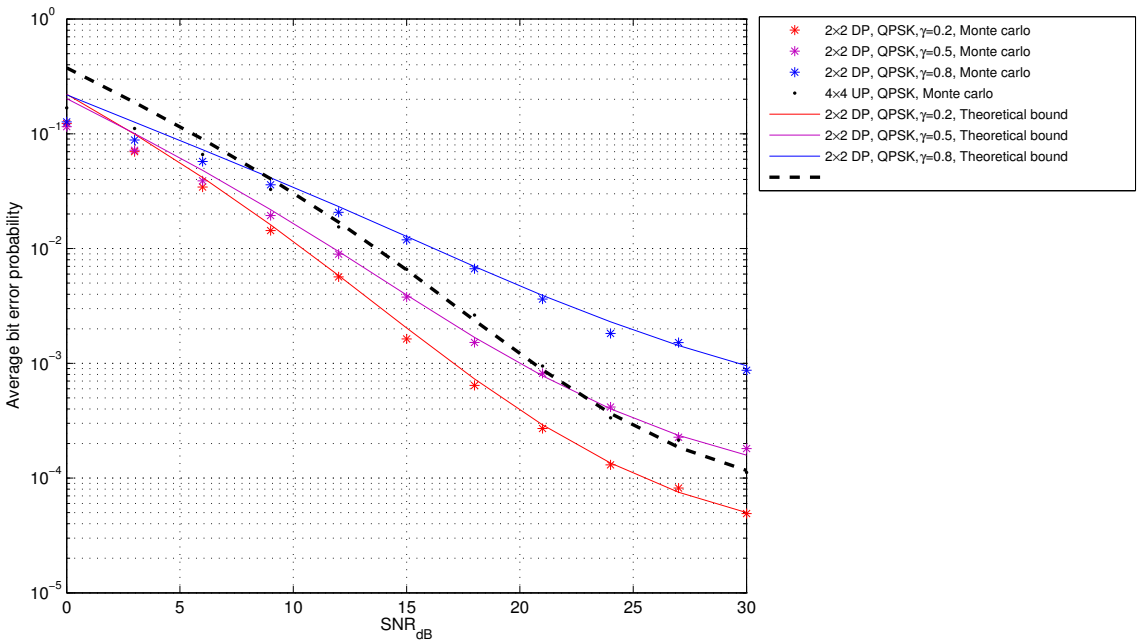

Figure 6.7: G-SM for correlated Rayleigh channel, $R = 4$, QPSK, $\sigma_e^2 = 0.01$.

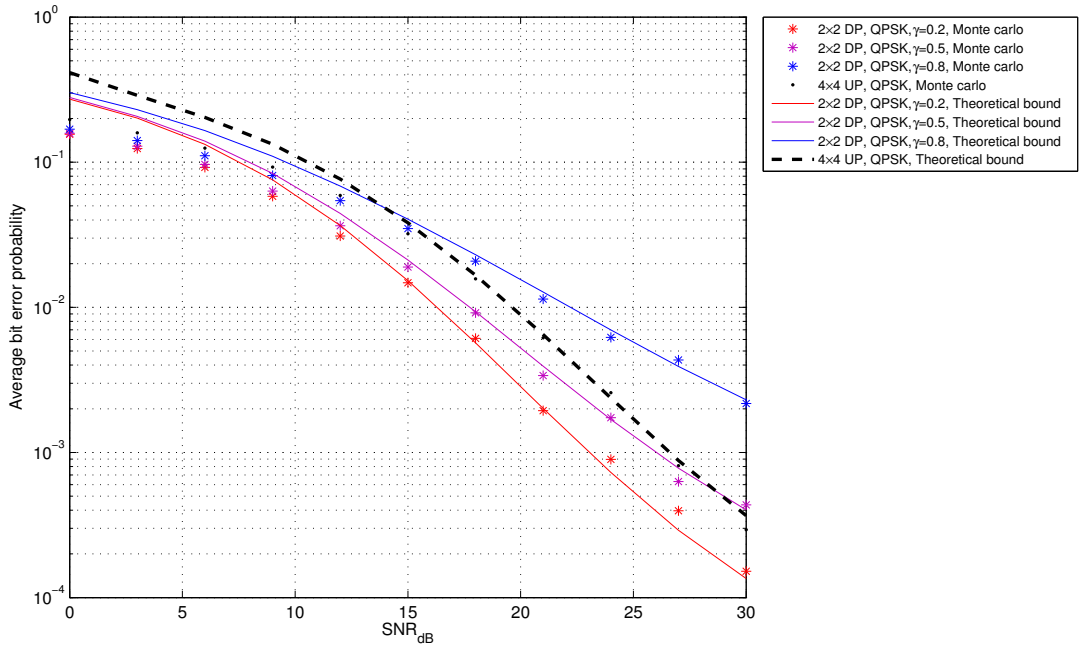

Figure 6.8: G-SM for correlated Rician channel, $R = 4$, QPSK, $\sigma_e^2 = 0.01$.

7. CONCLUSION

In this thesis, we have discussed the performance of wireless channel equipped with dual-polarized antennas. Not only taking advantageous of multi-polarization, but also SM can be employed to eliminate the channels and thus; reduce inter-channel interference. First, channel model has been presented for the general correlated Rician channel, where uncorrelated channel and Rayleigh channel are the special cases, using Kronecker model. Assuming perfect channel estimation PEP, APEP, and consequently ABEP are derived. Furthermore, using ABEP, the equilibrium point of dual-polarized channel and double ordered uni-polarized channel is simulated. Moreover, equilibrium points have been derived in terms of both Chernoff and mutual information and the results have been shown to be equal when numbers of transmitter and receiver are the same. It has been also shown that these equilibrium points are mostly affected by spatial correlation coefficient rather than Rician factor, K. Also, transmit ant receive spatial correlation do not effect these points equally.

Second, we have analyzed the performance of channel assuming that there is channel estimation error. Performance analysis has been considered for M-QAM and M-PSK and it has been shown that while ABEP analysis, which achieved theoretically is an exact result for M-PSK, it is a close approximation for M-QAM. Comparing to the perfect channel estimation, there is degradation in error performance due to the estimation error. It has been shown in simulation that depending on the polarization correlation, it is mostly worthy to use dual-polarized antenna, especially in correlated channels.

Finally, more than one activated antenna has considered which is known as G-SM. This system is mostly used to add diversity gain to all advantages of C-SM. As has been discussed, enhancement in number of transmit antennas ends up to the huge number of combinations from which several combinations might have the best performance as for uni-polarized system. Using the theoretical ABEP to find the best combinations is a time saving method. The best combination, which is independent of polarization correlation, has been derived. In addition to the best antenna index, equilibrium points have been also derived.

APPENDIX A: VARIABLE PART OF THE DUALl-POLARIZED MIMO CHANNEL

Putting Equations 3.13 and Equation 3.5 in Equation 3.12, we have

$$\begin{aligned}
\widetilde{\mathbf{H}} &= \widehat{\mathbf{H}} \otimes \breve{\mathbf{H}} = \mathbf{\Sigma}_r^{\frac{1}{2}} \widehat{\mathbf{H}}_w \mathbf{\Sigma}_t^{\frac{1}{2}T} \otimes \mathbf{Q}_r \mathbf{\Pi}_r^{\frac{1}{2}} \breve{\mathbf{H}}_w \mathbf{\Pi}_t^{\frac{1}{2}T} \mathbf{Q}_t \\
&= (\mathbf{\Sigma}_r^{\frac{1}{2}} \widehat{\mathbf{H}}_w \otimes \mathbf{Q}_r \mathbf{\Pi}_r^{\frac{1}{2}} \breve{\mathbf{H}}_w)(\mathbf{\Sigma}_t^{\frac{1}{2}T} \otimes \mathbf{\Pi}_t^{\frac{1}{2}T} \mathbf{Q}_t) \\
&= (\mathbf{\Sigma}_r^{\frac{1}{2}} \otimes \mathbf{Q}_r \mathbf{\Pi}_r^{\frac{1}{2}})(\widehat{\mathbf{H}}_w \otimes \breve{\mathbf{H}}_w)(\mathbf{\Sigma}_t^{\frac{1}{2}T} \otimes \mathbf{\Pi}_t^{\frac{1}{2}T} \mathbf{Q}_t) \\
&= \mathbf{\Psi}_r^{\frac{1}{2}} \widetilde{\mathbf{H}}_w \mathbf{\Psi}_t^{\frac{1}{2}T} \qquad \text{(A.1)}
\end{aligned}$$

.

REFERENCES

1. Gesbert, D., M. Shafi, D.-S. Shiu, P. J. Smith and A. Naguib, "From Theory to Practice: An Overview of MIMO Space-Time Coded Wireless Systems", *IEEE Journal on Selected Areas in Communicaions*, Vol. 21, No. 3, pp. 281–302, 2003.

2. Torlak, M. and T. Duman, "MIMO Communication Theory, Algorithms, and Prototyping", *20th Signal Processing and Communications Applications Conference (SIU)*, pp. 1–2, 2012.

3. Oestges, C., B. Clerckx, M. Guillaud and M. Debbah, "Dual-Polarized Wireless Communications: From Propagation Models to System Performance Evaluation", *IEEE Transactions on Wireless Communications*, Vol. 7, No. 10, pp. 4019–4031, 2008.

4. Sengul, E., E. Akay and E. Ayanoglu, "Diversity Analysis of Single and Multiple Beamforming", *IEEE Transactions on Communications*, Vol. 54, No. 6, pp. 990–993, 2006.

5. Lozano, A. and N. Jindal, "Transmit Diversity vs. Spatial Multiplexing in Modern MIMO Systems", *IEEE Transactions on Wireless Communications*, Vol. 9, No. 1, pp. 186–197, 2010.

6. Mesleh, R., H. Haas, S. Sinanovic, C. W. Ahn and S. Yun, "Spatial Modulation", *IEEE Transactions on Vehicular Technology*, Vol. 57, No. 4, pp. 2228–2241, 2008.

7. Jeganathan, J., A. Ghrayeb and L. Szczecinski, "Spatial modulation: Optimal Detection and Performance Analysis", *IEEE Communications Letters*, Vol. 12, No. 8, pp. 545–547, 2008.

8. Handte, T., A. Muller and J. Speidel, "BER Analysis and Optimization of Generalized Spatial Modulation in Correlated Fading Channels", *IEEE 70th Vehicular Technology Conference Fall (VTC) 2009*, pp. 1–5, 2009.

9. ElKalagy, A. and E. Alsusa, "A Novel Spatial Modulation Technique with Interference Free Simultaneous Transmission", *21st International Symposium on Personal Indoor and Mobile Radio Communications (PIMRC), 2010*, pp. 809–814, 2010.

10. Younis, A., N. Serafimovski, R. Mesleh and H. Haas, "Generalised Spatial Modulation", *Conference Record of the Forty Fourth Asilomar Conference on Signals, Systems and Computers (ASILOMAR) 2010*, pp. 1498–1502, 2010.

11. Wang, J., S. Jia and J. Song, "Generalised Spatial Modulation System with Multiple Active Transmit Antennas and Low Complexity Detection Scheme", *IEEE Transactions on Wireless Communications,*, Vol. 11, No. 4, pp. 1605–1615, 2012.

12. Basar, E., U. Aygolu, E. Panayirci and H. Poor, "Space-Time Block Coded Spatial Modulation", *IEEE Transactions on Communications*, Vol. 59, No. 3, pp. 823–832, 2011.

13. Jeganathan, J., A. Ghrayeb, L. Szczecinski and A. Ceron, "Space Shift Keying Modulation for MIMO Channels", *IEEE Transactions on Wireless Communications*, Vol. 8, No. 7, pp. 3692–3703, 2009.

14. Di Renzo, M., H. Haas, A. Ghrayeb, S. Sugiura and L. Hanzo, "Spatial Modulation for Generalized MIMO: Challenges, Opportunities, and Implementation", *Proceedings of the IEEE*, Vol. 102, No. 1, pp. 56–103, 2014.

15. Erceg, V., P. Soma, D. Baum and S. Catreux, "Multiple-Input Multiple-Output Fixed Wireless Radio Channel Measurements and Modeling Using Dual-Polarized Antennas at 2.5 GHz", *IEEE Transactions on Wireless Communications*, Vol. 3, No. 6, pp. 2288–2298, 2004.

16. Soma, P., D. Baum, V. Erceg, R. Krishnamoorthy and A. Paulraj, "Analysis and Modeling of Multiple-Input Multiple-Output (MIMO) Radio Channel Based on Outdoor Measurements Conducted at 2.5 GHz for Fixed BWA Applications", *IEEE International Conference on Communications, ICC 2002.*, Vol. 1, pp. 272–276, 2002.

17. Cho, K. and Y. Inoue, "Influence of Cross-Polarization Characteristics on Indoor MIMO Performance Using a Dual-Polarized Base Station Antenna", *IEEE Antennas and Propagation Society International Symposium (APSURSI), 2010*, pp. 1–4, 2010.

18. Prayongpun, N. and K. Raoof, "Correlation Effects and Channel Capacities for MIMO Polarization Diversity", *International Conference on Wireless Communications, Networking and Mobile Computing, WiCOM 2006*, pp. 1–4, 2006.

19. Raoof, K. and N. Prayongpun, "Impact of Depolarization Effects on MIMO Polarized Wireless Configuration", *International Conference on Wireless Communications, Networking and Mobile Computing, WiCom 2007*, pp. 1–4, 2007.

20. Quitin, F., C. Oestges, F. Horlin and P. De Doncker, "Polarization Measurements and Modeling in Indoor NLOS Environments", *IEEE Transactions on Wireless Communications*, Vol. 9, No. 1, pp. 21–25, 2010.

21. Xiao, H.-L., S. Ouyang and Z. Nie, "The Cross Polarization Discrimination of MIMO Antennas at Mobile Station", *International Conference on Communications, Circuits and Systems, ICCCAS 2008*, pp. 203–206, 2008.

22. Lempiainen, J. J. A. and J. Laiho-Steffens, "The Performance of Polarization Diversity Schemes at a Base Station in Small/Micro Cells at 1800 MHz", *Vehicular Technology, IEEE Transactions on*, Vol. 47, No. 3, pp. 1087–1092, 1998.

23. Jagannatham, A. and V. Erceg, "MIMO Indoor WLAN Channel Measurements and Parameter Modeling at 5.25 GHz", *IEEE 60th Vehicular Technology Conference, VTC2004-Fall*, Vol. 1, pp. 106–110 Vol. 1, 2004.

24. Katulski, R., "Polarisation Diversity in Mobile Communication", *13th International Conference on Microwaves, Radar and Wireless Communications. MIKON-2000.*, Vol. 2, pp. 387–389 vol.2, 2000.

25. Shafi, M., M. Zhang, A. Moustakas, P. Smith, A. Molisch, F. Tufvesson and S. Simon,

"Polarized MIMO Channels in 3-D: Models, Measurements and Mutual Information", *IEEE Journal on Selected Areas in Communications*, Vol. 24, No. 3, pp. 514–527, 2006.

26. Kwon, S.-C. and G. Stuber, "Geometrical Theory of Channel Depolarization", *IEEE Transactions on Vehicular Technology*, Vol. 60, No. 8, pp. 3542–3556, 2011.

27. Kwon, S.-C., G. Stuber, A. Lopez and J. Papapolymerou, "Geometrically Based Statistical Model for Polarized Body-Area-Network Channels", *IEEE Transactions on Vehicular Technology*, Vol. 62, No. 8, pp. 3518–3530, 2013.

28. Habib, A., "Multiple Polarized MIMO with Antenna Selection", *18th IEEE Symposium on Communications and Vehicular Technology in the Benelux (SCVT) 2011*, pp. 1–8, 2011.

29. Erceg, V., P. Soma, D. Baum and A. Paulraj, "Capacity Obtained from Multiple-Input Multiple-Output Channel Measurements in Fixed Wireless Environments at 2.5 GHz", *IEEE International Conference on Communications, ICC 2002.*, Vol. 1, pp. 396–400, 2002.

30. Coldrey, M., "Modeling and Capacity of Polarized MIMO Channels", *IEEE Vehicular Technology Conference, VTC 2008.*, pp. 440–444, 2008.

31. Oestges, C., V. Erceg and A. Paulraj, "Propagation Modeling of MIMO Multipolarized Fixed Wireless Channels", *IEEE Transactions on Vehicular Technology*, Vol. 53, No. 3, pp. 644–654, 2004.

32. Sellathurai, M., P. Guinand and J. Lodge, "Space-Time Coding in Mobile Satellite Communications Using Dual-Polarized Channels", *IEEE Transactions on Vehicular Technology*, Vol. 55, No. 1, pp. 188–199, 2006.

33. Liolis, K., J. Gomez-Vilardebo, E. Casini and A. Perez-Neira, "Statistical Modeling of Dual-Polarized MIMO Land Mobile Satellite Channels", *IEEE Transactions on Communications*, Vol. 58, No. 11, pp. 3077–3083, 2010.

34. Kyritsi, P., D. Cox, R. Valenzuela and P. Wolniansky, "Effect of Antenna Polarization on the Capacity of a Multiple Element System in an Indoor Environment", *IEEE Journal on Selected Areas in Communications*, Vol. 20, No. 6, pp. 1227–1239, 2002.

35. Eiceg, V., H. Sampath and S. Catreux-Erceg, "Dual-polarization Versus Single-Polarization MIMO Channel Measurement Results and Modeling", *IEEE Transactions on Wireless Communications*, Vol. 5, No. 1, pp. 28–33, 2006.

36. Nabar, R., H. Bolcskei, V. Erceg, D. Gesbert and A. Paulraj, "Performance of Multi-antenna Signaling Techniques in the Presence of Polarization Diversity", *IEEE Transactions on Signal Processing*, Vol. 50, No. 10, pp. 2553–2562, 2002.

37. Kilic, Y., M. Koca and E. Anarim, "Space-Time-Polarization Diversity in Multiple Input Multiple Output Communication Systems", *IEEE 17th Signal Processing and Communications Applications Conference, SIU 2009.*, pp. 480–483, 2009.

38. Loyka, S., "Channel Capacity of MIMO Architecture Using the Exponential Correlation Matrix", *IEEE Communications Letters*, Vol. 5, No. 9, pp. 369–371, 2001.

39. Maharaj, B., L. Linde and J. Wallace, "MIMO Channel Modelling: The Kronecker Model and Maximum Entropy", *IEEE Wireless Communications and Networking Conference, WCNC 2007.*, pp. 1909–1912, 2007.

40. Koca, M. and H. Sari, "Performance of Spatial Modulation Over Correlated Fading Channels with Channel Estimation Errors", *IEEE Wireless Communications and Networking Conference (WCNC) 2013*, pp. 3937–3942, 2013.

41. Veeravalli, V., "On Performance Analysis for Signaling on Correlated Fading Channels", *IEEE Transactions on Communications*, Vol. 49, No. 11, pp. 1879–1883, 2001.

42. Bahrami, H. and T. Le-Ngoc, "Precoder Design Based on Correlation Matrices for MIMO Systems", *IEEE Transactions on Wireless Communications*, Vol. 5, No. 12, pp. 3579–3587, 2006.

43. Asplund, H., J. E. Berg, F. Harrysson, J. Medbo and M. Riback, "Propagation Characteristics of Polarized Radio Waves in Cellular Communications", *IEEE 66th Vehicular Technology Conference, VTC 2007*, pp. 839–843, 2007.

44. Koca, M. and H. Sari, "Generalized Spatial Modulation Over Correlated Fading Channels: Performance Analysis and Optimization", *20th International Conference on Telecommunications (ICT) 2013*, pp. 1–5, 2013.